UNIVERSITY OF BELGRADE

FACULTY OF TECHNOLOGY AND METALLURGY

Ali Hussien Al-Eggiely

POSSIBLE APPLICATION OF THE POLYPYRROLE-ZINC SYSTEM AS A SEA-WATER BATTERY

Doctoral Dissertation

Belgrade, 2018

UNIVERZITET U BEOGRADU

TEHNOLOŠKO-METALURŠKI FAKULTET

Ali Hussien Al-Eggiely

MOGUĆNOST PRIMENE SISTEMA POLIPIROL-CINK KAO AKUMULATORA U MORSKOJ VODI

doktorska disertacija

Beograd, 2018

Mentor:

Dr Branimir Grgur, redovni profesor,
Univerzitet u Beogradu, Tehnološko-metalurški fakultet

Članovi komisije:

Dr Milica Gvozdenović, vanredni profesor,
Univerzitet u Beogradu, Tehnološko-metalurški fakultet

Dr Nebojša Nikolić, naučni savetnik,
Univerzitet u Beogradu, IHTM, Centar za elektrohemiju, Beograd

Datum odbrane: ___ ___ _____ god.

ACKNOWLEDGEMENT

I would like to express this appreciation to Professor Branimir Grgur, for his supervision, guidance, encouragements, and advice throughout the duration of study and experimental work.

I would also to thanks sincere appreciation to my Mentor Professor Branimir Grgur, Professor Milica Gvozdenović and Dr. Nebojša Nikolić, for guideless during the work on this doctoral dissertation.

Finally deep thanks to the Libyan Government, and my family, for their patent, and encouragements during my Ph.D study at Belgrade University.

Thank you.

POSSIBLE APPLICATION OF THE POLYPYRROLE-ZINC SYSTEM AS A SEA-WATER BATTERY

ABSTRACT

The polypyrrole is electrochemically synthetized from hydrochloric acid solution and pyrole monomer. Using the cyclic voltammetry and UV-visible spectroscopy it is shown that polypyrrole is in the polaron state with doping degree of 0.25 (one chloride anion per four pyrrole monomer units).

An environmentally friendly cell using polypyrrole-air regenerative cathode and zinc as anode is investigated in the 3% sodium chloride solution. The cell can operate in different charge and discharge modes. Polypyrrole can be reoxidized (doped) with chloride anions either by using dissolved oxygen or by an external power supply, e.g., small photovoltaic cell. In that way, after discharge, capacity retaining can be achieved by using sea-water as the electrolyte. During low discharge rate, the delicate balance between solid state diffusion-controlled dedoping and chemical oxidation of polypyrrole produced by hydrogen peroxide is achieved, generating stable voltage plateau of ~1 V. The cell is proposed to operate as a power supply for different devices used in a remote sensor buoy system for monitoring shallow marine environments in two modes. In the low discharge mode (10–20 mA g^{-1}), it can be used for data acquisition, and at the fast discharge mode (up to 2 A g^{-1}) for collected data transmission.

Keywords: Polypyrrole; Oxygen, Reduction, Hydrogen peroxide, Buoy system

Scientific field: Technological engineering

Specific scientific field: Chemical engineering

MOGUĆNOST PRIMENE SISTEMA POLIPIROL-CINK KAO AKUMULATORA U MORSKOJ VODI

REZIME

Polipirol je elektrohemijski sintetisan iz rastvora hlorovodonične kiseline i monomera pilora. Koristeći cikličnu voltametriju i UV-vidljivu spektroskopiju, pokazano je da je polipirrol u polaron stanju sa stepenom dopovanja od 0,25 (jedan hloridni anjon na četiri monomera pirol).

Ekološki prihvatljiva ćelija sa regenerativnnom katodom od polipirola i cinka kao anode ispitana je u 3% rastvoru natrijum hlorida. Ustanovljeno je da ćelija može da radi u različitim režimima punjenja i pražnjenja. Polipirol se može reoksidiovati (dopovati) sa hloridnim anionima bilo korišćenjem rastvorenog kiseonika ili spoljnim napajanjem, na primer, male fotonaponske ćelije. Na taj način, nakon pražnjenja, regeneracija kapaciteta se može postići korišćenjem morske vode kao elektrolita. Tokom pražnjenja sa niskim strujama postiže se delikatna ravnoteža između difuziono kontrolisanog dedopovanja i hemijske oksidacije polipirrola proizvedenim vodonik-peroksidom, stvarajući stabilni naponski plato od ~ 1 V. Predloženo je da ćelija može raditi kao izvor napajanja za različite uređaje autonomnih senzorskih plutajućih bova, koje se koriste u sistemu daljinskog praćenja kvaliteta plićih morskih voda. Pri režimu blagog pražnjenja (10-20 mA g^{-1}), može se koristiti za prikupljanje podataka i pri brzom pražnjenju (do 2 A g^{-1}) za radio prenos prikupljeni podataka.

Ključne reči: Kiseonik, Redukcija, Vodonik-peroksid, Plutajuća bova
Naučna oblast: Tehnološko inženjerstvo
Uža naučna oblast: Hemijsko inženjerstvo

CONTENTS

1. INTRODUCTION

In recent years, monitoring of the marine environment became an area of the considerable scientific interest [1]. Shallow marine ecosystems are especially vulnerable, because of the different human actions in the area of the industrial, touristic and municipal expansion. Consequently, pollution monitoring of these ecosystems became the main goal for the scientists concerned in the behavior of the marine environment [1]. It is of great importance to gather information using different sensor devices to ensure successful monitoring of the marine ecosystems [2, 3, 4]. A remote sensor buoy systems, shown in Fig. 1.1, for monitoring shallow marine environments include different electronics components like: sensors devices, radio frequency transmissions module, a power supply with corresponding controlling systems, a set of sensor interfaces, amplification modules, A/D converters, memory for data storage, an electronic timer clock, and finally a microcontrollers (CPU - central processing unit) to integrate the entire process and realized predefined monitoring tasks [5]. Autonomy marine monitoring systems require months of the constant power supply from a battery. In the remote buoy sensor system, the CPU is the main consumer of the power [1]. CPU usually works in an on-off mode with the most of the power, ~80%, consumed during the sleep period. Power consumption depends on the operation mode and range from few microamperes, in a sleep mode, to ~150 mA during the data acquisition, storage and transmission [1]. A power sources usually the Li-polymer battery connected to photovoltaic panel is considered [1, 6, 7]. However, such a power supply combination is very heavy, expensive and strongly depends on weather conditions. Namely, Li-polymer battery in combination with photovoltaic panel requires additional electronic components for overcharge and under-discharge limitations, while effective charge with relatively small photocell can be

accomplished only during the sunny days. In the occasion of cloudy or foggy days, photovoltaic panel should be oversized due small efficiency.

Figure 1.1. The YSI EMM68 buoy containing water quality and meteorological sensors, telemetry package, solar panels and batteries.

For long-lasting power supply, metal-air batteries [8,9,10], using dissolved oxygen in the sea-water as the cathode reactant, should be also considered. The operating voltage of such batteries depends on the metal anode e.g. Mg, Al or Zn, and range from ~1.8 to 1.4 for Mg and some Al alloys, to below 1 V for pure Al and Zn [11,12,13,14,15,16].

Conducting polymers, like polyaniline and polypyrrole are used as cathode with zinc anode as potentially promising electrochemical power sources in water based electrolytes [17, 18]. In some papers it is shown that zinc-polypyrrole cell in water based electrolytes possess cathode recharge characteristics (reoxidation) in the interaction with dissolved molecular oxygen [19]. The recharge is associated with the oxygen reduction reaction onto polypyrrole through two-electron, hydrogen peroxide path, accompanied by polypyrrole reoxidation (doping) in the chemical reaction with formed hydrogen peroxide [19].

Based on these findings, the aim of this thesis is to investigate the possibility of

Zn|PPy cell application as an environmentally friendly battery using the oxygen dissolved in sea-water as the electrolyte. Such cell is planned to work as a power supply for different buoy system devices in two modes: -in the low discharge mode for data acquisition and at fast discharge mode for transmission of the collected data. The processes of the polypyrrole reoxidation will be examined as a possible recharge mechanism of the Zn|PPy cell.

2. THEORETICAL PART

2.1. Seawater and metal-air batteries

Seawater batteries are of great importance for the long lasting, low-power supply of different devices [20], for example signal lights, lifejackets, GPS, sensors for the monitoring water temperatures and flow rate especially in measuring climate changes, deep sea applications *etc*. [21]. In Fig. 2.1, as an example the battery for lifejacket signal lights is shown.

Figure 2.1. Lifejacket light, using magnesium/cuprous chloride water-activated battery (*Electric Fuel Ltd.)*

Currently, the usages of such, immersion, batteries are a hot topic and has been recently emphasized in many countries [22]. Immersion batteries are designed to be activated by dipping into the electrolyte. Among different types, magnesium-cuprous chloride and magnesium-silver chloride are the front runners [23]. They have been constructed in sizes to produce from 1.0 V to several hundred volts at currents up to 50 A

[24]. Discharge times can vary from a few seconds to only several days depending on external load, as can be seen in Fig. 2.2 [24]. The principal overall and current-producing reactions for the water-activated magnesium batteries are as follows [24]:

1. Magnesium/silver chloride

Anode	$Mg - 2e \rightarrow Mg^{2+}$
Cathode	$2AgCl + 2e \rightarrow 2Ag + 2Cl^{-}$
Overall	$Mg + 2AgCl \rightarrow MgCl_2 + 2Ag$

2. Magnesium/cuprous chloride

Anode	$Mg - 2e \rightarrow Mg^{2+}$
Cathode	$2CuCl + 2e \rightarrow 2Cu + 2Cl^{-}$
Overall	$Mg + 2CuCl \rightarrow MgCl_2 + 2Cu$

A side reaction (corrosion) also occurs among the magnesium anode and the aqueous electrolyte, resulting in the formation of magnesium hydroxide, hydrogen gas, and heat:

$$Mg + 2H_2O \rightarrow Mg(OH)_2 + H_2 \qquad (2.1)$$

which is the main reasons for relatively fast discharge times.

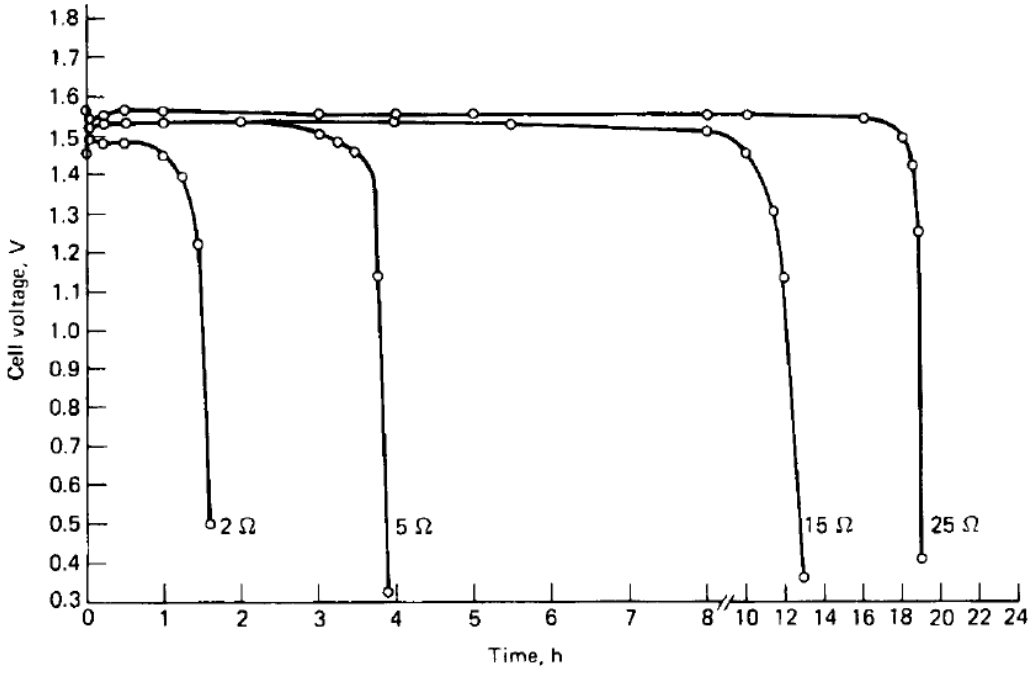

Figure 2.2. Magnesium/silver chloride seawater-activated cell discharged continuously at 35°C in simulated ocean water, 3.6% salinity [24].

Hereafter, for long-lasting power supply, modified metal-air seawater batteries, which could use dissolved oxygen as the cathode reactant and metal as anode should be considered.

The principles of the classical metal-air batteries, which use oxygen from the air as reactant are shown in Fig. 2.3 [25]. Due negative potentials, metal dissolves and behaves as anode with reaction:

$$M \rightarrow M^{n+} + ne \qquad (2.2)$$

while at cathode, oxygen is reduced:

$$O_2 + 2H_2O + 4e \rightarrow 4OH^- \qquad (2.3)$$

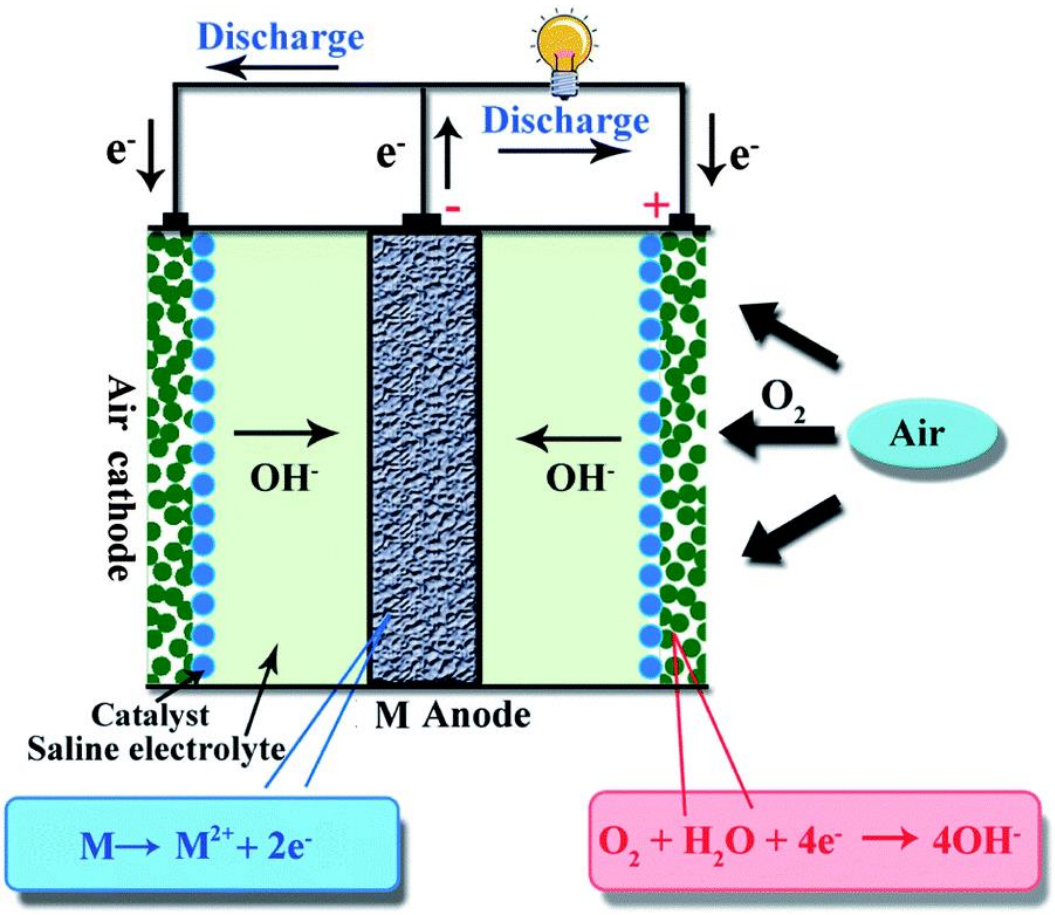

Figure 2.3. Typical structure and working principle of a metal–air battery [25].

Typically, a highly porous high surfaces cathode for the metal-air battery is constructed using high surface carbon with an expensive catalyst such as Pt. The catalyst is required due very slow reduction kinetics of the oxygen reaction on the carbon materials. The assembly of a typical air-gas diffusion cathode is composed of four layers: a waterproof breathable layer, a gas diffusion layer, a catalyst layer, and a current collector layer [25], as shown in Fig. 2.4. It should be mentioned that such system is effective only in a three-phase environment: gas-solid-liquid.

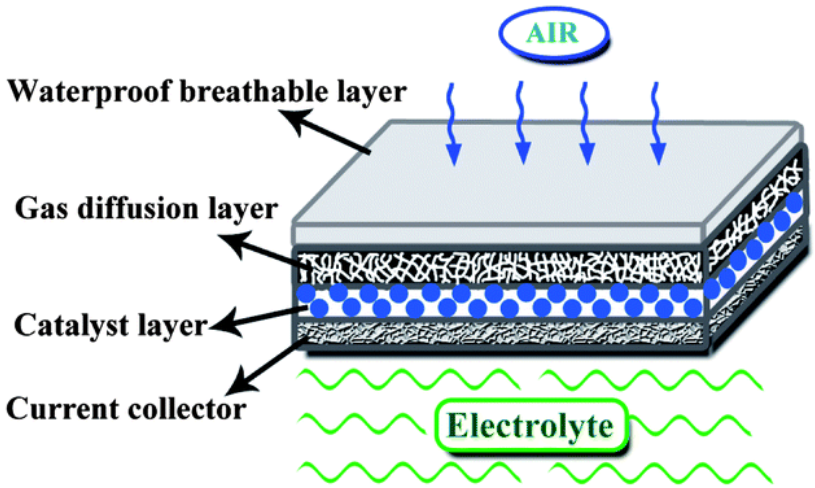

Figure 2.4. Structure of a typical air cathode with four layers [25].

2.1.1. Anodes for metal air batteries

Promising metals for that kind of applications are zinc, aluminum and magnesium [26]. Their characteristic electrochemical properties are shown in table 2.1.

Table. 2.1. Comparisons of specific (s) and volumetric (v) capacities (q), potentials, specific and volumetric energy (w) of aluminum, magnesium and zinc in 3.5% NaCl solution [26].

Metal	n	M g mol^{-1}	ρ g cm^{-3}	q_s Ah g^{-1}	q_v Ah cm^{-3}	E V (SHE)	w_s Wh g^{-1}	w_v Wh cm^{-3}
Aluminum	+3	26.98	2.70	2.98	8.05	–1.5	4.47	12.07
Magnesium	+2	24.3	1.74	2.2	2.83	–1.65	3.63	4.7
Zinc	+2	65.38	7.14	0.82	5.82	–0.76	0.62	4.42

Theoretical specific capacity (per 1 g of active materials) is given as:

$$q_{s,t} = \frac{nF}{M} \tag{2.4}$$

where F is Faraday constant (26.8 Ah g^{-1}), and M , g mol^{-1}, molar mass of the reacting metal. Theoretical volumetric capacity (per 1 cm^3 of active materials) is given as:

$$q_{v,t} = q_{s,t}\rho = \frac{\rho nF}{M} \tag{2.5}$$

where ρ, g cm^{-3}, is the density of the metal. On the other hand, specific and volumetric energies (w) are given as:

$$w_{s,t} = q_{s,t}E = \frac{nFE}{M} \tag{2.6}$$

and:

$$w_{v,t} = q_{v,t}E = \frac{\rho nFE}{M} \tag{2.7}$$

The operating voltage of such batteries, in combination with gas diffusion oxygen cathode, depends on metal anode, for example: Mg, Al or Zn, and range from ~1.8 V for pure Mg, 1.4-1.2 V for some Al alloys [27, 28, 29], to below 1 V for pure Al and Zn [26], as can be seen in Fig. 2.4 [30].

Mg has a very negative potential that provoke very high corrosion rates, and time limited applications. Among others, aluminum has the highest theoretical values of specific capacities and energies, but due formation of passive layer onto surface, the real values are significantly smaller. Zinc has the smallest specific capacities and energies, but due good corrosion stability and uniform corrosion, it could be considered as an optimal anode for sea-water based cells.

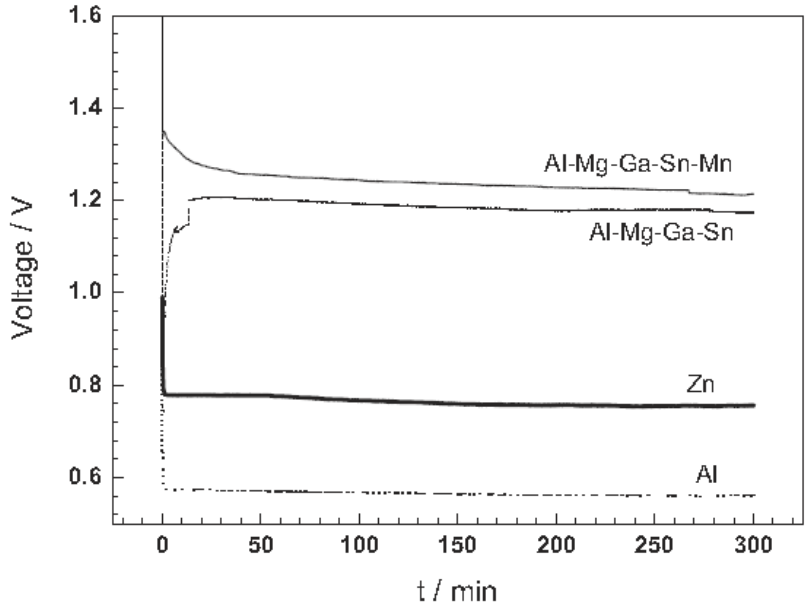

Figure 2.4. The discharge behavior of metal-air battery with different anodes at current densities of 20 mA cm^{-2}, and cathode is gas diffusion air electrode with MnO_2 catalyst in 2 M NaCl [30].

Many efforts have been invested in development of magnesium alloys to improve characteristics [31]. In Figure 2.5 the discharge behavior of Mg-air battery with different anodes at several constant current densities of 0.5, 2.5, 5 and 10 mA cm^{-2}, is shown, using the air gas diffusion cathode with sliver catalyst. The voltage–time curves are similar for all the anodes. The operating voltage decreased rapidly in the early discharging stage, which is caused by a film formed product during discharge on the anode surface, and then reached to an approximate constant value. It should be noted that the operating voltage of Mg-air battery with Mg–Li–Al–Ce is higher than those of Mg and AZ31-alloy (magnesium alloy with roughly 3 weight percent of aluminum and 1 weight percent of zinc) at various discharge current densities. In addition, as shown in Fig. 2.5(d), the operating voltage of Mg-air battery with AZ31 decreases rapidly to 0 V after 800 min of discharge, which means that the AZ31 anode is completely dissolved. For all the alloys, the corrosion was very high so, the operation of the battery is limited to only few days, before alloys is completely dissolved.

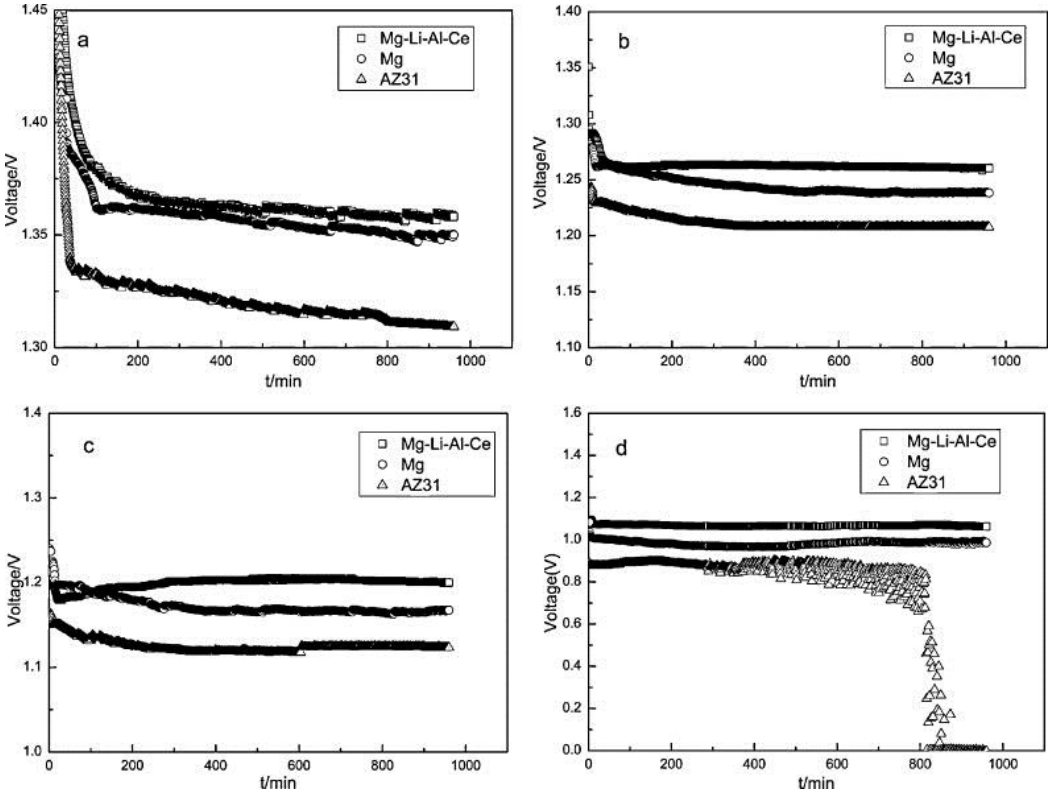

Figure 2.5. The discharge behavior of Mg-air battery with different anodes in 3.5% NaCl at currents (a) 0.5 mA cm^{-2}, (b) 2.5 mA cm^{-2}, (c) 5 mA cm^{-2}, and (d) 10 mA cm^{-2} [31].

On the other hand, aluminum is corrosion more stable than magnesium, but corrosion products (Al_2O_3, and $Al(OH)_3$) completely cover the electrode preventing them for the further operation by so called passivation [32]. Pino et al [32] introduced now method to improve characteristics of aluminum dissolution. They proposed treatment based on carbon layer deposition onto aluminum alloys, the principles are shown in Fig. 2.6, in order to enhance the performance of Al-air primary batteries with neutral electrolyte pH. Carbon treatment is consisted of the uniform covering of the aluminum surface by carbon-based paste. The paste is prepared by mixing two parts of carbonaceous material, one part of binder and seven parts of solvent (by weight). During discharge the carbon covering decreases the jellification of aluminates at the anode surface, and exance the battery characteristics.

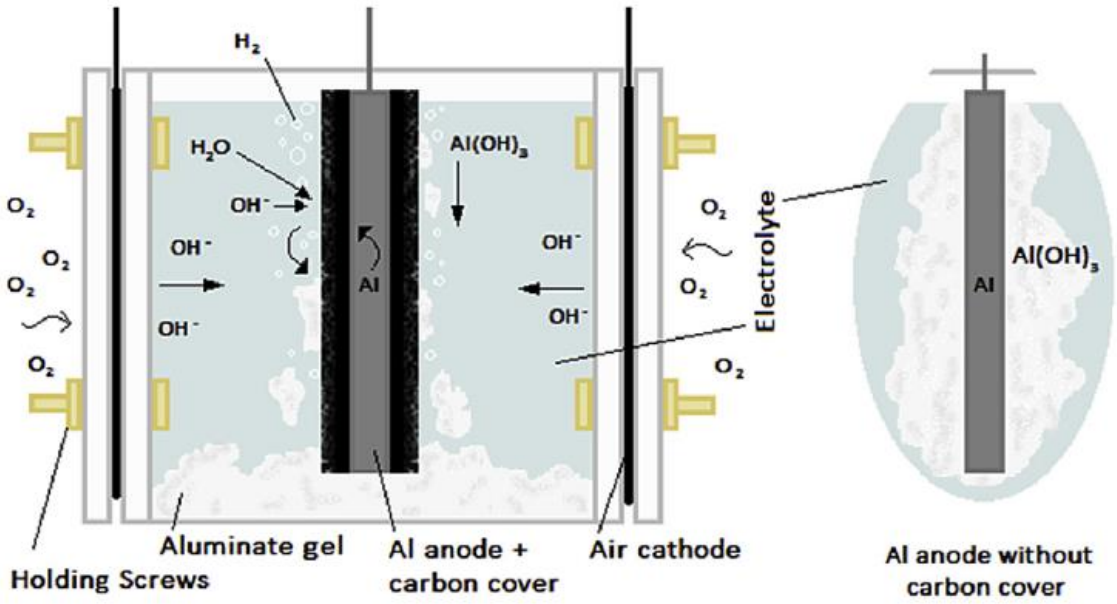

Figure 2.6. Schematic representation of aluminate accumulation in Al-air neutral pH cell with and without carbon treatment [32].

Treated and untreated commercial Al alloys (Al1085 and Al7475) are tested as anodes in the battery achieving specific capacities above 0.6 Ah g^{-1} *vs* 0.2 to 0.3 Ah g^{-1} without carbon covering, as can be seen in Fig. 2.7. However, still discharge voltage is relatively low, below 0.7 V, and energy is far from the theoretical values.

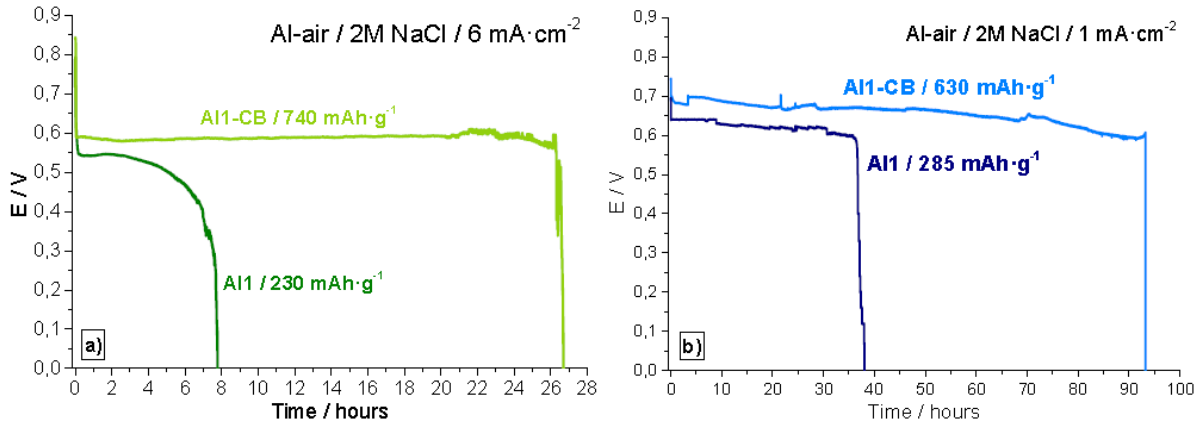

Figure 2.7. Discharge plot of Al1-air cell with and without carbon cover at constant current density of: a) 6 mA cm^{-2}; b) 1 mA cm^{-2}. [32]

Among these three metals, magnesium shows high corrosion rate, while aluminum passivated due formation of low soluble aluminum oxy(hydroxides) owing low discharge voltage. So, even the zinc possess lowest specific capacity, Table 2.1, due good electrochemical characteristics and low price it should be considered as a good candidate for metal-air batteries.

The corrosion potentials of the pure zinc in seawater is below –1 V (vs. SCE), and can be discharged with relatively high current densities up to 25 mA cm^{-2}, as can be seen in Fig. 2.8 [33].

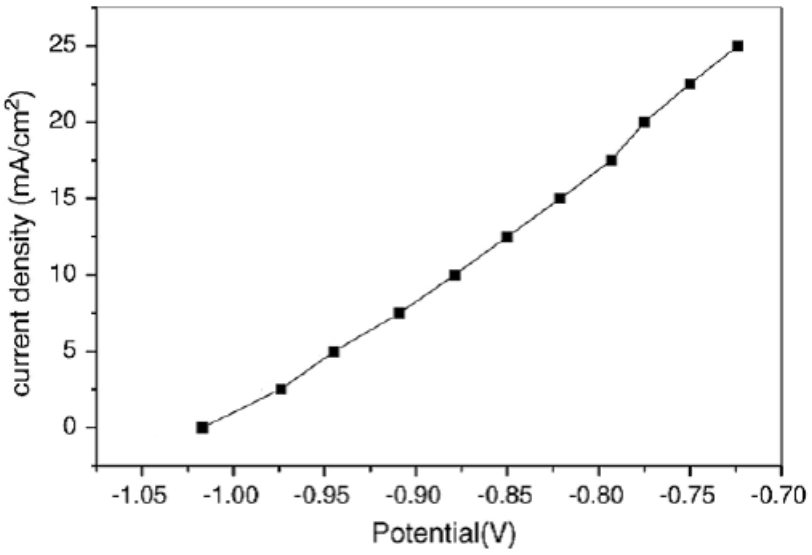

Figure 2.8. Variation of anode polarization curves for pure zinc sample in 3.5 wt.% NaCl solution (potential is vs. reference saturated calomel electrode) [33].

2.1.2. Oxygen reduction reaction

Theoretical potential of the oxygen electrode can be given as:

$$E(O_2|H_2O) = 1.23 - \frac{2.3RT}{F}\,pH - \frac{2.3RT}{4F}\log\frac{p(O_2)}{p^{\theta}} \qquad (2.8)$$

or approximately at room temperature:

$$E(O_2|H_2O) \approx 1.23 - 0.06pH - 0.015\log y(O_2) \qquad (2.9)$$

Hence, at neutral pH~7, and oxygen from the air where 21% of oxygen is present, $y(O_2)$~0.21, the potential will be ~0.82 V vs SHE. For the theoretical potentials of zinc ~–0.76 V vs SHE, the open circuit voltage of zinc-air battery will be 1.58 V. Unfortunately, during the discharge this voltage is usually below 1 V. The main limiting factor is the high overpotentials of the oxygen reaction reaction during discharge process. These are mostly a result of insufficient catalysts used on the cathode for the oxygen reduction reaction while discharging [34, 35]. In Fig. 2.9 can be seen that among other electrolytes, in NaCl based electrolyte at 1 mA cm^{-2} (10 A m^{-2}) the potential of platinum cathode is only 0.15 V (SHE) [36], which is for 0.67 V more negative than theoretical potential.

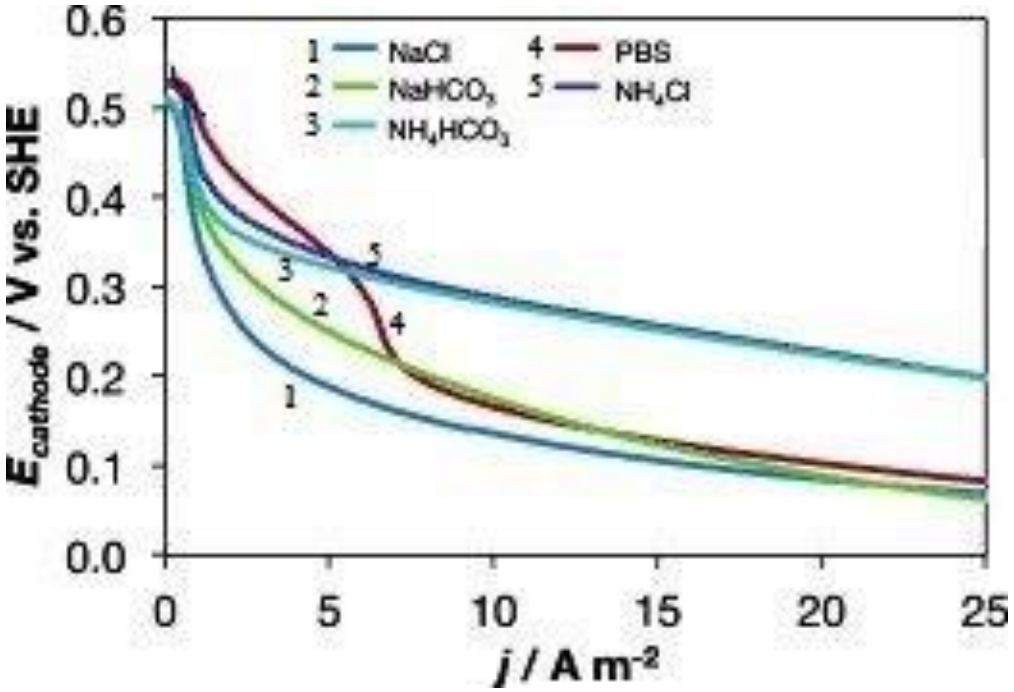

Figure 2.9. Polarization curves of the oxygen reduction reaction on platinum cathode in different electrolytes at pH~7 [36].

In a near neutral electrolyte (pH~7), oxygen is reduced to OH^- at the interface of the gas–solid–liquid ternary phases of the air cathode. As the oxygen reduction reaction (ORR) occurs in the three-phase interface, it involves complex physical and chemical reactions. In general, the possible reaction pathways involved in the ORR in a neutral solution can be expressed [37]:

as a direct four electron path (on active catalyst like Pt):

$$O_2 + 2H_2O + 4e^- \rightarrow 4OH^- \quad (2.10)$$

or via indirect two electron path (formation of hydrogen peroxide ions, on usually carbon materials):

$$O_2 + H_2O + 2e^- \rightarrow HO_2^- + OH^- \quad (2.11)$$

$$HO_2^- + H_2O + 2e^- \rightarrow 3OH^- \quad (2.12)$$

It should also be mentioned that high surface area cathode usually works in three phases namely solid to liquid to gas environments. However, it is not the case with sea-water whereby there is dissolved oxygen. Dissolved oxygen enters water through the air or as a plant byproduct. As shown in Fig. 2.10, from the air, oxygen can slowly diffuse across the water surface from the adjacent atmosphere, or can be mixed in quickly through aeration, whether natural or man-made [38]. Wind (creating waves), rapids, waterfalls, ground water discharge or other forms of running water can cause the aeration of water. Dissolved oxygen is also produced as a waste product of photosynthesis from phytoplankton, algae, seaweed and other aquatic plants.

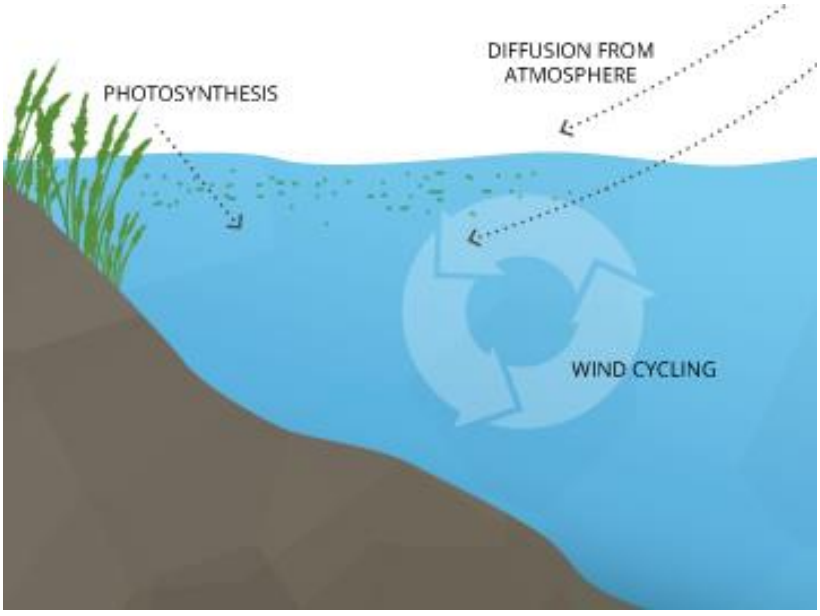

Figure 2.10. Schematic presentation of the sea-water аератион [38].

Operating current density of the oxygen cathode in seawater is limited to ~0.1 mA cm^{-2}, due to the limited solubility of oxygen [39], which ranges from 0.35 mM at 0°C to ~0.2 mM at 30°C as can be seen in Table 2.2.

Table 2.2. Solubility of the oxygen in sea-water (s*alinity ~ 35)*

***т*/ °Ц**	**µмол/Л**	**мг/Л**	**мл/Л**
0	349	11.2	7.8
5	308	9.9	7
10	275	8.8	6.4
15	248	7.9	5.9
20	225	7.2	5.4
25	206	6.6	5
30	190	6.1	4.7
35	176	5.6	4.5
40	165	5.3	4.2
45	154	4.9	4
50	146	4.6	3.8

The oxygen content of sea-water over water depth is shown in Fig 2.11 [40]. Gas content is high, around 6 mg dm^{-3}, at the surface where mixing occurs. At depth, oxygen is used to oxidize organic matter and carbon dioxide is released. This produces an oxygen minimum zone, between 500 to 1000 m. Gas content again increase with depth thereafter due to deep ocean water masses. Consequently, from the Fig. 2.11 can be seen that among 0 and 500 m of depth, a reasonable concentration between 6 and 3 mg dm^{-3} of dissolved oxygen exists.

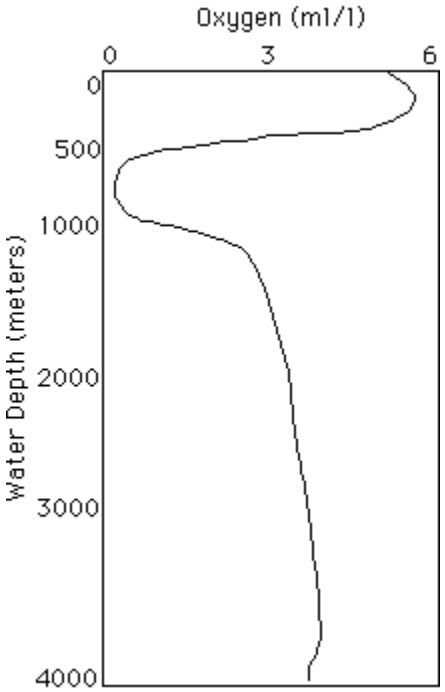

Figure 2.11. The oxygen content in seawater over water depth [40]

2.2. Possible application of the conducting polymers in the batteries

Electrochemical properties of conducting polymers due to their low specific weight when compared with classical inorganic compounds; high energy and power density and ability to reversible exchange counter ions, have stimulated the interest in their use as electrode materials of the electrochemical power sources [41]. According to Rüetschi, and elaborated by Beck and Rüetschi [42, 43], determining factors of the battery system success are the 'three E' criteria: **Energy** (high energy content with respect to unit weight and volume), **Economics** (low manufacturing costs, low maintenance during use, long service life), **Environment** (free of toxic materials, safe, low energy consumption during manufacture and use, long service life, high reliability, easy to recycle).

There are many different types of the conducting polymers [44], but the most investigates are polyaniline (PANI), polypyrrole (PPy), polythiophene (PTh) and poly(3,4-ethylenedioxythiophene) (PEDOT), which structures are shown in Fig. 2.12. [45].

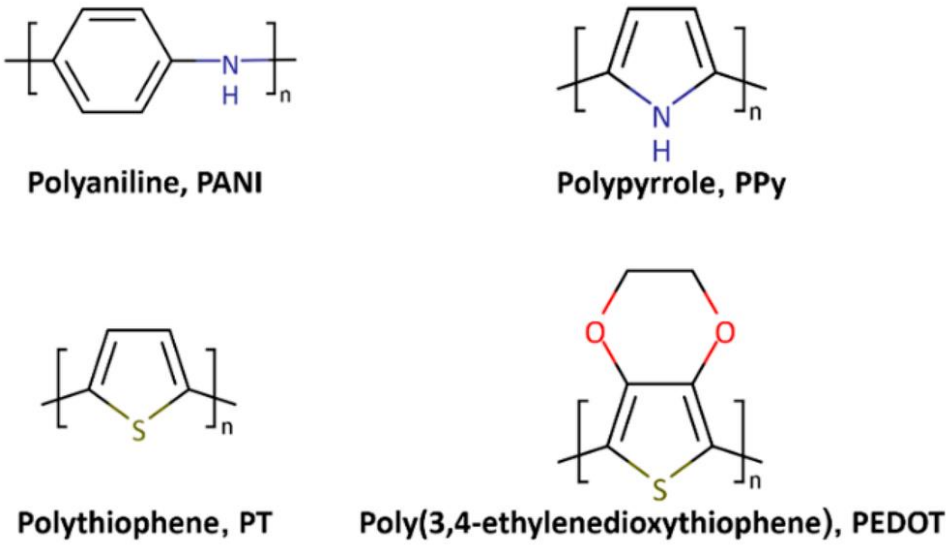

Figure 2.12. Chemical structures of the most representative conducting polymers [45].

Some of the typical characteristics of common conducting polymers are given in Table 2.3 [46].

Table 2.3. Characteristics of most common conducting polymers [46]

CP's	***M* (monomer) g mol^{-1}**	**Doping level *y***
PANI	93	0.5
PPy	67	0.33
PTh	84	0.33
PEDOT	142	0.33

Conducting polymers has ability to be chemically or electrochemically reversible reduced (dedoped) and oxidized (doped), through simultaneous deinsertation or insertion of the anions. For example, polyaniline, which is consisted of 4 monomer in the polymer units cloud undergo different changes depending on potentials or pH. Transition occurs through leucoemeraldine – emeraldine – perningraniline with corresponding anion insertion (dopind), as shown in Fig. 2.13 [47]. All the oxidation states could have certain numbers of anions in the polymer units, which is called doping degree. For example, in

emeraldine salt state, two anions are banded to four monomer units, so doping degree is 0.5.

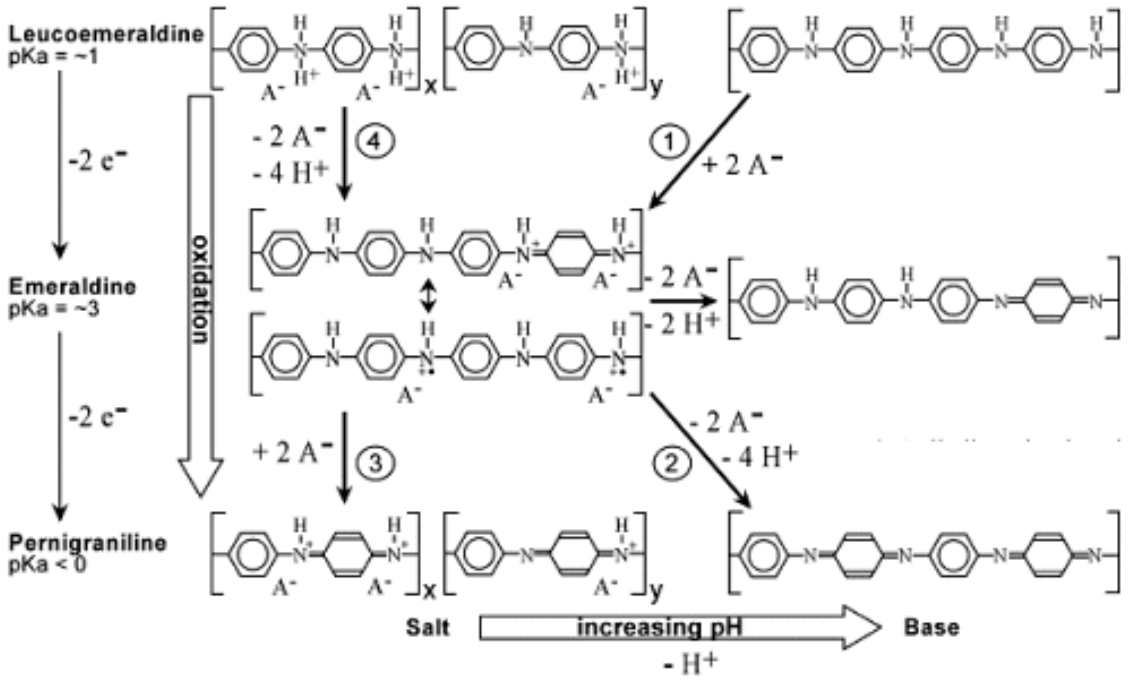

Figure 2.13. Electrochemical oxidation states of polyaniline. In the fully protonated states (left), the polymer comprises only x units, but in most acids the chains are mixtures of x and y units, the ratio depending on pH. During electrochemical oxidation in aqueous electrolytes, the gain or loss of anions and protons, and thus the strain, depends on solution pH. (Anion and proton counts are taken from the x units to the emeraldine salt.) [47].

Electrochemical systems based on the conducting polymers, electronegative metals (*e.g.* Zn, Mg, Al) and aqueous based electrolytes, have potentials to accomplish most of the three *E'* criteria. Even, the variety of the conducting polymers are high, up to now only few of them has been investigated and tested for the application in aqueous based electrochemical power sources. Polyaniline combined electronegative metals (mainly zinc) are the most extensively investigated systems [48, 49, 50, 51]. This type of the electrochemical power sources has not been commercialized, even the electrochemical characteristics are in principles very good. The main reasons for this are degradation process of polyaniline electrode at potentials more positive than ~0.5 V [52, 53].

Even the polypyrrole, together with the polyaniline, is one of the most investigated conducting polymer, practically there in the past little attempt in his use as an electrode material for aqueous based electrochemical power sources. Main investigations are focused for applications in aprotonic electrolytes [41]. In recent years, batteries which used polypyrrole (PPy) as cathode materials and aqueous electrolyte have gained popularity due to their high discharge specific capacity of ~115 mAh g^{-1}, environmental stability, easy synthesis, electroactivity in different pH *etc.*, especially for application in a micro power devices, biocompatible power sources, or stretchable electronics [54, 55, 56, 57, 58, 59, 60, 61, 62, 63, 64, 65].

2.2.1. Oxygen reduction and reoxidation of the conducting polymers

Some of the conducting polymers can be oxidized or doped during interaction with the molecular oxygen in the electrolyte. Kitani et al. [50] observed that Zn-polyaniline battery possess recharge characteristic after complete discharge, and being exposed to dissolved molecular oxygen in the electrolyte, Fig. 2.14. In contrast to nitrogen contained solution, cell voltage of 1.1 V was completely regenerated in the electrolyte contained oxygen during ~60 min. Authors did not explained seen phenomena. Authors only concluded that "*At the present stage of our knowledge, we have no evidence to confirm the reaction mechanism. Further studies from various viewpoints are necessary to solve this problem.*" [50]

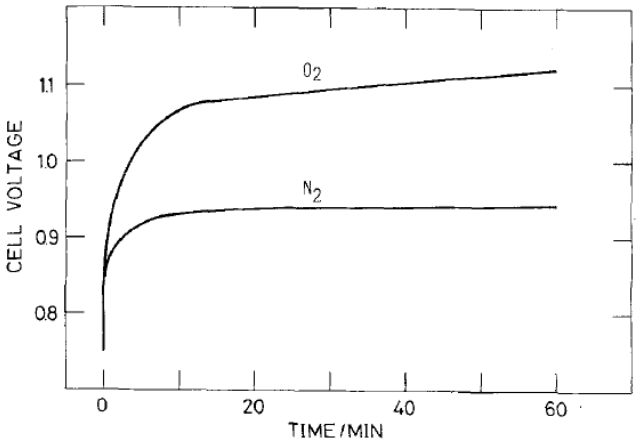

Figure 2.14. Change of open-circuit voltage under nitrogen or oxygen atmosphere after complete discharge of Zn/polyaniline battery [50].

Barsukov et al. [66, 67, 68, 69] investigated the characteristics of mostly polyaniline as the replacement of relatively expensive carbon based oxygen catalysts in metal-air batteries and fuel cells. The Authors investigated the reduction of oxygen on conducting polymers like polyaniline (PANI), polypyrrole (PPy), polythiophen (PTh), and poly(3-methyl)thiophen (PMeT), poly(3,4-ethylenedioxythiophene) (PEDOT) [67], as shown in Fig. 2.15. The electrochemical investigations of conducting polymer based catalytic electrodes in oxygen-saturated electrolytes indicate the existence of electrocatalytic activity toward oxygen reduction at different CPs with the exception of PEDOT. Using the 0.5 M KI solution as an indicator, Authors qualitative proved that H_2O_2 or HO_2^- is formed in the solution after the oxygen reduction reaction.

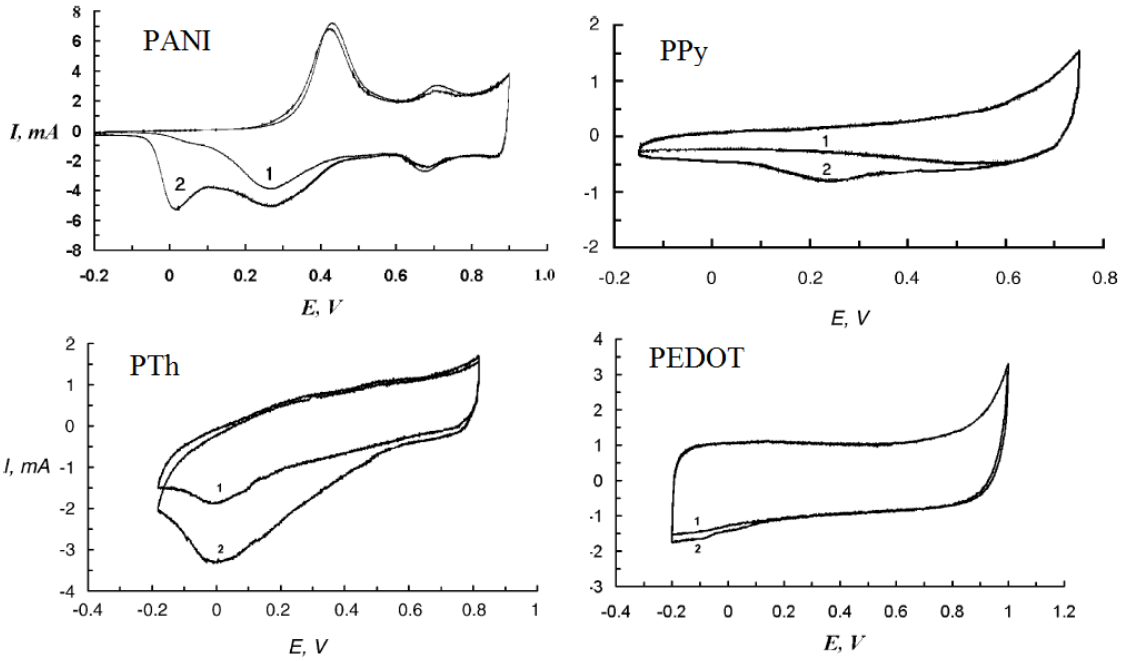

Figure 2.15. Cyclic voltamogramms (2 mV s^{-1}) of a conducting polymers electrode in argon saturated (1) and oxygen-saturated (2) 1M HCl solution. (Adopted from reference [67]).

The Authors also provided the discharge and reoxidation curves for the coin type Zn/polyaniline cell [68], Fig 2.16. They explained the cell capacity of retaining charge after eight hours, by the oxidative transformation of the polyaniline in the form of

leucoemeraldine, which is chemically non-stable in the presence of oxygen, to emeraldine form.

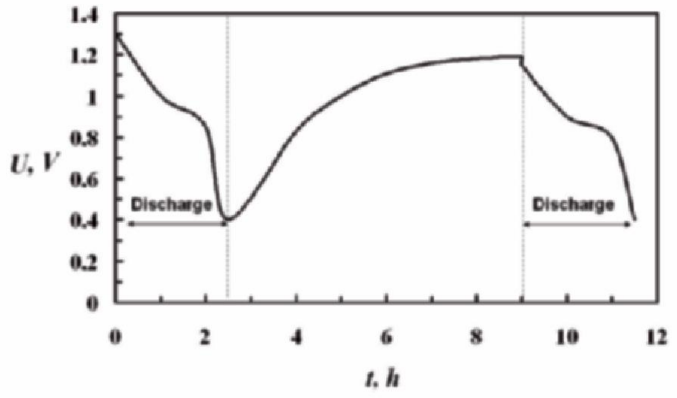

Figure 2.16. The galvanostatic discharge curves and self-charge curve for Zn-Air coin battery with PANI/TEG gas-diffusion electrode [68].

Wu et al. [70] described a similar behavior, measuring the open circuit potentials, Fig 2.17, and short circuit currents, Fig. 2.18, of the zinc–polyaniline and zinc–polypyrrole systems after discharge in oxygen and nitrogen containing electrolyte. They showed that the short-circuit current of these systems can be regenerated by oxygen after discharge. It is worth to mention that zinc-polypyrrole systems shows better characteristics than zinc-polyaniline.

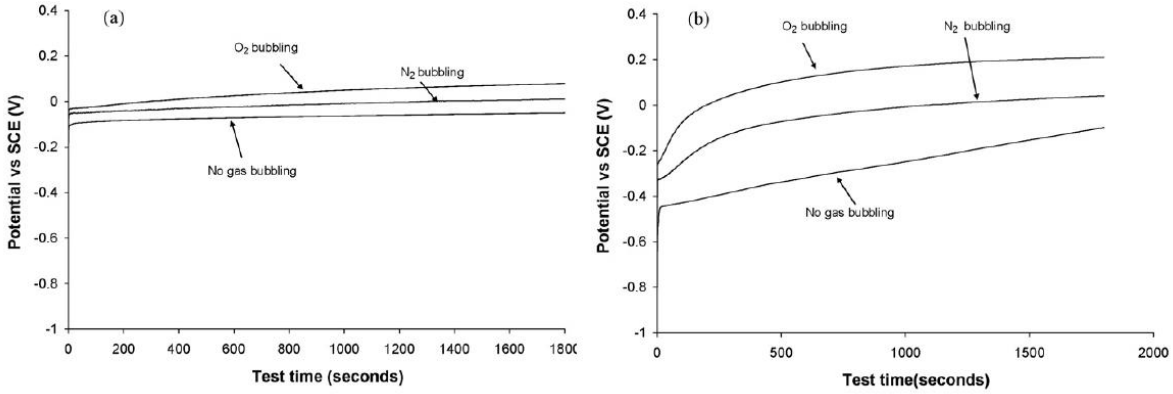

Figure 2.17. Effect of gas bubbling (O_2 or N_2) and no gas bubbling on the potential of (a) reduced polyaniline and (b) reduced polypyrrole in 1.0 M $ZnCl_2$ + 0.5M NH_4Cl [70].

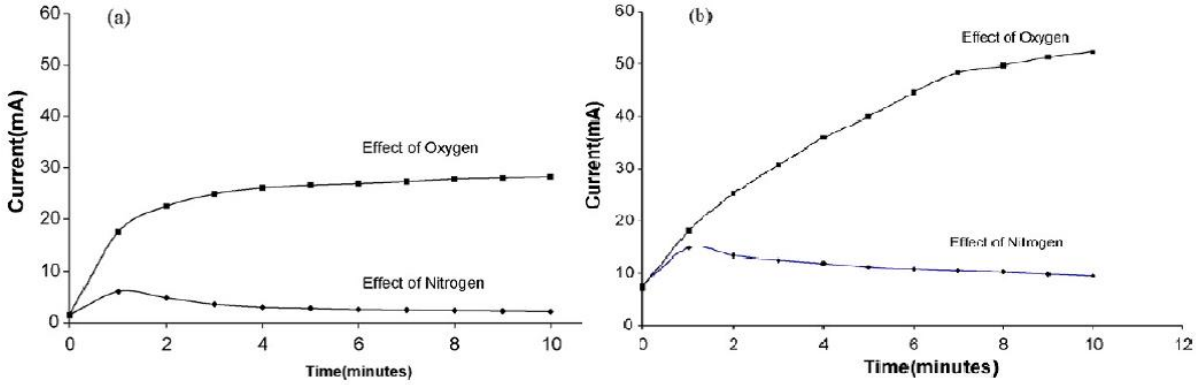

Figure 2.18. Effect of gas (O_2 or N_2) on the short-circuit current in (a) Zn–polyaniline and (b) Zn–polypyrrole battery in 1.0 M $ZnCl_2$ + 0.5M NH_4Cl [70].

The application of bare electroconductive polymers as oxygen reduction catalysts in microbial fuel cells (MFCs), which used electrolytes with neutral pH is also reported [71]. However, conducting polymers in MFC applications are usually combined with other active electrocatalytic materials to improve performance. For example, with respect to carbon black/PPy composite, the peak potential (-0.34 V) has a more positive value than pure carbon black (-0.60 V), as shown in the cyclic voltammetry curves in Fig. 2.19 [72]. Also the onset potential for oxygen reduction is at –0.1 V for carbon black/PPy composite, which is almost 0.5 V more positive than on carbon black.

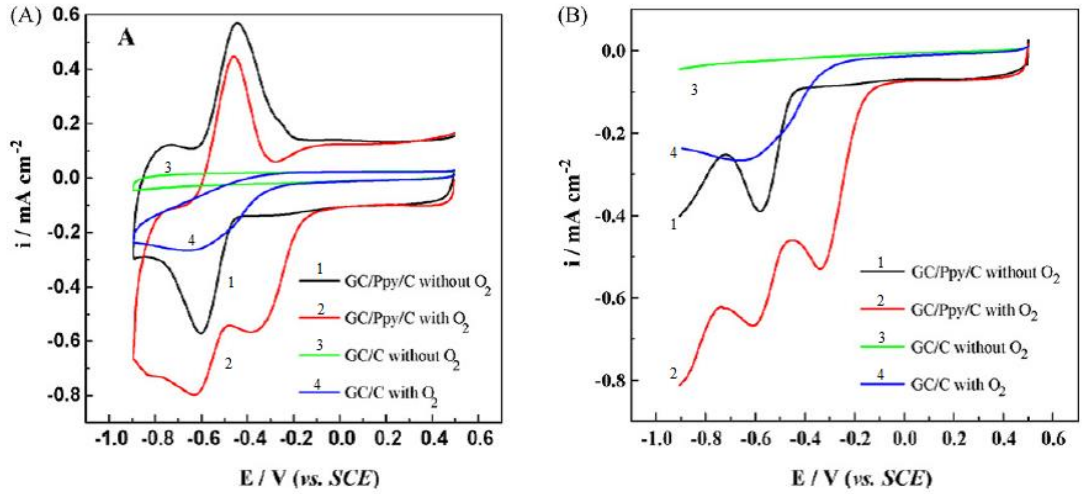

Figure 2.19. CV (A) and LSV (B) of various materials for the oxygen reduction in phosphate buffer solution at pH = 7 [72].

Li et al. [59] investigated polypyrrole as cathode materials for Zn-polymer battery with various biocompatible aqueous electrolytes. Figure 2.20a presents the discharge curves of the Zn/aqueous electrolyte/PPy batteries, which showed very high capacities calculated based on the mass of the polypyrrole. For example, in NaCl the discharge capacity is 5000 mAh g^{-1} of PPy, but the PPy avaiable capacity is only 120 mAh g^{-1} of PPy. In order to understand the reversibility of the Zn/PPy batteries, the cells with SBF as electrolyte are charged and discharged at a current density of 160 μA mg^{-1} for another cycle, Fig. 2.20b. It can be seen that the Zn/PPy batteries delivered a more than double of the charged capacity, suggesting that some other reactions are responsible for high discharge capacities.

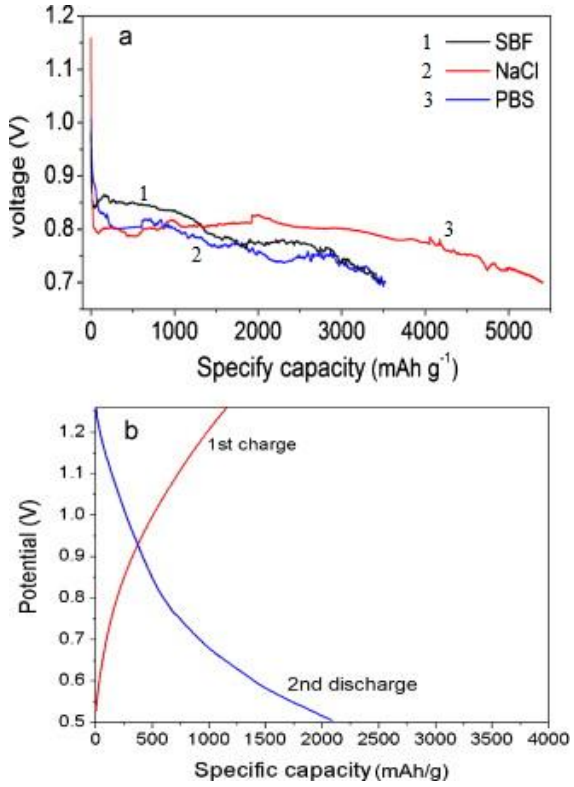

Figure 2.20. (a) Discharge curves of Zn/PPy batteries (40 μA mg^{-1}) with different electrolytes: simulated body fluid (line 1), 0.1 M NaCl (line 2), PBS buffer solution (line 3); (b) the 1st charge and the 2nd discharge curves of Zn/PPy batteries in SBF electrolyte (160 μA mg^{-1}) [59].

Authors concluded that if the mechanism of the battery is simply explained as the redox reactions between the Zn foil and the polypyrrole film, there is definitely not enough polypyrrole to be reduced and thus maintain the long discharge plateaus. This

means that the cathode reaction cannot be simply explained as the reduction of polypyrrole. Authors also concluded "*Not much evidence has ever been provided to investigate the role of polypyrrole in batteries*" [59]

Kong et al. [57] investigated AZ61 magnesium based alloy | PPy cell in different biocompatible aqueous based electrolyte. They used PPy–DS (DS, dextran sulfate as anion dopant) electrode which cyclic voltammograms in different electrolytes are shown in Fig. 2.21.

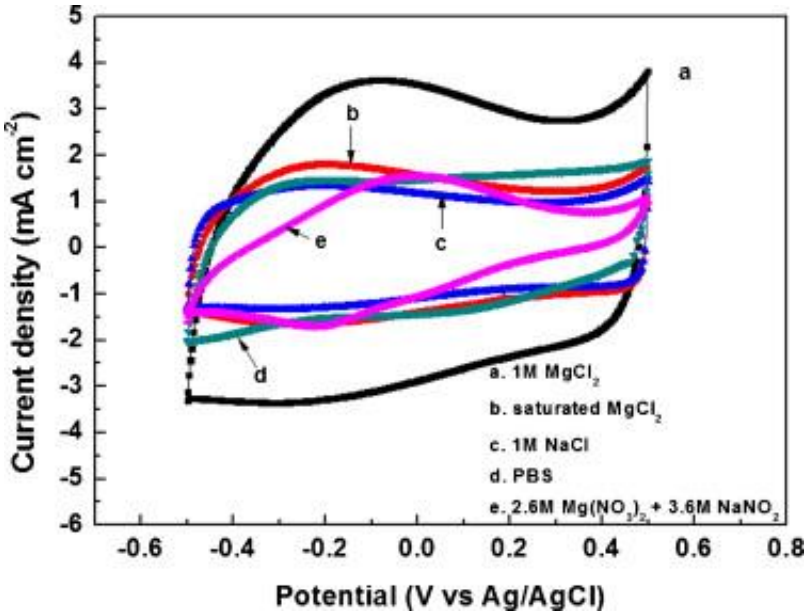

Figure 2.21. Cyclic voltammograms of PPy–DS (dextran sulfate) in different electrolytes at a scan rate of 25 mV s^{-1}. (a) 1.0 M $MgCl_2$; (b) saturated $MgCl_2$; (c) 1 M NaCl; (d) PBS; (e) mixed electrolyte of 2.6 M $Mg(NO_3)_2$ and 2.6 M $NaNO_2$ [57].

In some of the investigated electrolytes, Fig. 2.22, Authors observed and explained remarkably high discharge capacities of the system, with relatively small discharge current density of 30 μA g^{-1}, by the reoxidation of polypyrrole with the dissolved oxygen contained in the electrolyte, retaining its electroactivity. In addition, the discharge voltage of ~1.4 V is observed in 1 M NaCl and PBS, but unfortunately Authors did not explained the possible mechanism of the polypyrrole reoxidation [57].

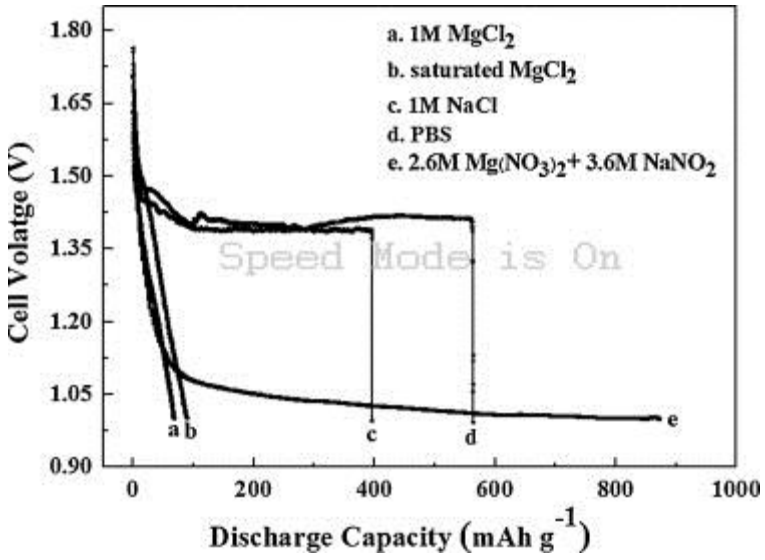

Figure 2.21. The discharge curves of the cell composed of a PPy–DS cathode and AZ61 anode in different electrolytes at the discharge current density of 30 μA g^{-1}. (a) 1 M $MgCl_2$; (b) saturated $MgCl_2$; (c) 1 M NaCl; (d) PBS and (e) mixed electrolyte of $Mg(NO_3)_2$ (2.6 M) and $NaNO_2$ (3.6 M) [57].

Jia et al. [73] investigated biodegradable Mg–Air batteries composed of silk fibroin (SF) – polypyrrole film in PBS based electrolyte. The cathode materials shows activity toward oxygen reduction reaction as can be seen in Fig. 2.22a, and ability to be reoxidated after discharge, Fig. 2.22b.

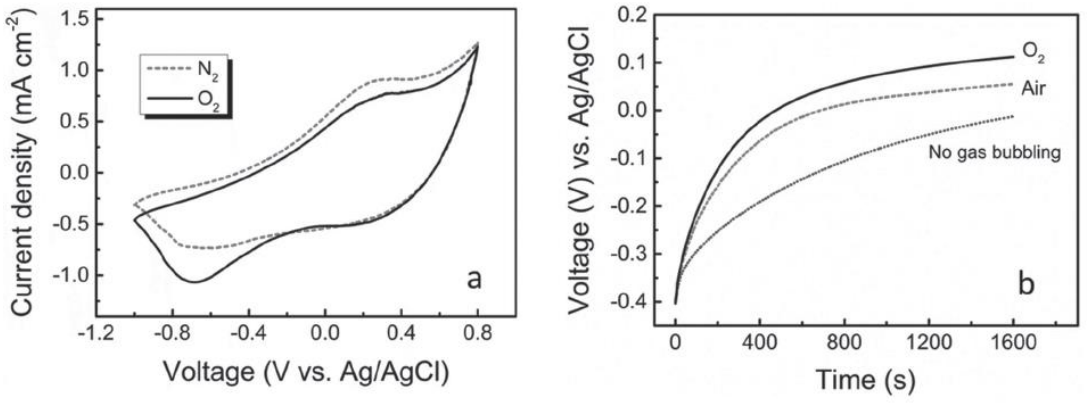

Figure 2.22. a) CV of SF-PPy film in N_2 - or O_2 -saturated PBS electrolyte at a scan rate of 5 mV s −1 . b) Potential response of reduced SF-PPy film in PBS electrolyte with N_2, O_2 or no gas bubbling after the applied potential (−0.85 V vs Ag/AgCl) is switched off [73].

For the very small discharge current densities in the range of 5 to 50 μA cm^{-2}, Fig. 2.23a-b, the authors observed plateau during discharge of the battery, above 1 V.

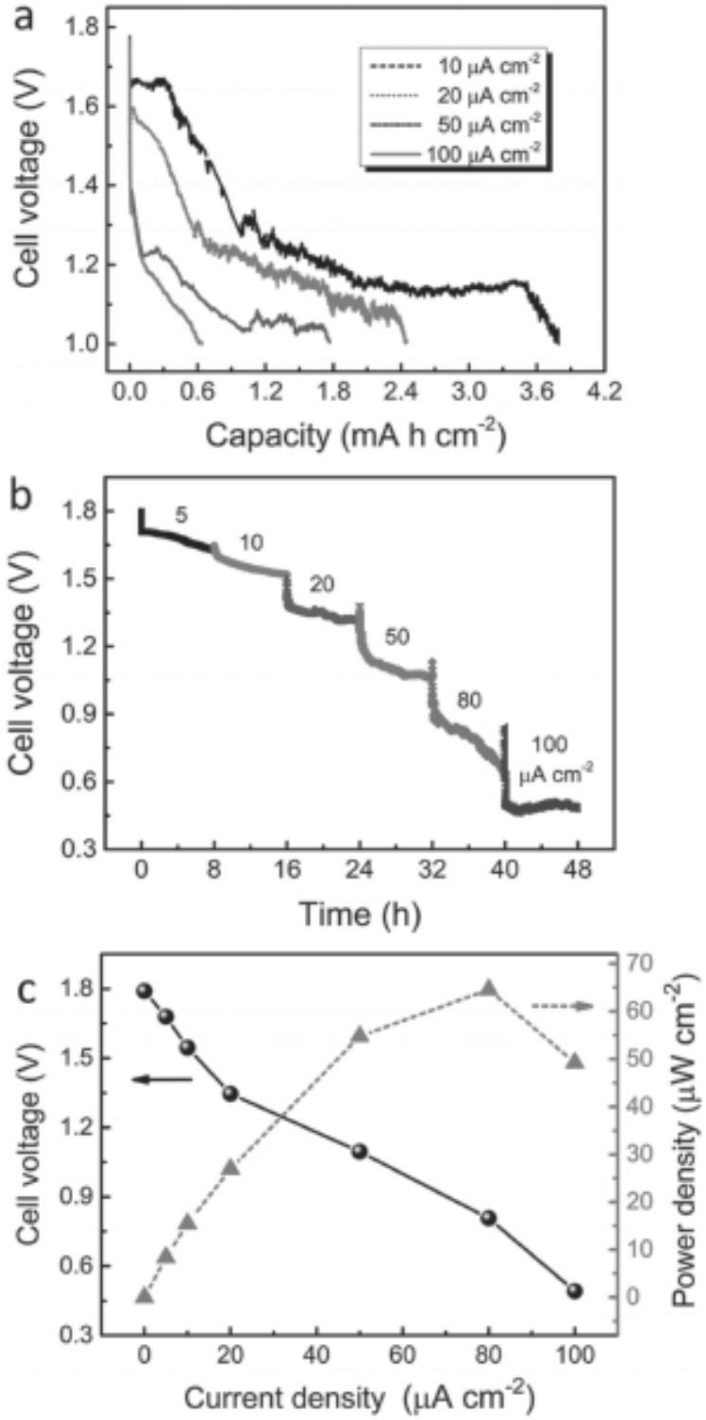

Figure 2.23. a) Galvanostatically discharge curves, b) rate capabilities, c) plateau voltage and the corresponding power density of Mg-air biobatteries composed of SF-PPy film at various current densities in PBS electrolyte at room temperature [73].

Grgur [19] investigated discharge and recharge characteristics of the battery based on the electrochemically synthesized polypyrrole cathode and aluminum, zinc and magnesium anode in 2 M NH_4Cl, which discharge curves are shown in Fig. 2.24. Author showed that the capacity of the polypyrrole electrode could be regenerated after discharge by the reoxidation with dissolved oxygen from the air. Such behavior is explained by the complex interaction of polypyrrole and hydrogen peroxide produced during the oxygen reduction reaction. Reoxidation, inset a in Fig 2.24, which occurred mainly above –0.3 V (SCE) is described to be similar as in the corrosion processes by the oxygen reduction occurred as a cathodic reaction, and polypyrrole doping with chloride anions occurred as the anodic reaction. The discharge potentials of the PPy electrode above –0.5 V at current density could not be explained simply by the oxygen reduction reaction, for which the potential is –1 V at current density of 0.1 mA cm^{-2}, inset b) in Fig. 2.24.

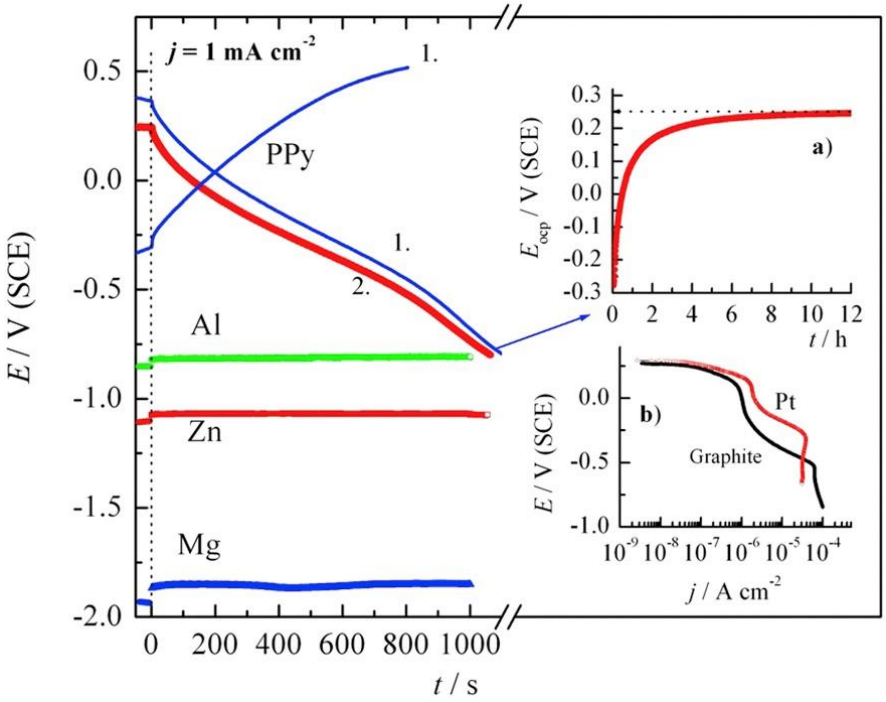

Figure 2.24. Galvanostatic charge–discharge curves (1), discharge curves after reoxidation (2) of the PPy, and anodic curves of the aluminum, zinc, and magnesium electrodes in the 2 M NH_4Cl at current density of 1 mA cm^{-2}. Insets: a) Dependence of the open-circuit potential of PPy electrode over time after discharge; b) Cathodic polarization curves (v =1 mV s^{-1}) of graphite and platinum electrode in the same solution [19].

The cell voltages of the investigated systems, Fig. 2.25, after reoxidation of the discharged polypyrrole, are above 1 V for the Mg|PPy and among 1.2 to 0.6 for Zn|PPy and Al|PPy. The high corrosion rate of Mg anode is also observed. It is also shown that all three investigated systems possess superior characteristics in comparisons with pure graphite-zinc system [19].

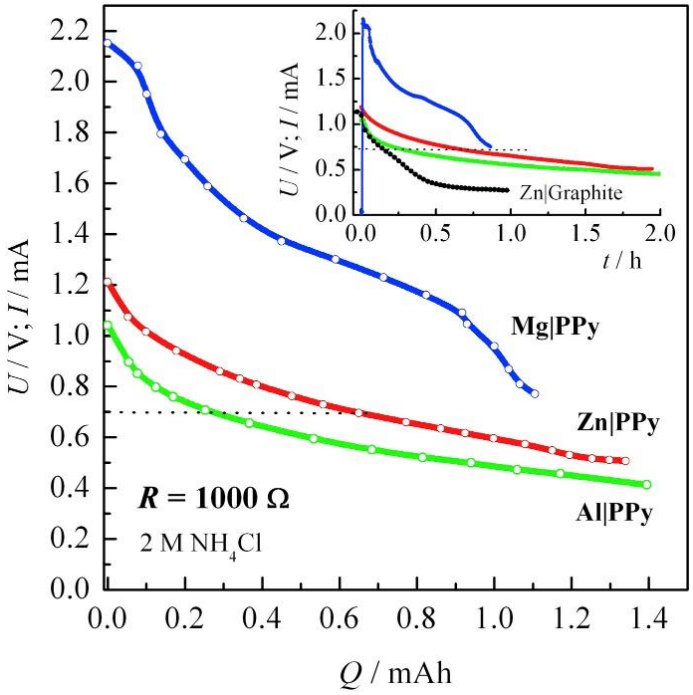

Figure 2.25. Discharge characteristics at a constant load of 1000 Ω, of the metal | polypyrrole recharged cells [19].

2.2.2. Spectroscopic evidence of the interactions of polypyrrole with oxygen

In contrast with other conducting polymers, pristine neutral polypyrrole can be easily oxidized, due to its relatively low redox potential [74]. Oxygen is usual the most common oxidizing agent, present in typical polypyrrole applications. Even though oxidized polypyrrole is relatively stable, the neutral polymer is readily oxidized by oxygen present either in the air or in aqueous electrolytes [75,76,77,78,79,80,81]. The mechanism of the polypyrrole interactions with oxygen is rather complex, depending on

time, oxygen pressure and presence of the water. In such a case polypyrrole properties change, confirming transition from the typical states for neutral polymer to that of doped polypyrrole, accompanied by doping and weight increase [77]. Some signs point to multistep process; for example, the conductivity of the neutral pristine polypyrrole quickly growths in the initial stages of oxidation, while optical changes are observed later [77]. The open circuit potential, after discharge, increase for neutral polypyrrole in aqueous solutions, Fig. 2.26., suggesting the polymer oxidation [79,82]. It is also observed that thinner polypyrrole film (synthetized with 30 mC) undergoes faster reoxidation than thicker one (synthetized with 150 mC).

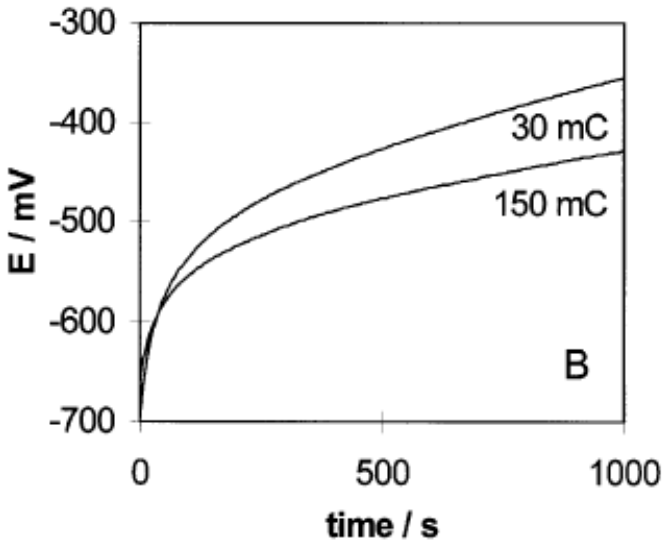

Figure. 2.26. The dependence of the polypyrrole open circuit potential over time after prepolarization at –0.8 V in 1 M KCl solution [82].

Some Authors observed changes in UV-vis, FTIR [80,83,84,85,86] and electron spin resonance (ESR) spectra [77,87,88,89] during the interaction of oxygen with polypyrrole. Figure 2.27 shows that in the UV-visible spectra of the neutral polypyrrole, reduced at –0.9 V, after short contact with aqueous solution containing oxygen, absorption at 460 nm (connected to polarons) and at 800 nm (connected to bipolarons) increases, while absorption at 420 nm ($\pi - \pi^*$ transition), typical for the neutral polymer, decreases [83]. Besides, for longer times, absorption at 560 nm starts to decrease, indicating decreasing contents of polarons, and that at 800 nm increases as a result of bipolaron presence.

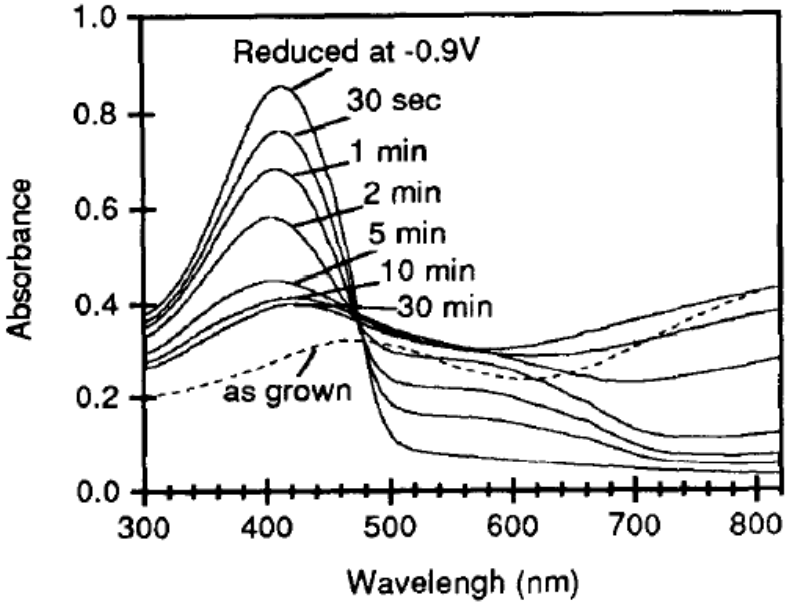

Figure 2.27. UV-visible spectra of the fully reduced PPy with time in wet state without applied potential [83].

The obvious connections with UV-visible spectra changes, can be seen in comparisons with open circuit potentials increase, Fig. 2.28 during the interaction of the polypyrrole with oxygen [82,83]

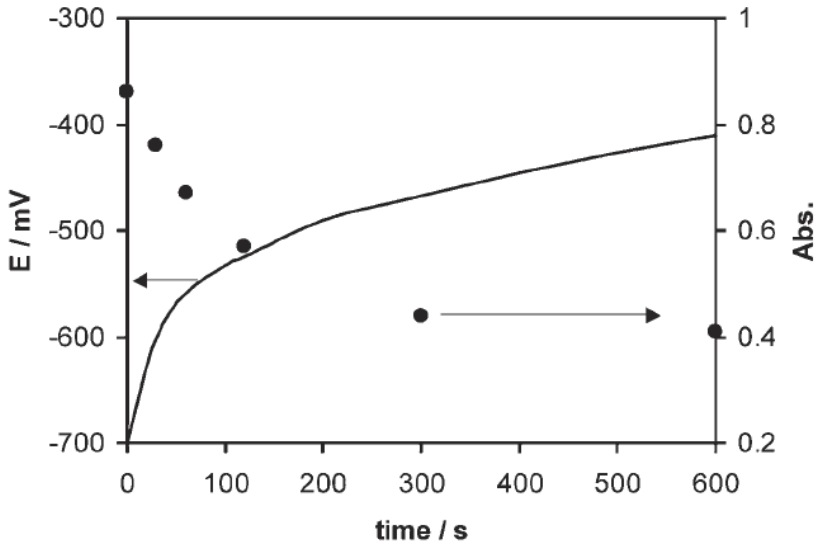

Figure 2.28. Changes of the open circuit potential (line) [82] and UV-visible absorption peak at 420 nm [83] (points) of neutral polypyrrole in the presence of oxygen.

The oxidation process of the polypyrrole can be also followed using FTIR spectroscopy, as can be seen in Fig 2.29 [80,85]. In the presence of oxygen, the spectra typical for neutral polymer gradually transforms to that characteristic of oxidized polypyrrole, with increase of signal at 4000 cm^{-1}. Additionally bipolaron bands appear in the range of 1000 cm^{-1}

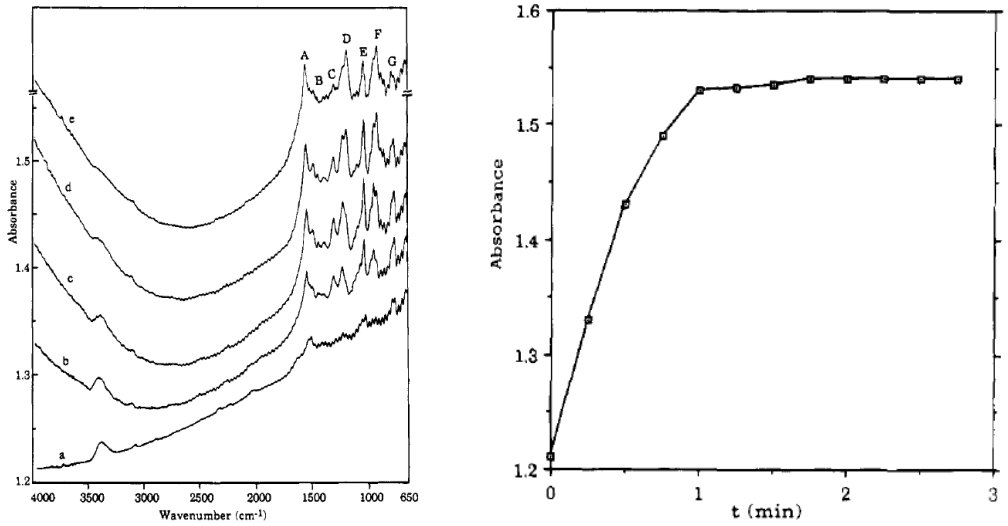

Figure 2.29. Left: FTIR spectra for a pristine polypyrrole film after various times of exposure to 1 atm of O_2. Exposure times: (a) 0 s, (b) 15 s, (c) 30 s, (d) 60 s, (e) 30 min [80]. Right: FTIR absorbance at 4000 cm^{-1} as a function of time after admitting 1 atm of O_2 to the cell [80].

2.2.3. Mechanism of the interactions of the polypyrrole with the oxygen

The possible mechanism of the polypyrrole interaction with oxygen is investigated in a lower extent, even the evidence of reoxidation are clear.

Combination of different techniques gives opportunity to elucidate the mechanism of oxygen–polypyrrole interactions. ESR (electron spin resonance) spectroscopy enabled visualization of polaron formation and their decay upon transformation to bipolarons, as shown by the signal increase and decrease, respectively. Kanemoto et al. [90] based on ESR results, Fig. 2.30, suggested that the first step of polypyrrole – oxygen interaction is

oxygen reversible adsorption both on the polymer surface and inside the film. Accordingly, broadening of the ESR signal with time and rising oxygen pressure in air is observed. After reaching the maximal value, after prolonged time, the ESR signal width gradually decreases probably because of the oxygen replacement by other molecules, e.g., water if available.

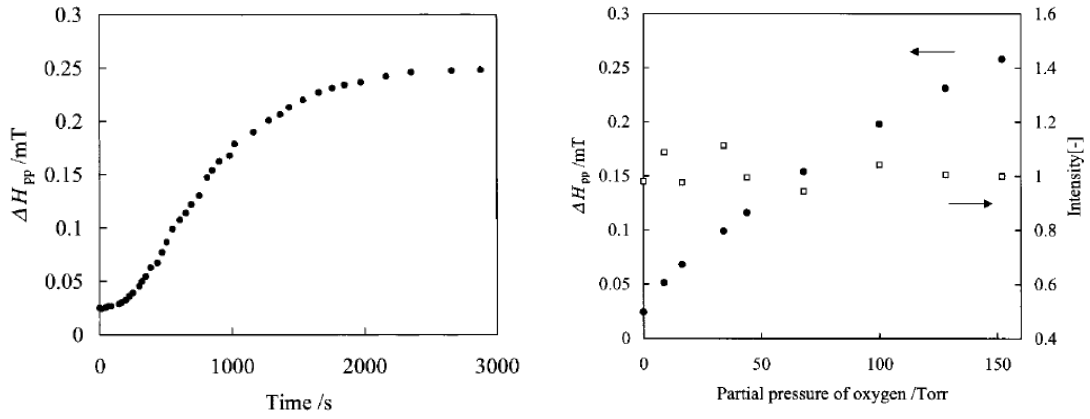

Figure 2.30. Left: Initial time variation of ESR line width when the PPy sample under vacuum was open to the atmosphere (a152 Torr of oxygen). Right: Oxygen pressure dependences of ESR line width (filled circles) and ESR intensity (open square). ESR intensities are normalized at 152 Torr [90].

Based on FTIR and XPS analysis, Lei and Martin [80] postulated existence of two forms of oxygen interacting with pristine polypyrrole. The first oxygen form are O_2^- anions (present only in anhydrous media) because of charge transfer between the polymer and oxygen molecule. The O_2^- anions play a role as a dopant [80]:

$$x\mathrm{O}_2 + -(\mathrm{Py})_n- \rightarrow -[\mathrm{Py}_{n-x}-(\mathrm{Py}^+\mathrm{O}_2^-)_x]-$$

where Py represents the neutral (unoxidized) pyrrole unit in the polymer chain, Py^+ is the oxidized unit. Nevertheless, the obtained doping degree is lower than for a fully doped polymer as the conductivity is ca. 2 orders of magnitude lower than for a typicaly electrochemical doped polypyrrole. The low doping degree is also confirmed by significantly lower absorbance in the free-carrier region of the FTIR spectra. The second form of oxygen, being in major excess compared to O_2^-, are molecular association

complexes between O_2 and polypyrrole. In a relatively short time scale (30 minutes), exposure of polypyrrole to oxygen does not result in formation of carbonyl or hydroxyl groups in the polymer, which are characteristic for irreversible degradation of the material. However, after longer exposure (hours) the superoxide anions participate in irreversible process of deprotonation of the pyrrole nitrogen atom, yielding an imine derivative of polypyrrole [77,80]. On the other hand, the ring oxidation can result in appearance of C-O and C=O groups [91].

Khomenko et al. [69] based on the electrochemical and DFT (density functional theory) calculations proposed the mechanism of the electrocatalytic oxygen reduction in acidic media at the surface of PPy/C and PANI/C. The mechanism is explained by the formation of a bridge-type adsorption complex, as shown in Fig. 2.31.

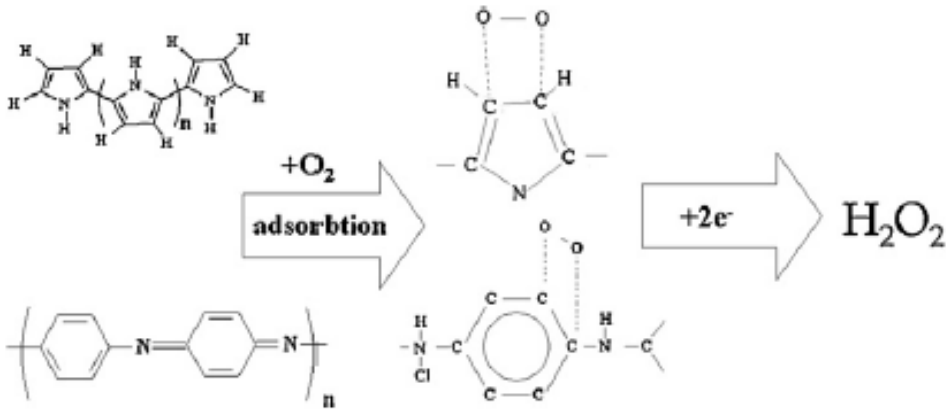

Figure 2.31. Proposed mechanism of the oxygen reduction reaction of polypyrrole and polyaniline via formation of a bridge-type adsorption complex [69].

In according to this scheme, the molecules of oxygen dissolved in the electrolyte chemisorb on the surface of conducting polymers. After absorption, noticeable weakening and extension of the bonds between oxygen atoms take place up to breaking of the double bonds. The interaction between the oxygen activated in this way and hydroxonium ions in acidic solution becomes easier and results in the formation of hydrogen peroxide. Thus, the 2-electron mechanism of ORR on the films of PANI and PPy catalysts, which proceeds via the formation of bridge-type adsorption complexes on the ECP surface, is possible.

Wu et al. [70], proposed that simultaneously with oxygen reduction in acidic media, anion insertion (doping) into the polypyrrole chain occurred, as schematically shown in Fig. 2.32. This scheme is similar to the corrosion processes where oxygen is reduced and base material (polypyrrole) is oxidized.

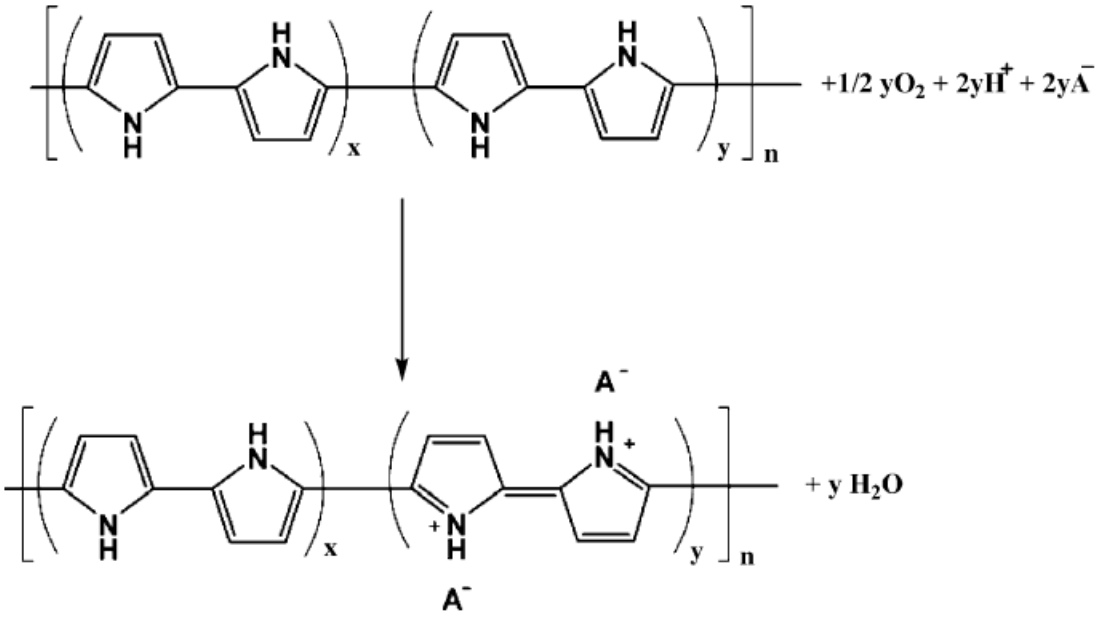

Figure 2.32. Schematic presentation of the simultaneous oxygen reduction and anion insertion onto polypyrrole [70].

The question of polypyrrole active centers on the oxygen reduction reaction is disputable. Among proposed bridge-type adsorption complexes mechanism proprosed by Khomenko et al. [69], it is also possible that active centers could be quinone-like species, which was always produced during electrochemical and chemical polypyrrole synthesis [92] as proposed by Grgur [19]. Similarly like in the (anthra)quinone processes of the hydrogen peroxide production [93, 94], quinone-like moieties could be involved in the oxygen reduction reaction. In this mechanism Fig. 2.33, during discharge (dedoping) of the polypyrrole simultaneously on the quinone-like moieties hydrogen peroxide is formed, which is able to chemically oxidize dedoped parts of the polypyrrole chains.

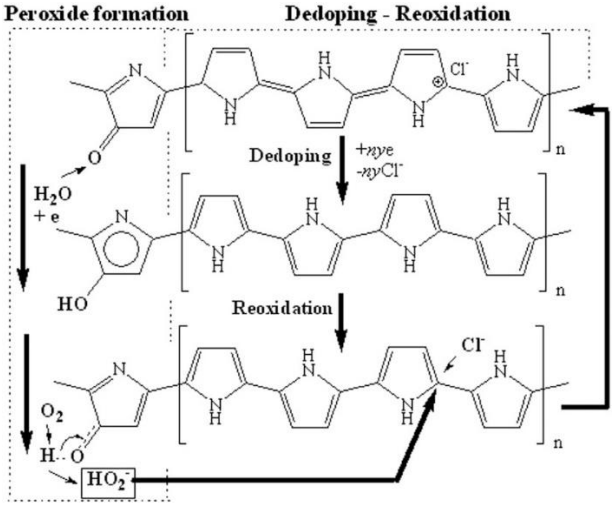

Figure 2.32. Schematic presentation of proposed polypyrrole discharge and reoxidation charge mechanism [19].

2.3. Synthesis and characterization of the polypyrrole

2.3.1. Electrochemical synthesis of the polypyrrole

Besides polyaniline, polypyrrole is certainly one of the most extensively investigated conducting polymer, which possess reoxidation characteristics. Both electrical conductivity and chemical stability of polypyrrole originate from heteroatomic and extended π conjugated backbone structure. This structure is not sufficient for conductivity on its own. However, conductivity achieved by doping largely exceeds those of other electroconducting polymers, which is a good prerequisite for practical application [95]. Unlike polymerization of aniline, polymerization of pyrrole can be successfully performed in neutral aqueous environment and variety of organic solvents [96].

Polypyrrole can be synthetized chemically using an oxidizing agents (for example ammonium persulfate) or electrochemically [97,98]. Pyrrole, similarly to aniline, is easily electrochemically polymerized in both aqueous and organic based electrolytes containing pyrrole on inert anodes, including graphite, gold or platinum. Electrochemical synthesis can be made potetiodynammially (using cyclic voltammetry, CV), galvanostatically (under constant current, GS), and potentiostatically (at constant potential, PS) techniques, as shown in Fig. 2.33 [99].

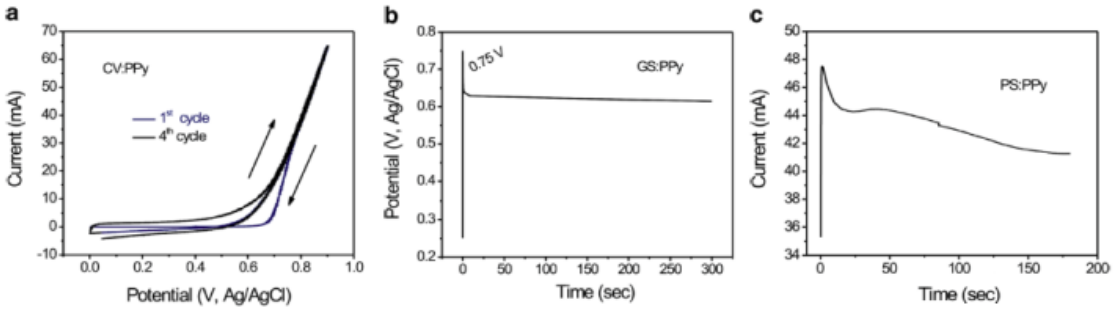

Figure 2.33. Synthesis of polypyrrole thin films by different electrodeposition modes: a) cyclic voltammetry (CV) mode by scanning between 0 and + 0.9 V for 12 cycles; b) galvanostatic (GS) mode at 10 mA cm^{-2} for 5 min; and c) potentiostatic (PS) mode at 0.8 V (vs Ag/AgCl) for 3 min. 0.1 mol dm^{-3} of distilled pyrrole and 0.5 mol dm^{-3} of H_2SO_4 [99].

Due simplicity and mass control, just by measuring the passed charge, galvanosatatic method is preferable for polypyrrole synthesis. Figure 2.34 shows galvanostatic polymerization of pyrrole from aqueous electrolyte together with cyclic voltammogram obtained after galvanostatic synthesis in the same electrolyte in order to show characteristic doping/dedoping processes, inset in Fig. 2.34) [97].

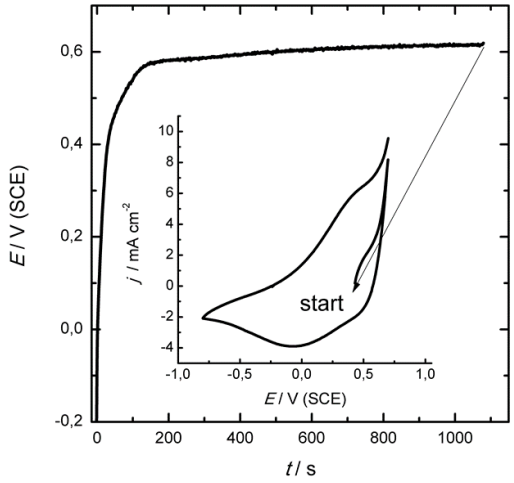

Figure 2.34. Galvanostatic curve of the electrochemical polymerization of pyrrole at graphite electrode (j = 2 mA cm^{-2}) from 0.1 mol dm^{-3} HCl and 0.2 mol dm^{-3} pyrrole. Insert: Cyclic voltammogram (v = 20 mV s^{-1}) recorded after 1100 s of galvanostatic synthesis of polypyrrole from the same electrolyte [97].

From Fig. 2.34 can be seen that chronoamperometric curve is characterized, by fast increase of the potential during which the electrode is covered with a layer of polypyrrole. The succeeding plateau of the potential refers to further polymerization on already formed polymer. It can be noticed that after galvanostatic synthesis polypyrrole is almost completely in its doped state which is reflected in rapid increase of the potential during cyclic voltammetry. The cathodic part of the voltammogram is characterized by wide peak attributed to dedoping of ions from polypyrrole, after which anodic part of the voltammogram refers to doping. [100].

2.3.2. The mechanism of the electrochemical polymerization of pyrrole

According to generally accepted mechanism of electrochemical polymerization of pyrrole, the first step refers to formation of the primary radical cation as proposed by Diaz [101], as shown in Fig. 2.35 [102].

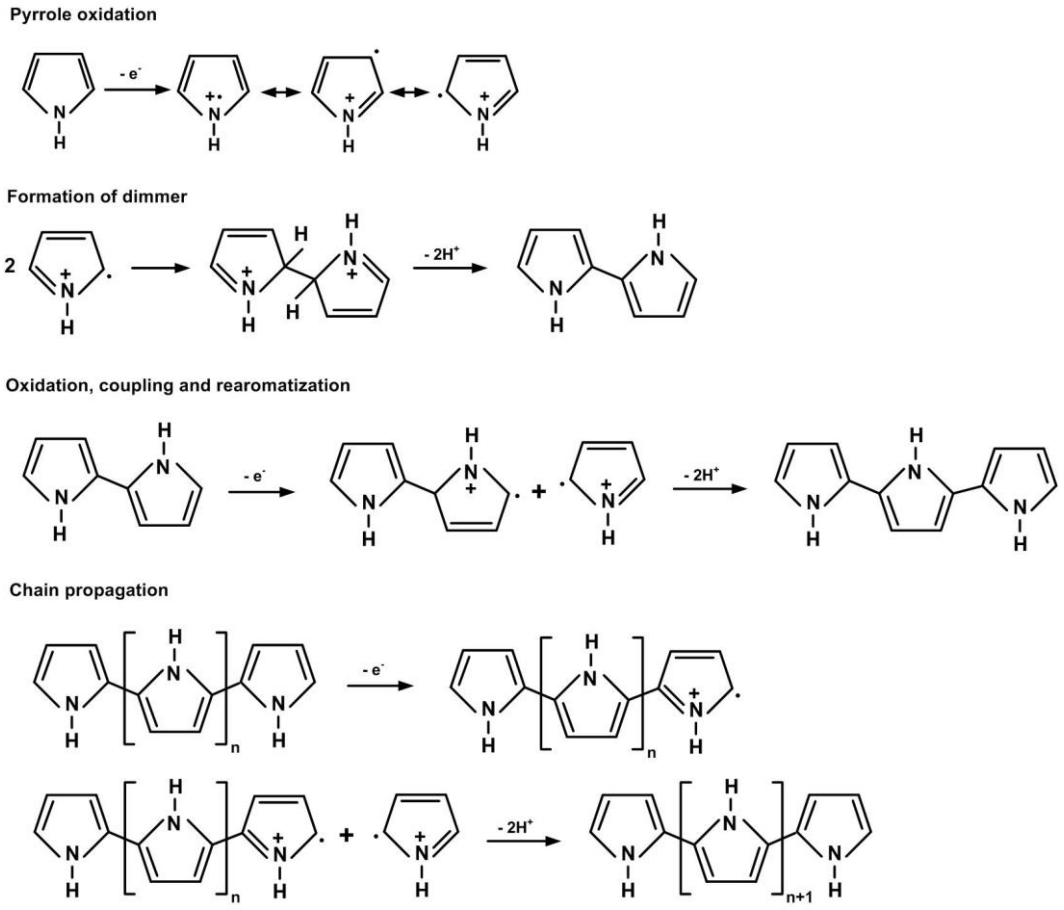

Figure 2.35. Proposed mechanism for pyrrole electropolymerization by Diaz et al. [101].

Unpaired electron and positive charge are delocalized and quantum mechanical calculations reveals that electron spin density is the greatest at *o* – positions, therefore they are the most reactive so radical coupling takes place in these positions [103]. By coupling of two primary radical cations, positively charged dimer is formed. Because two protons of the positively charged dimer distort the conjugation, rearomatization is likely to occur through deprotonation leading to formation of energetically favorable neutral dimer [104]. According to alternative, but not accepted mechanism, radical cation can react with neutral pyrrole molecules leading to formation of a new radical cation [104]. Neutral dimer is, in further step, oxidized at anode giving new radical cation. As expected, oxidation of the dimer is easier comparing to neutral pyrrole, therefore occurring at the lower potential. In the forthcoming steps coupling of dimer radical cations (lately, oligomer radical cations) and primary radical cations occur, followed by a release of protons and rearomatization. Oxidation, coupling and rearomatization are repeated leading to formation of polypyrrole. Although the electron spin density is the largest at *o* – position, by development of the conjugation length, spin density is spreading over conjugating system, so the radicals might be coupled in other positions, resulting in disturbing of the linearity and branching [104]

2.3.3. Molecular structure of the polypyrrole

The molecular structures of protonated polypyrrole (polypyrrole salt) proposed in the literature to a certain degree vary [105], but there is agreement about the structure of the polypyrrole base (undoped state) obtained after deprotonation, which is composed of both the oxidized and reduced pyrrole constitutional units, Fig. 2.36. The localization of positive charges on polymer chain, as well as the presence of unpaired spins, polarons, detected by electron paramagnetic resonance, is still open to discussion.

The rearrangement of electrons within polypyrrole chain that lead to the formation of charge carriers was proposed by Stejskal et al. [105] (Fig. 2.37). The rearrangement of the electrons in polypyrrole salt may generate bipolarons and finally polarons by delocalization over the polymer chain, as shown in Fig. 2.37. Polarons act as charge carriers.

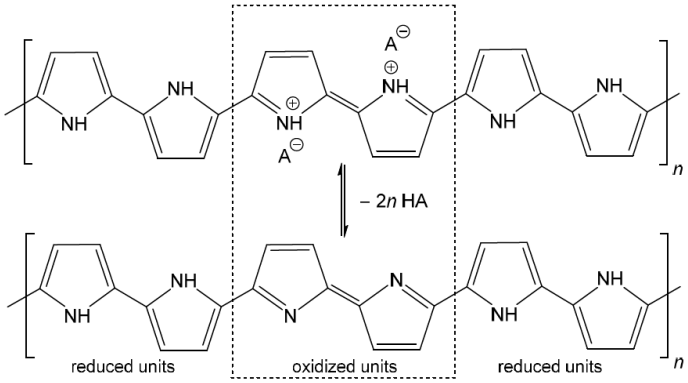

Figure 2.36. Conducting polypyrrole salt converts to non-conducting polypyrrole base under alkaline conditions. HA is an arbitrary acid, A^- a corresponding counter-ion [105].

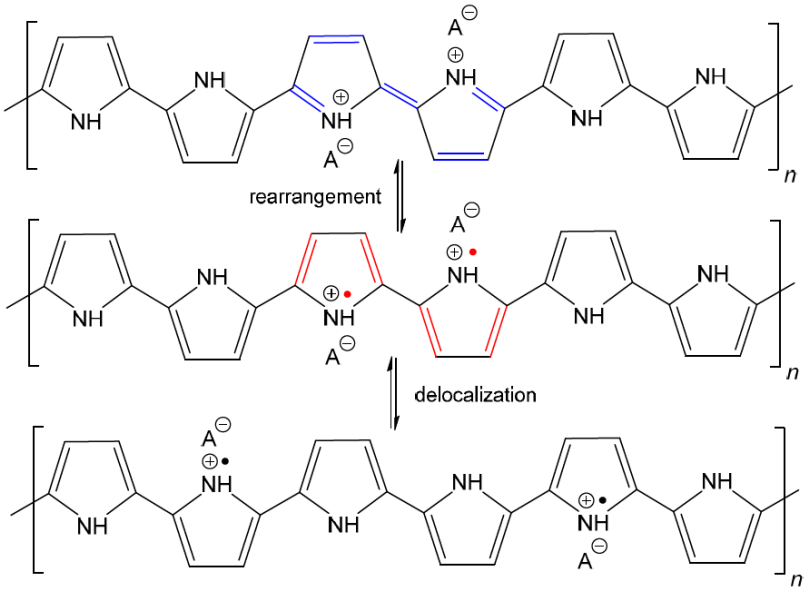

Figure 2.37. The rearrangement of electrons in polypyrrole salt [105].

In the literature, there is no agreement about the structure of the polypyrrole in a doped states. [105]. The anodic oxidation, which results in the formation of conducting polymer, has the stoichiometry of $(2+y)F$ per mole of monomer [96]. Of those, only $2F$ mol^{-1} is related to the polymerization, and extra charge yF is linked, to the oxidation (doping) of the polymer film with chloride anions. In the literature y or doping degree, vary between 0.2 to 0.6. Doping degree represents the number of inserted anions in the

polymer unit. Therefore, *y* equal to 0.2 means that one anions is inserted within five monomer units, *y* equal to 0.25 means that one anions is inserted within four monomer units and *y* equal to 0.33 means that one anions is inserted within three monomer units as schematically presented in Fig. 2.38. In all three structure double bond conjugations, responsible for the conductivity exists.

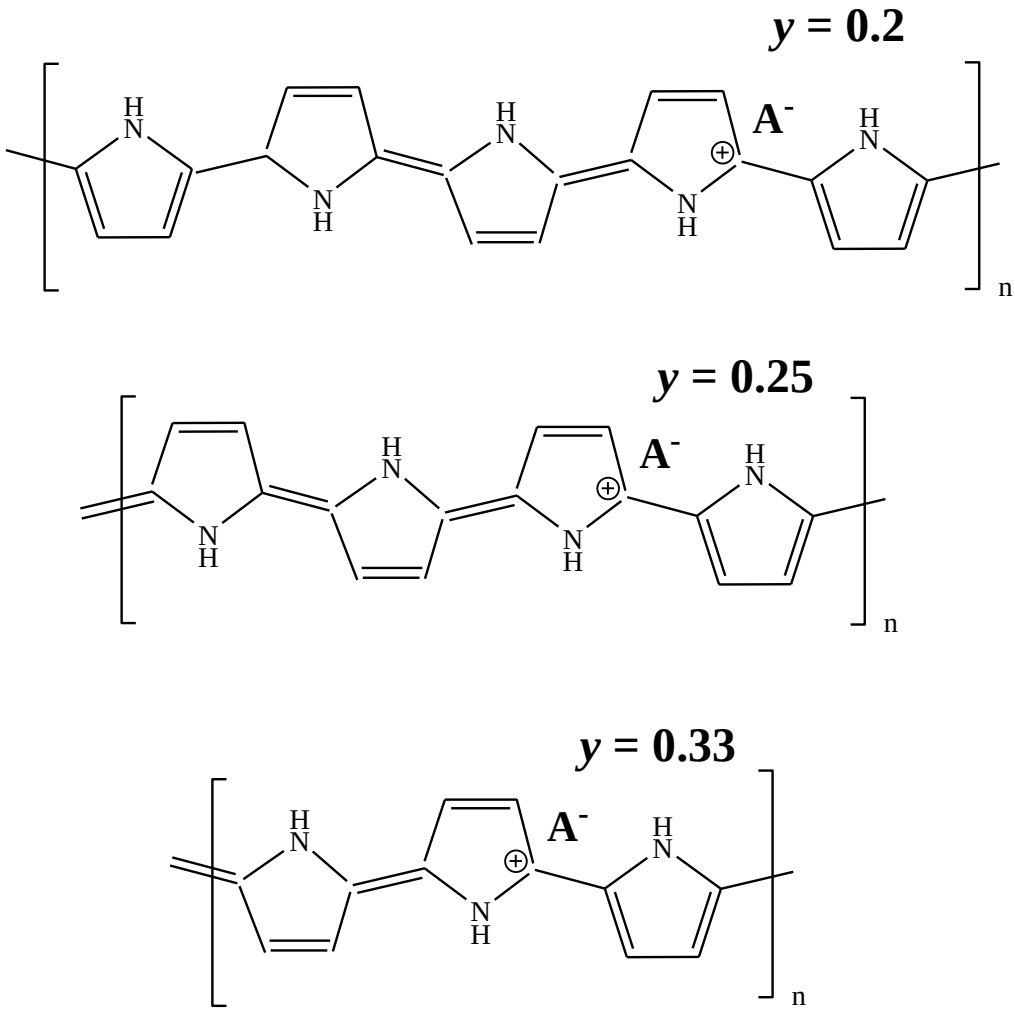

Figure 2.38. Theoretical structures of the polypyrrole with different doping degrees, *y*.

2.3.3. Morphological structure of the polypyrrole

Usually, polypyrrole can be electrochemically obtained by galvanostatic, potentiodinamic, and potentiostatic techniques. Liu and Oliviera [106], investigated galvanostatic, Fig. 2.39 and the potentiodynamic, Fig. 2.40 electrodepozition of the polypyrrole.

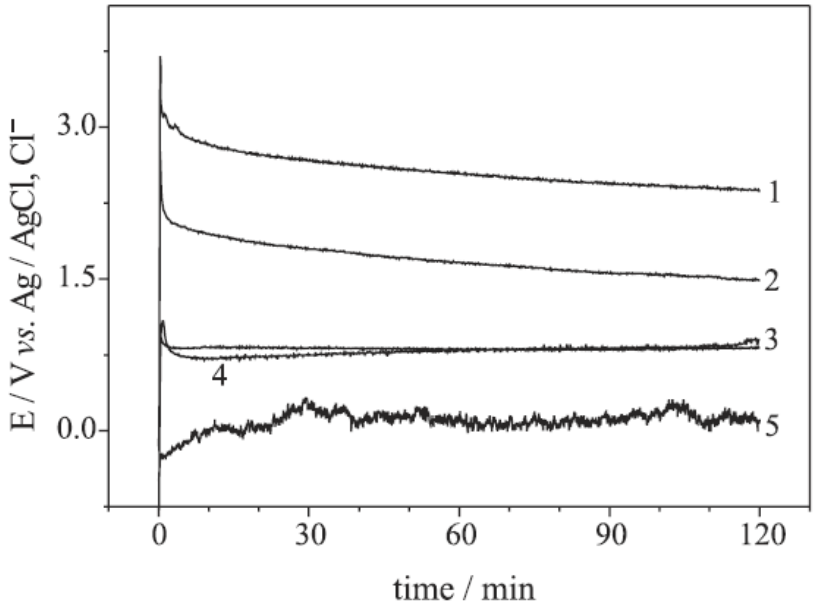

Figure 2.39. Potential transients for electropolymerization of pyrrole on aluminum electrode from 0.2 mol L^{-1} tartaric acid + 0.5 mol L^{-1} pyrrole, pH 1.7. The applied current densities (mA cm^{-2}) were: (1) 10; (2) 5; (3) 2.5; (4) 1.0 and (5) 0.5 [106].

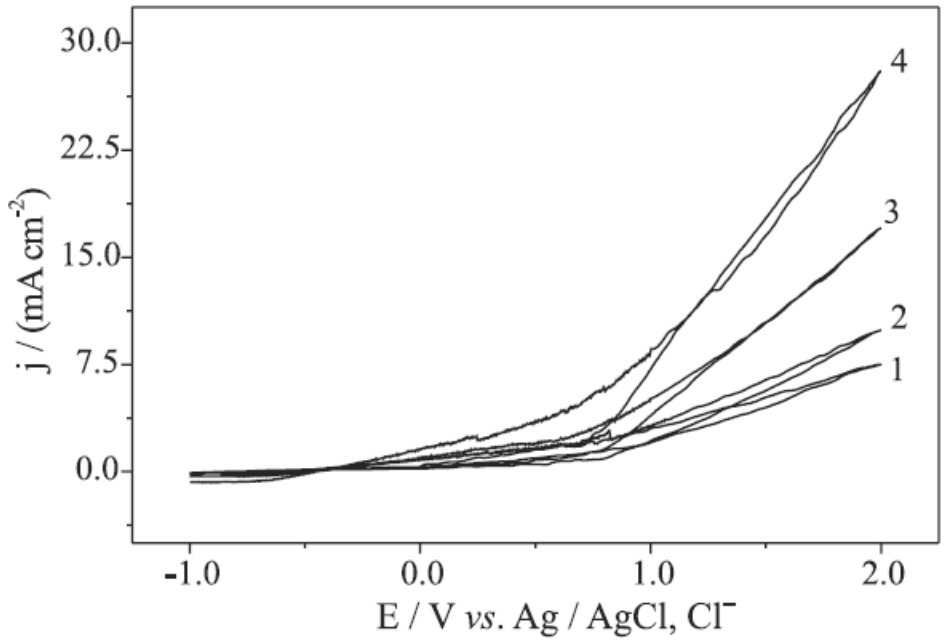

Figure 2.40. Voltammetric profiles (first cycle), for the electrodeposition of PPy from 0.5 mol L^{-1} pyrrole aqueous solutions and tartaric acid concentrations of: (4) 0.8 mol L^{-1}, (3) 0.4 mol L^{-1}, (2) 0.2 mol L^{-1} and (1) 0.1 mol L^{-1}. Sweep rate 5 mV s^{-1} [106].

From SEM images, shown in Figs. 2.41a-c, it can be seen that films formed potentiodynamicallycally are much less uniform than films formed galvanostatically. Films formed galvanostatically are more homogeneous presenting a cauliflower-like structure constituted by micro-spherical grains.

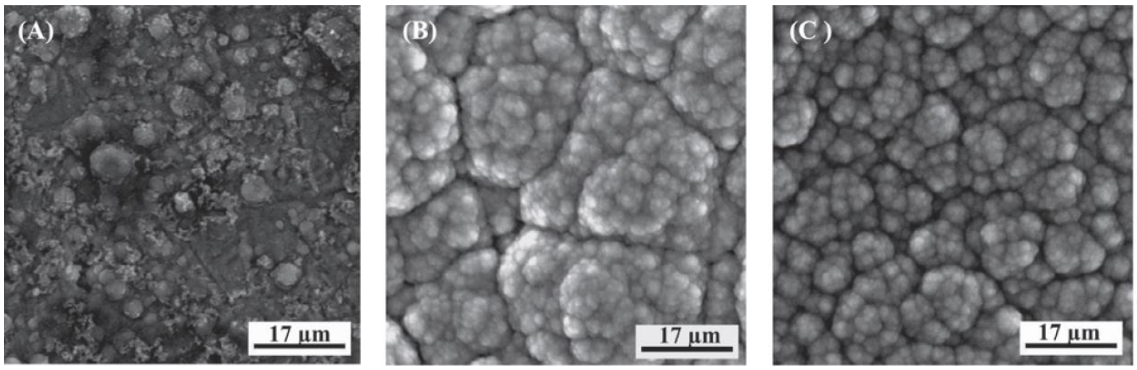

Figure 2.41. SEM of aluminum surfaces coated with PPy films electrodeposited from solutions containing 0.2 mol L^{-1} tartaric acid + 0.5 mol L^{-1} pyrrole: (A) potentiodynamically at 5 mV s^{-1}; galvanostatically at (B) 2.5 and (C) 10 mA cm^{-2}. [106]

Because, the galvanostatic method is more favorable for the practical applications, Liu et al. also investigated the influence of current density on electrodeposition of polypyrrole films on aluminum surfaces from a p-toluene sulfonic acid medium [107], and the results are shown in Fig. 2.42. With increased current density, the electrodeposition potentials increased as well.

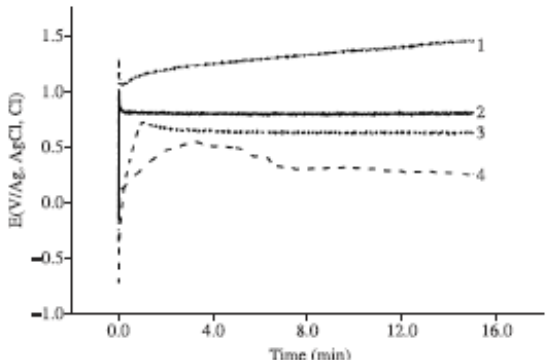

Figure 2.42. Potential-time curves for PPy electrodeposition from 0.2 mol.L^{-1} p-toluene sulfonic acid + 0.5 mol L^{-1} pyrrole. The applied current densities (mA cm^{-2}) were: 1) 10.0; 2) 5.0; 3) 2.5 and 4) 0.5 mA.cm^{-2} [107].

The morphology of electrodepozited polypyrrole, shown in Fig. 2.43, present a cauliflower-like structure which is open and suitable for the interaction with dissolved molecular oxygen, in the possible applications as cathode battery in the sea water.

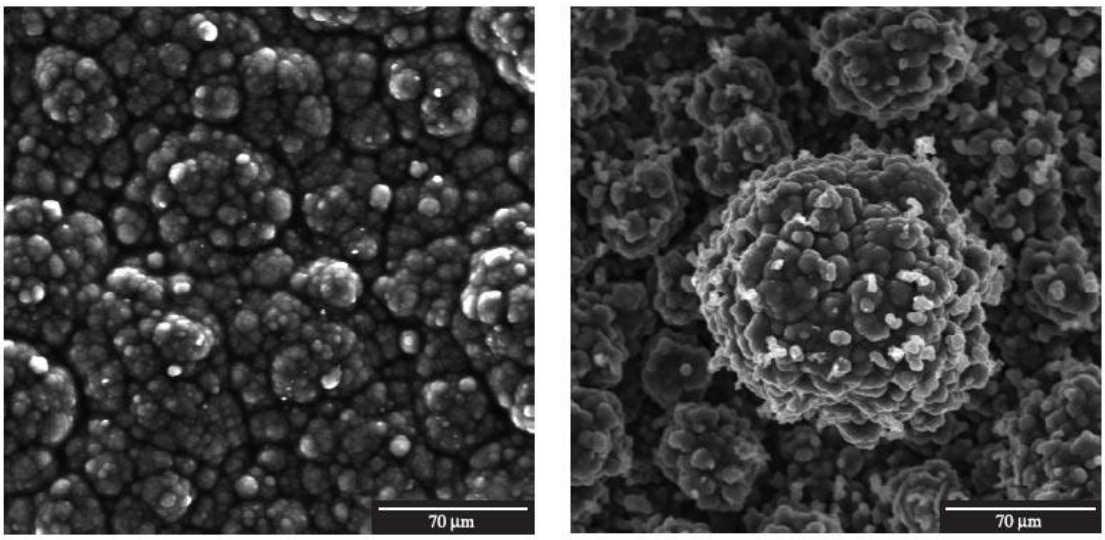

Figure 2.43. SEM of the aluminum surfaces coated with PPy films galvanostatically deposited at a) 5.0 and b) 10.0 $mA.cm^{-2}$ [107]

3. EXPERIMENTAL

3.1. Synthesis and characterization of thin film electrode

Thin polypyrrole film electrode is obtained from hydrochloric acid solution (0.1 M) with addition of 0.2 M of pyrrole monomer (p.a. Merck, distilled in argon atmosphere), at constant current densities of 2 mA cm^{-2} on graphite electrode. Electrolytes were prepared from p.a. grade chemicals (Merck) and bidistiled water. After polymerization, electrode is washed with bidistiled water and transferred in the three-compartment electrochemical cell, shown in Fig. 3.1, with 0.1 M HCl electrolyte for further investigations.

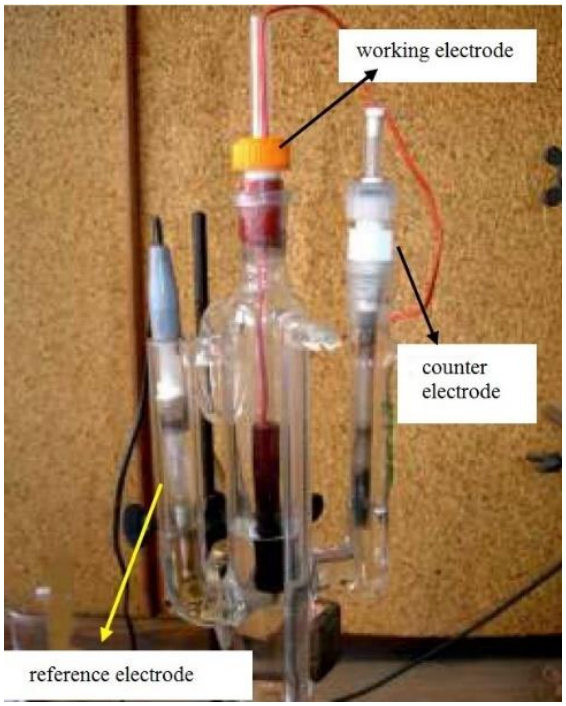

Figure 3.1. Three compartment electrochemical cell used for polypyrrole synthesis.

After transfer, electrode is conditioned at potential of –0.8 V for 600 s to be completely discharged. The working electrode, cylindrically shaped graphite inserted in

Teflon holder (S=0.64 cm^2) is mechanically polished with fine emery papers (2/0, 3/0 and 4/0, respectively) and then with polishing alumina of 1 μm (Banner Scientific Ltd.) on the polishing cloths (Buehler Ltd.). After mechanical polishing the traces of polishing alumina are removed from the electrode surface in an ultra-sonic bath in ethanol during 5 min. For characterization experiments three compartment electrochemical cell, with platinum foil (S=2 cm^2) is used as counter, and saturated calomel electrode as a reference, as shown in Fig. 3.2. Experiments are performed using Gamry PC3 potentiostat/galvanostat.

The oxidation states of polypyrrole are investigated in N-methylpyrrolidone with an UV–vis LLG uniSPEC 2 spectrometer.

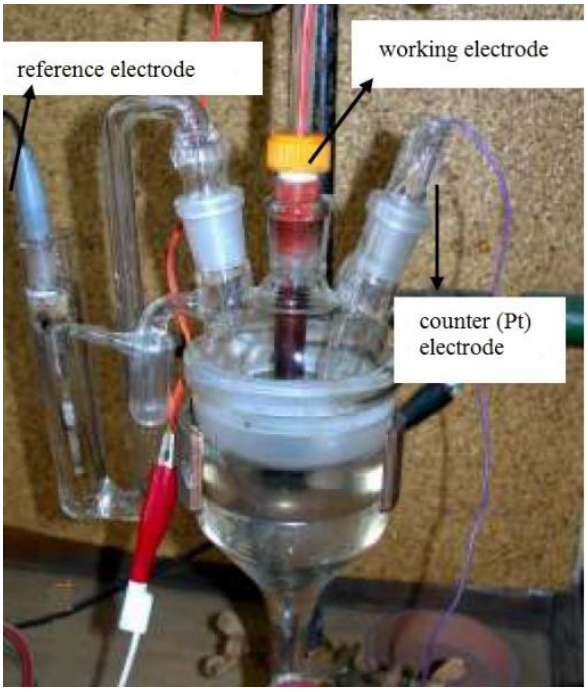

Figure 3.2. Three compartment electrochemical cell used for polypyrrole characterization.

3.2. Polypyrole-zinc cell

Polypyrrole is synthesized galvanostatically with current density of 2 mA cm^{-2} from electrolyte contained 0.1 M pyrrole (Aldrich p.a., previously distilled under reduced pressure), and 1 M HCl (p.a., Merck) onto the plane 1.5 cm × 4 cm, A = 6 cm^2, graphite

electrode with polymerization charges of 3.6 mAh and 12 mAh. Electrode is on one side protected by the epoxy. Before the experiments are conducted, the electrode is mechanically polished with fine emery papers (2/0, 3/0 and 4/0, respectively) and degreased in ethanol in an ultrasonic bath. Pure (>99.9%) zinc, (Alfa Aesar GmbH & Co KG, Germany) of 1.5 cm × 4 cm, A = 6 cm^2 from the one side protected by epoxy, is used as the anode.

All experiments are conducted in 0.5 M (~3%) NaCl (p.a. Merck) as electrolyte using saturated calomel electrode as the reference, and in some cases Pt-mesh as a counter electrode. One compartment electrochemical cell is made of Plexiglas, with a volume of 250 cm^3, equipped with an external reference electrode compartment via Luggin capillary. The plane-parallel electrode in a vertical position with an inter distance of 20 mm is used. The oxygen is supplied from the air by natural convections or by the air pump with the flow rate of 5 ml s^{-1}, with an oxygen equilibrium concentration of ~0.2 mM at room temperature. For the pulsed charge-discharge experiments combinations of the homemade programmable electronic on-off timer- switcher (1 s to 24 h), and R-substitution box (MA 2200, Iskar, Slovenia), are used. For the charge with Si-photovoltaic cell, the 1.5 V toy-photovoltaic cell (1 cm x 2 cm) is used. The light source is a polychromatic 300 W Osram Ultra-Vitalux light bulb that has a sun-like spectral distribution between 280 nm to 780 nm, and an IR region. Experiments are performed using Gamry PC3 potentiostat/galvanostat, and cell voltage is acquired with digital voltmeter ISO-Tech IDM 73, interfaced to a PC via RS-232.

3.3. High area carbon felt-polypyrrole cell

Polypyrrole is synthesized galvanostatically using the current of 48 mA (2 mA cm^{-2}) from electrolyte contained 0.15 M pyrrole (Aldrich p.a., previously distilled under reduced pressure), and 1 M HCl (p.a., Merck) onto both sides of the 3.18 mm thick carbon felt (Alfa Aesar, No: 43199) electrode, with the active area of 24 cm^2, which construction is shown in Fig. 3.3. The polymerization charge was 30 mAh. During electropolymerization, using saturated calomel electrode as the reference, and two plane-

parallel stainless steel plane, 5 cm × 6 cm, as the counter electrodes, electrolyte is mixed with magnetic stirrer at 400 rpm. Two identical pure (>99.9%) zinc plane 4 cm × 6 cm, from the one side isolated by epoxy, are used as the anode.

All experiments are conducted in 3.5% NaCl (p.a. Merck) as the electrolyte. One compartment electrochemical cell made of Plexiglas, with a volume of 500 cm^3 is used. The cathode was inserted between two plane-parallel zinc electrode in a vertical position with an inter distance of 20 mm. Oxygen was supplied from the air using the glass-frit tube as a bubbler, and the air pump with the flow rate of 2 ml s^{-1}, with an oxygen equilibrium concentration of ~0.2 mM at room temperature. For the pulsed charge-discharge experiments combinations of the homemade programmable electronic on-off timer- switcher (1 s to 24 h), and R-substitution box (MA 2200, Iskar, Slovenia), are used. Experiments are carried out using Gamry PC3 potentiostat/galvanostat, while the cell voltage was collected with digital voltmeter ISO-Tech IDM 73, interfaced to a PC via RS-232.

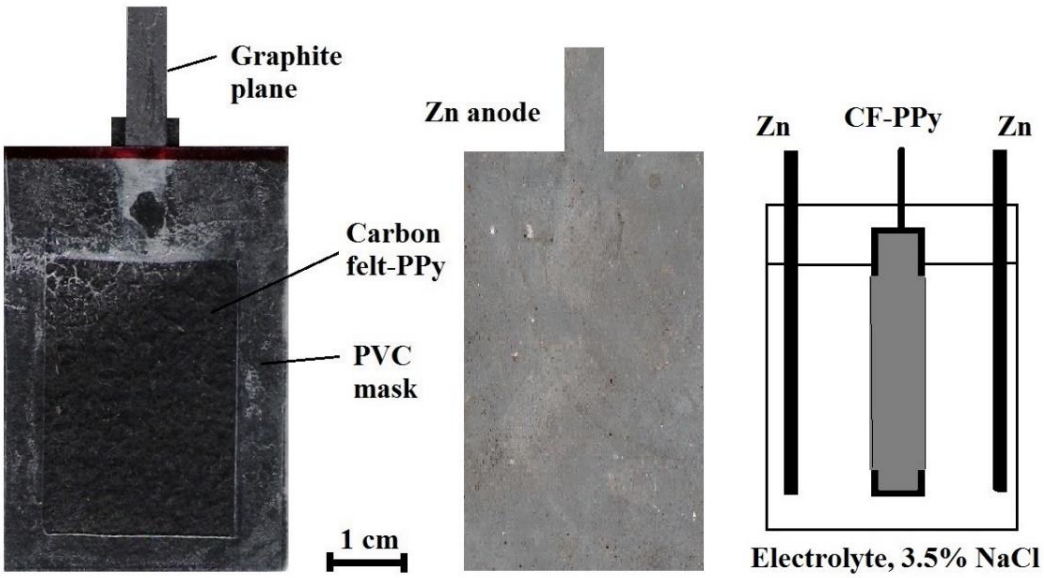

Figure 3.3. Left: image of the high area graphite felt-polypyrrole electrode, middle: zinc anode, right: scheme of the cell configuration.

4. RESULTS AND DISCUSSION

4.1. Synthesis and characterization of the polypyrrole thin film electrode

Figure 4.1 shows the galvanostatic curve for the polymerization of pyrrole on graphite from solution containing 0.10 M HCl and 0.20 M monomer on graphite electrode at the current density of 2 mA cm^{-2} with polymerization charge, q_{pol}, of 0.6 mAh cm^{-2} (1080 s).

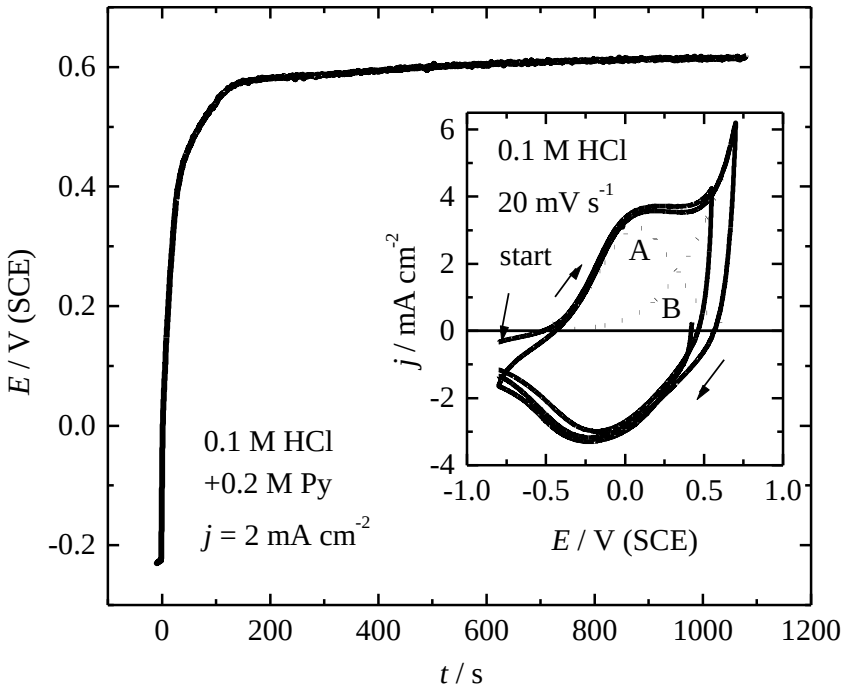

Figure 4.1. Galvanostatic curve for pyrrole polymerization from 0.1 M HCl and 0.2 M monomere at 2 mA cm^{-2} on graphite electrode. Inset: cyclic voltammograms of the PPy electrode in pure 0.1 M HCl for the anodic potential limits of 0.7 and 0.5 V

Polypyrrole polymerization proceeds according to equation:

$$n(\mathrm{Py}) + ny\mathrm{Cl}^- \rightarrow [\mathrm{PPy}^{y+}(\mathrm{Cl}^-)_y]_n + nye^- \quad (4.1)$$

in the potential range between 0.55 and 0.6 V.

In the inset of Fig. 4.1 cyclic voltammograms (CV) of the PPy electrode in pure 0.1 M HCl for the anodic potential limits of 0.7 and 0.5 V are shown. Full line represents experimental data, while dot line represents peak deconvolution. As it can be seen from insert of Fig. 4.1, doping of the PPy electrode starts from the potentials region between ~ –0.4 and 0.55 V (A), with maximum peak potentials at ~ 0.15 V. In the same potential range some other reaction take place, probably overoxidation of the PPy (B). According to the cyclic voltammograms it seems that optimum anodic potential lies near to 0.55 V. Discharging of the PPy electrode starts at potentials of ~ 0.5 V, thought one broad peak in the potential range between 0.5 and –0.8 V, with maximum peak potentials at ~ –0.22 V. After synthesis, PPy electrode are further characterized in 0.1 M HCl.

Figure 4.2 shows the cyclic voltammogram response of PPy for the different sweep rate in the solution of 0.1 M HCl for the anodic potential limit of 0.55 V, while insert of Fig. 4.2 shows magnification of CV response for the sweep rate of 2, 3, 7 and 10 mV s^{-1}.

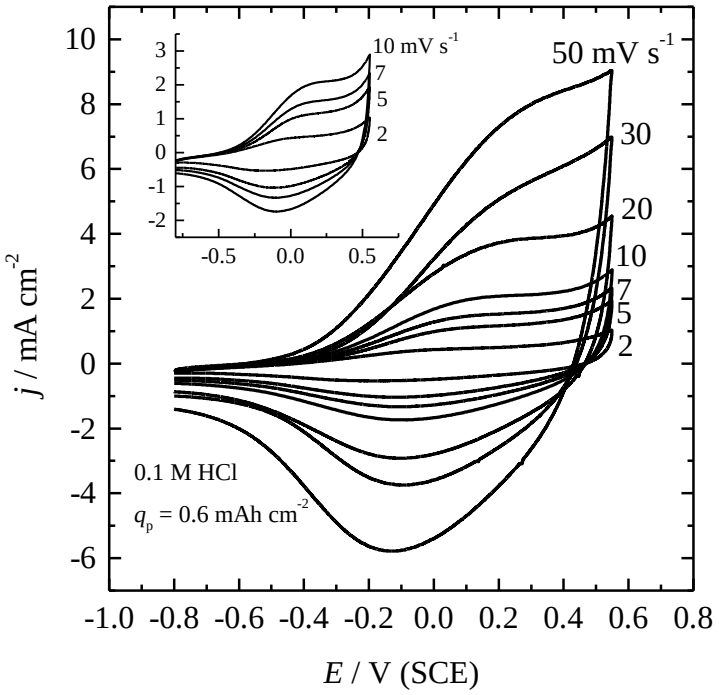

Figure 4.2. Cyclic voltammograms of PPy electrode for the different sweep rate in the solution of 0.1 M HCl.

Figure 4.3 shows dependence of the anodic and cathodic peak current density as a function of the scan rate square root, determined from Fig. 4.2.

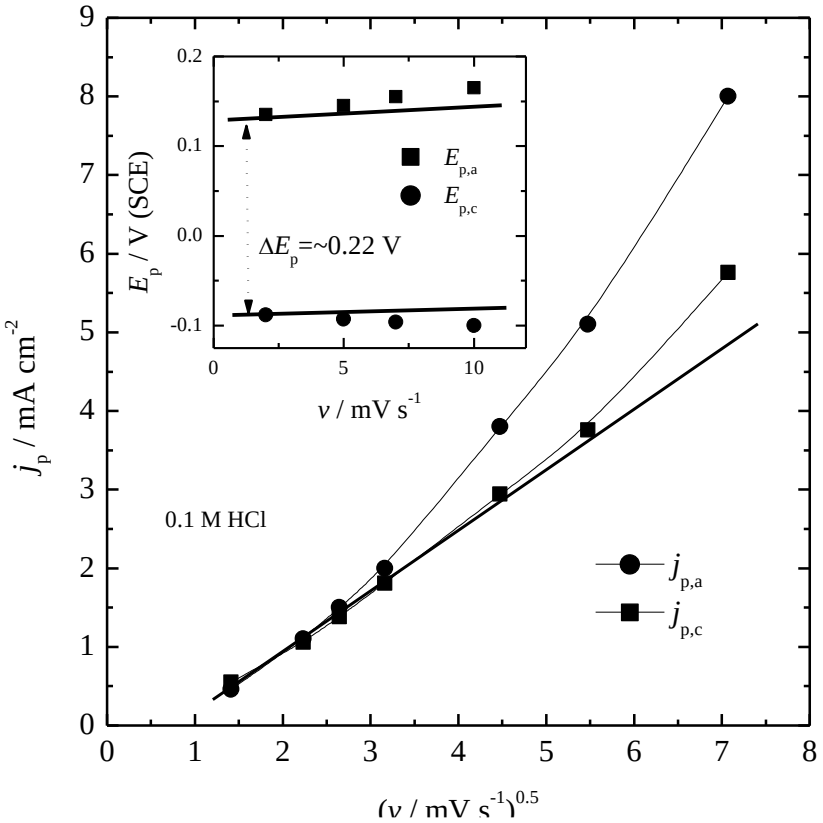

Figure 4.3. Dependence of the anodic and cathodic peak current density as a function of the scan rate square root in 0.1 M HCl. Inset: Dependence of the peak potentials on the sweep rate.

Linear dependence of the peak current density as a function of the scan rate square root below ~10 mV s^{-1} indicates the reversible charge transfer reaction controlled by diffusion of counter (chloride) ions. Above ~10 mV s^{-1} reaction could be considered as irreversible. The dependence of the peak potentials on the sweep rate (for reversible case) are shown as insert of Fig. 4.3. Symbols represents measured peak potentials, while full line represents peak potentials corrected for the Ohmic drop determined by the impedance measurements of the graphite electrode in solution of 0.1 M HCl at the same conditions. The dependence of the peak potentials for relatively low sweep rate is practically independent on sweep rate (> 10 mV s^{-1}), suggesting reversible doping/dedoping reaction

of the PPy film in the investigated potential region. Since, the difference between anodic and cathodic peak potential (for the reversible couple) of ~0.22 V is equal to:

$$E_{\mathrm{p,a}} - E_{\mathrm{p,c}} = \Delta E_p = 2.303\frac{RT}{nF} = 0.22 \text{ V} \qquad (4.2)$$

Equation 4.2 could be used to determine the total numbers of exchanged electrons which is equal to the doping degree, *y*:

$$n = y = \frac{2{,}303RT}{\Delta E_p F} \approx 0.26 \qquad (4.3)$$

To obtain maximum available electrode capacity of PPy films the following procedure is used. Integrating the anodic and cathodic parts of the CV for the anodic potential limit of 0.55 V, the dependence of capacity for different sweep rate is calculated and shown on Fig 4.4. The capacity of the electrode is affected by the sweep rate, and decrease by increasing the sweep rate, which could be attributed to the difficulties for counter-chloride ions exchange along the pores present in the PPy film. If the diffusion of counter (chloride) ions is rate controlling, it has been found that the reciprocal values of the voltammetric charge vary linearly on square root of sweep rate [108], as shown on insert of Fig. 4.4. Intercept at $v \rightarrow 0$, gives the total available charge in steady state conditions of the PPy film of ~0.1 mA h cm^{-2}.

The total polymerization charge, Q_p, of the polypyrrole electropolymerization reaction, Eq. 1, can be given as [19]:

$$Q_\mathrm{p} = I_\mathrm{p}\, t_\mathrm{p} = (2+y)n\mathrm{e}F \qquad (4.4)$$

On the other hand, for the p-doping/dedoping reaction with chloride anions theoretically available doping/dedoping capacity is given as:

$$Q = It = ny\mathrm{e}F \qquad (4.5)$$

Combining equation. (4.4) and (4.5), available capacity is connected with polymerization charge with the following equation:

$$Q = \frac{y}{2+y} Q_{\mathrm{p}} = \frac{y}{2+y} I_{\mathrm{p}} t_{\mathrm{p}} \tag{4.6}$$

from which the doping degree can be estimated as:

$$y = \frac{2Q}{Q_{\mathrm{p}} - Q} \tag{4.7}$$

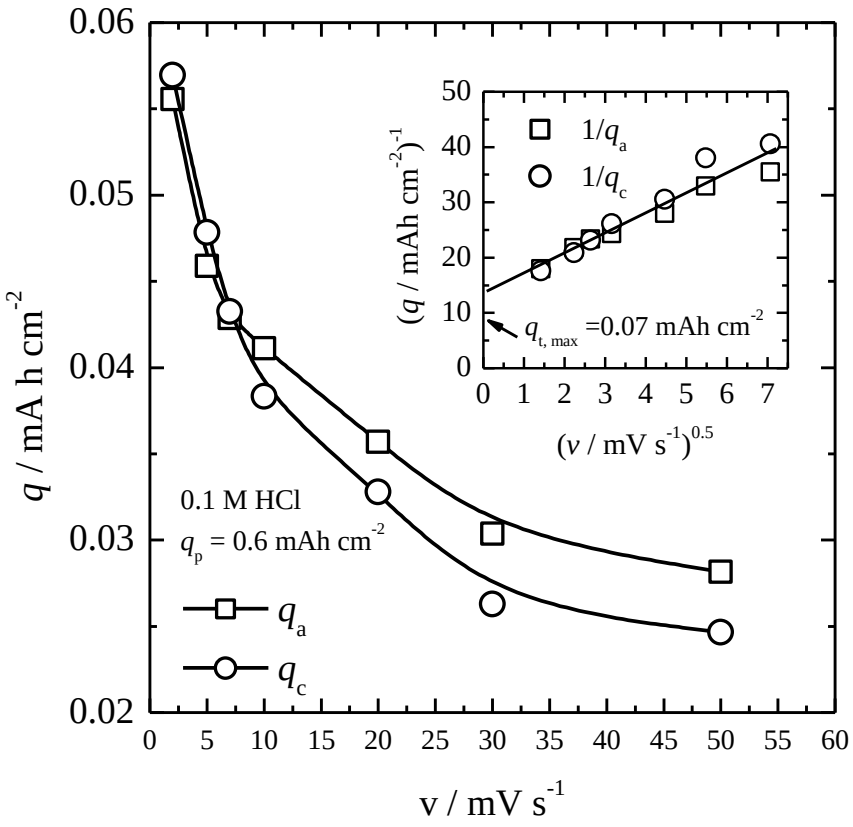

Figure 4.4. The dependence of the PPy electrode capacity for different sweep rate in 0.1 M HCl. Insert: Reciprocal values of the voltammetric charge of PPy electrode on square root of sweep rate in 0.1 M HCl.

Hence, for the polymerization charge of 0.6 mAh cm^{-2} and available charge of 0.07 mAh cm^{-2}, it could be estimated that doping degree is ~0.26, which is in excellent agreement with value obtained from cyclic voltammetry experiments.

In Fig. 4.5 the charge/discharge curve at current density of 0.2 mA cm^{-2} for the anodic potential limits of 0.55 and 0.75 V in 0.1 M HCl are shown. Charging of the electrode starts at potential of ~ –0.5 V, and linearly increase relatively fast up to the potentials of ~0.45 V. After that potential, increase of the potential is much smaller. Discharging of the electrode starts at the potential of 0.45 V, in the potential range of 0.45 to –0.6 V, without pronounced potential plateau. Below potentials of –0.6 V, it seems that some other reaction take place. This reaction could be attributed to the hydrogen evolution reaction. Obtained discharge capacity was ~0.09 and 0.11 mA h cm^{-2} for the charging potential limits of 0.55 and 0.75 V, respectively. Taking in to account that charging time for the anodic potential limits of 0.75 V was more than two and the half time higher than for the potential limits of 0.55 V, it seems that optimal potential limit for the charging of the PPy electrode is near to 0.55 V.

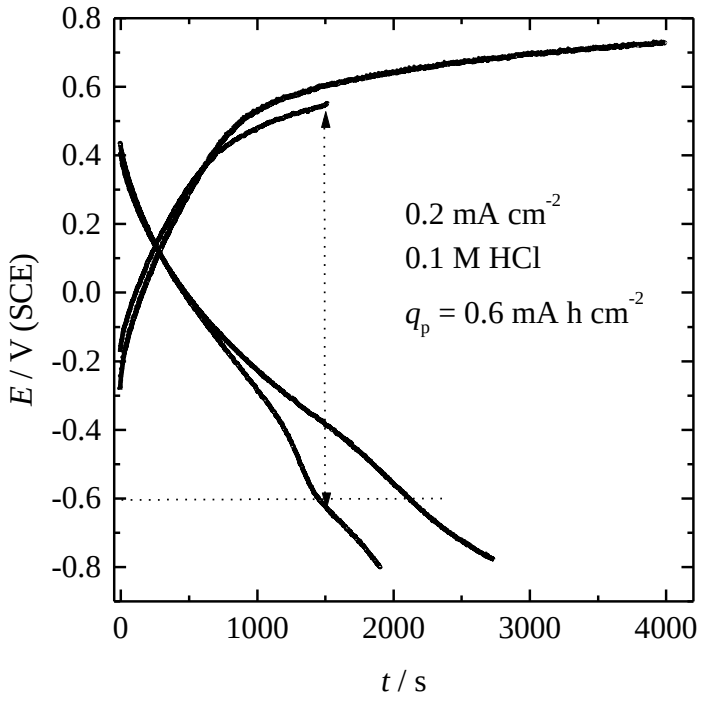

Figure 4.5. Charge/discharge curve for current density of 0.2 mA cm^{-2} for the anodic potential limits of 0.55 and 0.75 V in 0.1 M HCl

To obtain information about the polypyrrole structure, the as synthesized PPy is dissolved in N-methylpyrrolidone. Figure 4.6. shows UV-vis spectra of as synthetized product in N-methylpyrrolidone. In as synthetized PPy, one well-defined band is present at 445 nm. which can be connected to polarons [83]. Because absorption at 345 which corresponds to bipolaron formation [109] is not present it is logical to conclude that polypyrrole is in polaronic states. Intense, broad absorptions are also occurred above 550 nm [110]. This broad absorption is attributed to electron transitions from the polypyrrole valence band to a second bipolarons band in the band gap. So, as synthetized PPy has the well-defined features of a polaron formation with existence of some bipolaronic states, showing the film to be in a doped state [109, 110].

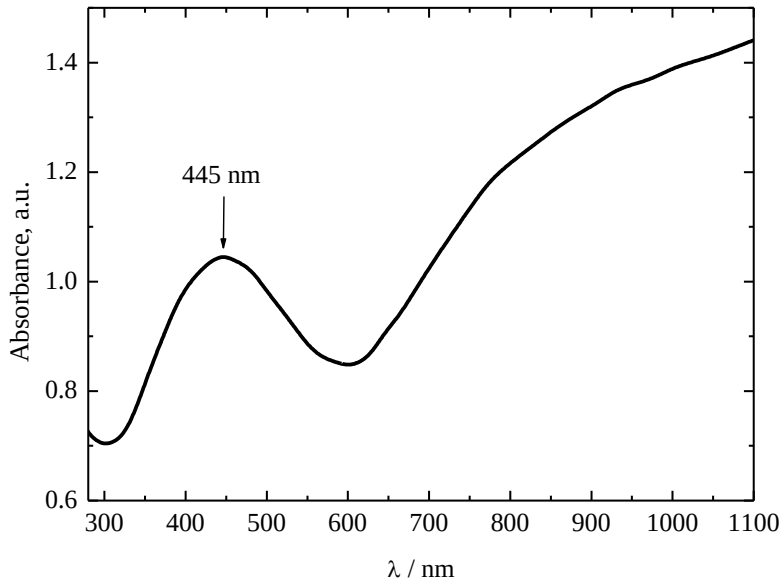

Figure 4.6. UV-vis spectra of as synthetized polypyrrole in N-methylpyrrolidone.

Based on the obtained doping degree of 0.25, one chloride anion per four pyrrole units, and on presence of polaronic states, the structure of the polypyrrole chain shown in the Fig. 4.7 could be suggested.

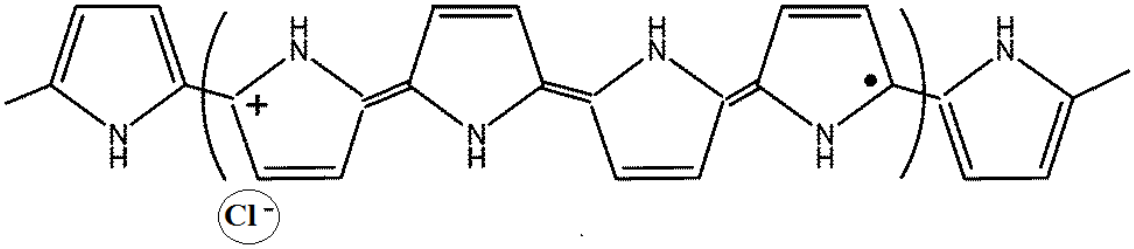

Figure 4.7. The proposed structure of the polypyrrole chain for doping degree of 0.25 in polaronic states.

4.2. Polypyrrole-zinc cell

4.2.1. Synthesis and characterization of the polypyrrole

Galvanostatic synthesis of the polypyrrole for the two different charges, 3.6 mAh and 12 mAh, are shown in the inset of Fig. 4.8. Electropolymerization of the pyrrole occurred in the potential range of 0.65 to 0.6 V via following reaction, as described above [19]:

$$n\mathrm{Py} + ny\mathrm{Cl}^- = [\mathrm{PPy}^{y+}(\mathrm{Cl}^-)_y]_n + 2n\mathrm{H}^+ + (2+y)n\mathrm{e} \qquad (4.1)$$

whereby y is the degree of doping. The anodic oxidation, which results in the formation of conducting polymer, has the stoichiometry of $(2+y)F$ per mole of monomer [96]. Of those, only $2F$ mol^{-1} is related to the polymerization, and extra charge yF is linked, to the oxidation (doping) of the polymer film with chloride anions. The yield in charge terms is close to 100%; providing a possibility of controlling the mass and thickness of the film [111].

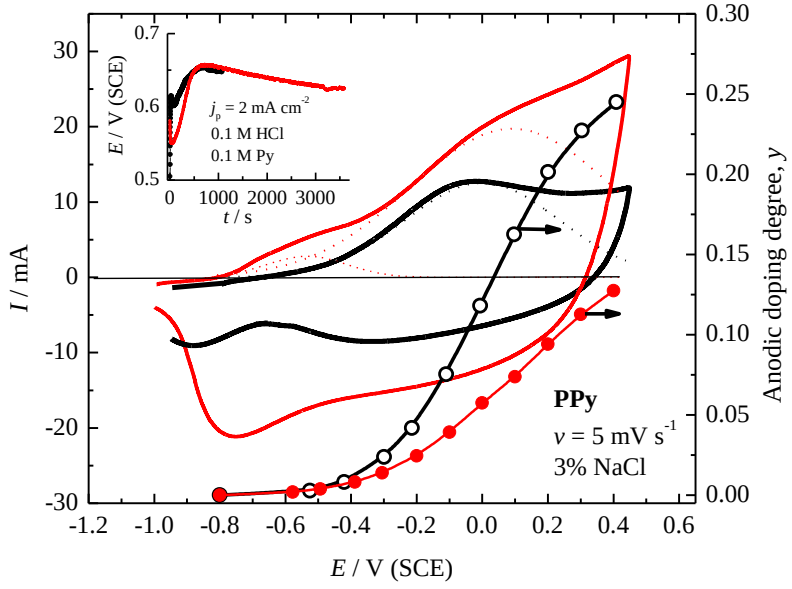

Figure 4.8. Cyclic voltammograms and galvanostatic synthesis (inset) of PPy electrode deposited with polymerization charges of 3.6 mAh (1) and 12 mAh (2) and corresponding anodic doping degree. Doted lines in cyclic voltammograms: deconvolution using Gaussian peak fit.

In Fig. 4.8, cyclic voltammograms of the investigated materials are also shown. Polypyrrole electrode has pceudocapacitive behavior accompanying with the doping-dedoping reaction in the broad range of studied potential. In anodic direction, doping (charge) with chloride anions started at –0.8 V to –0.7 V, and increased up to the potentials of ~0.4 V. Dedoping (discharge) occurred in the potential range of 0.3 to –0.7 V. The, broad peak, especially at the electrode polymerized with 12 mAh at the potentials more negative than –0.4 V could be associated with the oxygen reduction reaction [73] accompanied by cation insertion (n-doping) [112].The dependence of the doping degree with potential, can be estimated by partial integration of deconvoluted anodic part of the cyclic voltammograms, and calculated by rearranging equation Eq. 4.7, according to:

$$y = \frac{2Q}{Q_{\mathrm{p}} - Q} \tag{4.7}$$

$$Q = \frac{1}{\nu} \int_{E(j=0)}^{E_{\mathrm{a,n}}} I \mathrm{d}E \tag{4.8}$$

where ν, is the sweep rate in V h^{-1}, Q_{p} is the polymerization charge in mAh, and I in mA. In the sample with a polymerization charge of 12 mAh, cation (Na^{+}) deinsertion overlapped with chloride doping and due to possible degradation at higher potentials [113], anodic part of the voltammogram is deconvoluted using Gaussian peak fit function, and results are shown in Fig. 4.9 and 4.10.

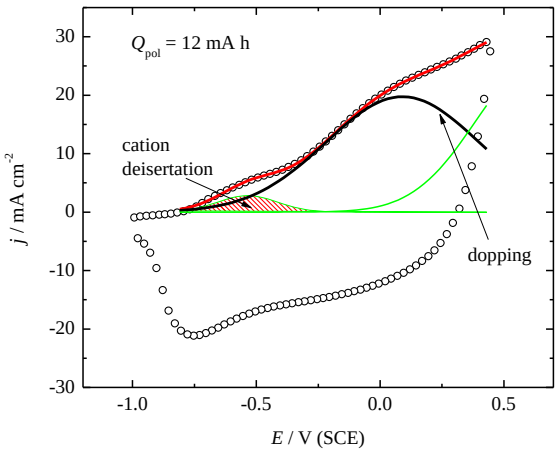

Figure 4.9. Cyclic voltammogram deconvolution using Gaussian peak for the polymerization charge of 12 mAh.

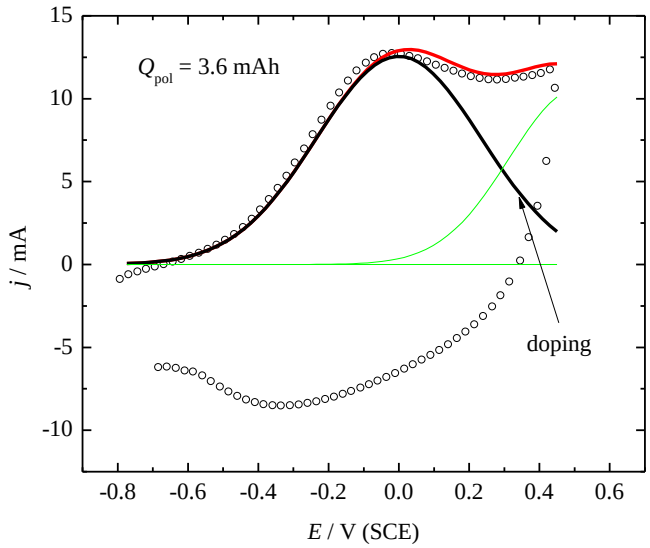

Figure 4.10. Cyclic voltammogram deconvolution using Gaussian peak for the polymerization charge of 3.6 mAh.

The maximum doping degree, for the given conditions are estimated to be 0.26 for PPy polymerized with 3.6 mAh, and 0.125 for PPy polymerized with 12 mAh. This can be explained by the slow solid-state diffusion limitations during doping. The outer PPy layer is practically fully charged, and due to the slow chloride solid-state diffusion, $D(Cl^-)_{PPy} \sim 2-4\times10^{-11}$ m^2 s^{-1} [114] the PPy inner layer cannot be sufficiently fast charged, and some other reaction for example overoxidation, can be started at the charged outer PPy layer.

Using the Eq. 4.6, for the polymerization charge of 3.6 mAh and 12 mAh, and for the doping degrees of 0.25 and 0.125 (estimated from Fig. 4.8), available dedoping charge can be estimated estimated to 0.4 mAh and 0.71 mAh respectively. For further calculations of the specific capacity based on PPy as a limiting electrode material in the investigated system, it is necessary to calculate the mass of polypyrrole. The mass of the electropolymerized polypyrrole is associated with the total polymerization charge (Q_P), and can be represented by the following equation [115]:

$$m(\mathrm{PPy}) = \frac{I_p t_p [M_M - 2M(H^+) + yM_A]p}{(2/\eta + y)(p-1)F} \qquad (4.9)$$

where, η is the polymerization current efficiency, p is the degree of polymerization, F is the Faraday constant, M_M and M_A the molar masses of the monomer, pyrrple, unit and the chloride anion, respectively. Taking that $\eta \sim 1$, and a large value for p, the mass of the electropolymerized PPy for $y = 0.25$ was estimated at 4.35 mg for $Q_p = 3.6$ mAh, and 14.6 mg for $Q_p = 12$ mAh for $y = 0.125$. Using the value of the doped PPy density of ~1.5 g cm^{-3} [115] corresponding thickens of the PPy layers are estimated to 5 μm and 17 μm. From Eqs. 4.5 and 4.8, it is possible to recalculate specific capacity of the fully dopped doped PPy ($y = 0.33$) in the range of 115 mAh g^{-1}. Available specific charge for the electrode synthetized with 3.6 mAh will be 92 mAh g^{-1} (PPy), while for the electrode synthetized with 12 mAh will be 49 mAh g^{-1} (PPy)

4.2.2. Polypyrrole reoxidation charging mode

To investigate potential reoxidation characteristics, PPy electrodes are galvanostatically charged to 0.4 V (lines 1 and 2) with a current of 3 mA, fully discharged to –1 V (lines 1’ and 2’), Fig. 4.11a. The discharge capacity for electrode synthesized with 3.6 mAh is 0.56 mAh, and for electrode synthesized with 12 mAh is 1.26 mAh, which is 109% and 75% of the theoretical value respectively. After the electrodes are completely discharged, the open-circuit potentials are recorded over time in the naturally aerated solution, as illustrated in the inset of Fig. 4.11. From the inset, it can be seen that a stable open circuit potential of ~0.13 V is reached after approximately twelve hours for electrode polymerized with 3.6 mAh, while for the electrode polymerized with 12 mAh the stable open circuit potential is not reached even after 24 hours. After twenty-four hours, the electrodes are discharged with the same current density of 3 mA. Reoxidized electrode (3.6 mAh) has a practically identical discharge capacity as galvanostatically charged, but the discharge potential is ~100 mV lower. On the contrary, electrode (12 mAh) has 75% smaller discharge capacity, and ~0.3 V lower discharge potential. As for converting time of the charge-discharge curves from Fig. 4.11a to the specific capacity, Fig. 4.11b, it can be seen that thinner electrode (3.6 mAh) after 24 hours reoxidation

charging has practically theoretical specific discharge capacity (~115 mAh g^{-1} of PPy), while thicker electrode has only 65% of the theoretical value.

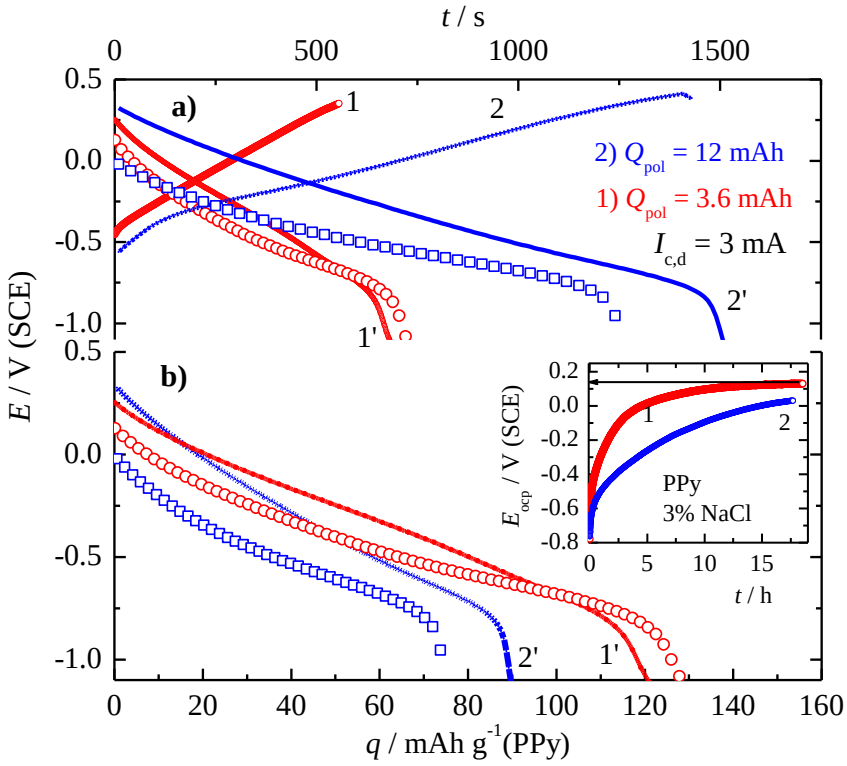

Figure 4.11. a) Galvanostatic charge-discharge (lines), 3 mA, of the electrode polymerized with 3.6 mA (1-1') and 12 mAh (2-2') in comparison with discharge curves after 24 h of the reoxidation charging shown in the inset, (Q_p, ○-3.6 mAh, □-12 mAh). b) The dependence of the potential on the specific PPy capacity during galvanostatic discharge.

Reactions, which are likely to occur during PPy, discharge and reoxidation charge can be anticipated by the following reaction scheme [19]. During discharge at higher potentials, partial dedoping of PPy is the main reaction:

$$[PPy^{y+}(Cl^-)_y]_n = [PPy^{y+}(Cl^-)_y]_{(n-m)} - [PPy^0]_m + myCl^- + mye \qquad (4.10)$$

accompanied by oxygen reduction to the hydrogen peroxide as a side reaction, on the quinone-like PPy moieties [19], via followed simplified scheme:

$$[PPy^{+}(Cl^{-})_y]_n–Py=O + H_2O + e = [PPy^{+}(Cl^{-})_y]_n–Py–OH + OH^{-} \quad (4.11)$$

$$[PPy^{+}(Cl^{-})_y]_n–Py–OH + O_2 = [PPy^{+}(Cl^{-})_y]_n–Py=O + HO_2^{-} \quad (4.12)$$

The produced hydrogen peroxide ion (HO_2^{-}) is able to chemically reoxidize partially dedoped PPy:

$$[PPy^{y+}(Cl^{-})_y]_{(n-m)}\text{-}[PPy^{0}]_m + myCl^{-} + my\,HO_2^{-} + myH_2O \rightarrow$$
$$\rightarrow [PPy^{y+}(Cl^{-})_y]_n + 3myOH^{-} \quad (4.13)$$

The potential of the PPy electrode is determined mainly by the proportion of the oxidized and reduced forms of PPy, and by the potential difference on the PPy/electrolyte solution interface. In the case of PPy doped with mobile anions, potential is given by the simplified equation [116]:

$$E_r(PPy^{+} \mid PPy^{0}) \approx E_f(PPy^{+} \mid PPy^{0}) + \frac{RT}{yF}\ln\left[\frac{a(PPy^{+})}{a(PPy^{0})}\right] - \frac{RT}{F}\ln a^{y}(Cl^{-}) \quad (4.14)$$

which can be rearranged to:

$$E_r(PPy^{+} \mid PPy^{0}) \approx E_f(PPy^{+} \mid PPy^{0}) + \frac{2.3RT}{yF}\log\left(\frac{y}{y_{max}-y}\right) - \frac{2.3RT}{F}\log a(Cl^{-}) \quad (4.15)$$

where: y_{max} is a maximum doping degree, y is actual doping degree at any potential, and $E_f(PPy^{+}|PPy^{0})$ is the formal electrode potentials. E_f of ~0 V can be estimated from Fig. 4.8 for electrode polymerized with 3.6 mAh at conditions $y = 0.5y_{max}$. Therefore, by increasing y, the first logarithmic term increases as well, provoking an increase of the PPy electrode potential.

Figure 4.12a shows the dependence of the cell voltage over discharge time at a constant load of 2 kΩ, after 24 hours of the reoxidation charge, shown in the inset. In the same figure, the discharge curve of the pure graphite-zinc cell is also shown. The voltage

characteristics of this system are rather poor. Electrode (12 mAh) has slightly higher discharge voltage than electrode (3.6 mAh), Fig. 3a. However, by converting the discharge time to the specific discharge capacity, electrode (3.6 mAh) has much better characteristics, as can be seen in Fig. 4.12b.

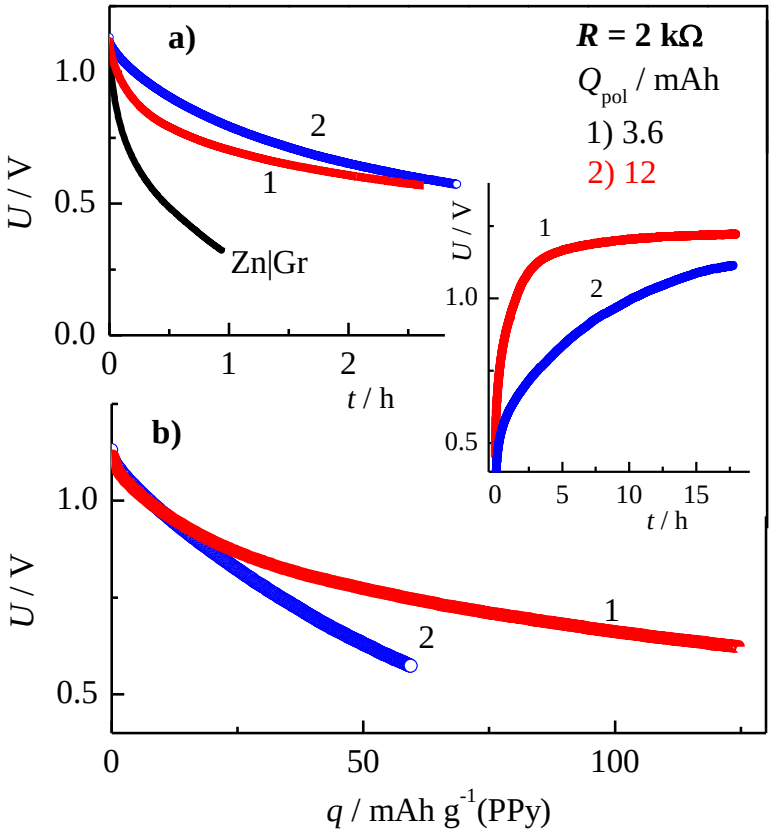

Figure 4.12. a) The dependence of the cell voltage over discharge time at constant load of 2 kΩ, after 24 h of the reoxidation charge, shown in the inset (Q_p, 1-3.6 mAh, 2-12 mAh). b) The dependence of the cell voltage on specific PPy capacity.

Figure 4.13 shows polarization curves after 24 hours of the reoxidation charge of the investigated systems, applying the different constant loads for 60 s per point. For example, the discharge voltage of 1 V is reached for the current of 1.8 mA for the electrode synthesized with 3.6 mAh, and 3 mA for the electrode synthesized with 12 mAh, which corresponds to the specific currents of 400 and 200 mA g^{-1} of the PPy, respectively, as can be seen at top axis of the Fig. 4.13.

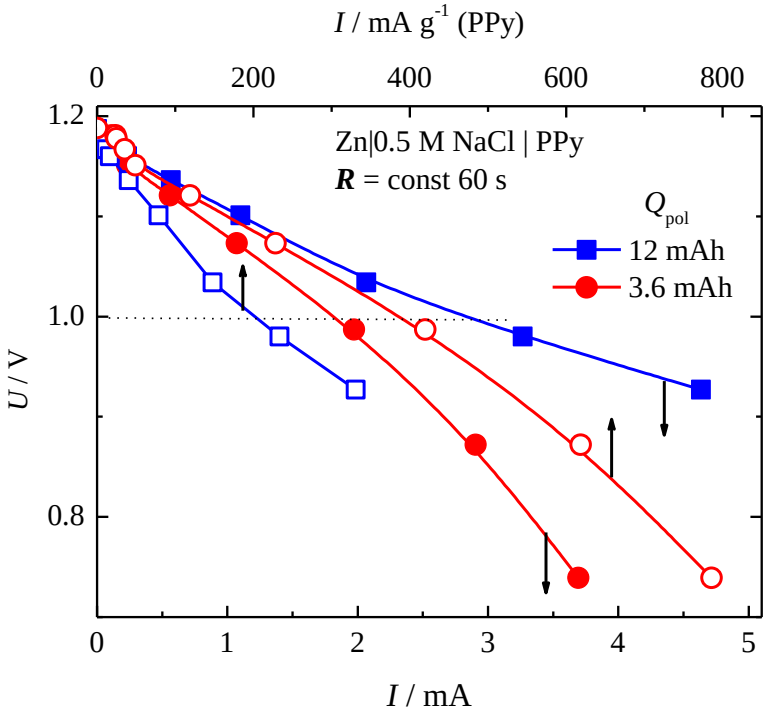

Figure 4.13. Polarization curves of the 24 h charged PPy electrodes in the reoxidation mod, filled symbols-dependence of the voltage on current, open symbols- dependence of the voltage on specific current.

In order to investigate the characteristic of the impulse discharge and reoxidation charge, electrodes are charged 24 h in the reoxidation mode, and continuously discharged 20 s under 2 kΩ load, and 120 s charged in the reoxidation mod, and results are shown in Fig. 4.14. During initial five hours of discharge, both electrodes show similar behavior, but following that, a decrease in the voltage in the electrode (12 mAh), indicating that there is an imbalance in the rate of doping and oxygen reduction has occurred. On the contrary, discharge of the electrode (3.6 mAh) has a relatively stable plateau with the voltage of approximately 0.95 V, Fig. 4.14a, with corresponding current of ~0.5 mA or 110 mA g^{-1} of PPy. After 48 h, the zinc anode is replaced with new, freshly polished one, because an accumulation of zinc hydroxide could deteriorate characteristic of the cell. Only a small increase in the voltage is observed, suggesting that zinc anode does not limit the cell characteristics, in higher contributions. After 68 hours, the external load is increased to 5 kΩ provoking an increase in the voltage for ~90 mV. Further increase of the external load to 10 kΩ contributed to an increase of the cell voltage to ~1.04 V, Fig.

4.14a. Under these conditions, electrode is discharged for additional 100 hours, with a stable voltage plateau of ~ 1 V, Fig. 4.14b. The same figure shows a comparison of the polarization curve for pure graphite electrode in the same solution. The oxygen reduction current which corresponds to the voltage of ~1 V is ~6 µA, while current of the electrode is ~100 µA (~20 mA g^{-1} of PPy). Hence, the steady state current and voltage is probably accompanied by two reactions: during discharge under external load, the main reaction is dedoping of PPy, and during the reoxidation charge without load, by oxygen reduction to peroxide, which chemically oxidized PPy. Consequently, the balance between dedoping and chemical oxidation of PPy by produced hydrogen peroxide is achieved, generating stable voltage plateau. The balance can only be achieved with thinner, 5 µm, electrode that suggested the importance of the solid-state diffusion of the counter ions. For that reason, in the following experiments only electrode synthesized with a charge of 3.6 mAh are investigated.

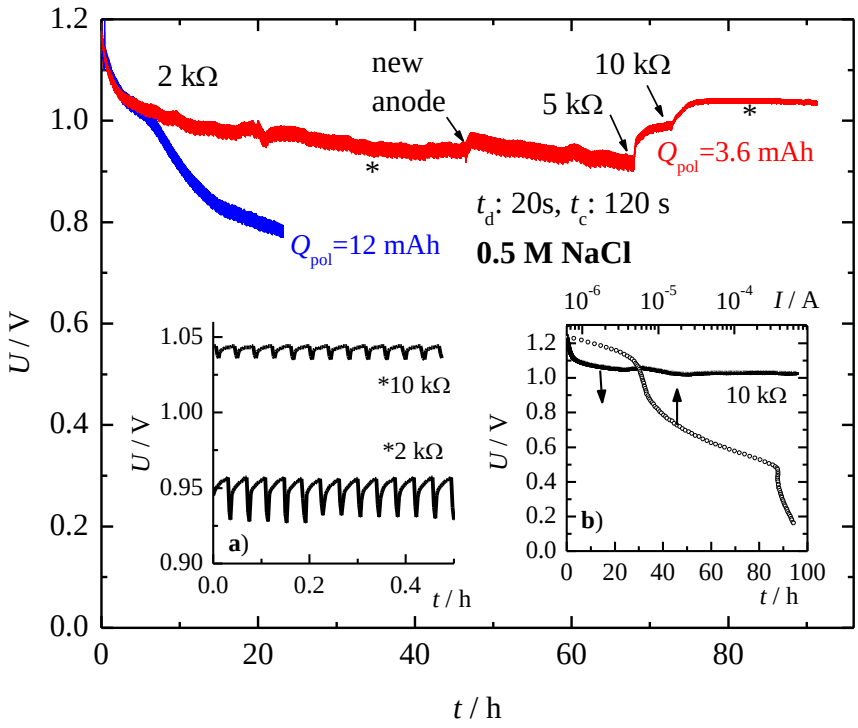

Figure. 4.14. The dependence of voltage over time during impulse discharge (20 s) - reoxidation charge (120 s). a) Magnification of the curves marked with asterisk (*) under external load of 2 kΩ and 10 kΩ. b) The dependence of voltage over time during impulse discharge (20 s) - reoxidation charge (120 s) under external load of 10 kΩ in comparison with polarization curve of the oxygen reduction from air on pure graphite electrode.

Figure 4.15 shows continues discharge of the electrode (3.6 mAh) after 10 hours of reoxidation charge for different external loads. It can be seen that with increase the value of the external load, discharge time increase, and the voltage plateau appears. For example, with the load of 15 kΩ the voltage plateau is near 1 V. The discharge current over time can be calculated using the Ohm law:

$$I(t) = \frac{U(t)_{actual}}{R} \tag{4.16}$$

By decrease of the external load value, the discharge current increase from ~70 μA for load of 15 kΩ; to ~1.5 mA load of 1 kΩ, as can be seen in the inset of fig. 4.15. Obtained discharge capacity for the load of 15 kΩ is in the range of 1 mAh, which twice overcomes capacity connected with dedoping reaction (0.51 mAh).

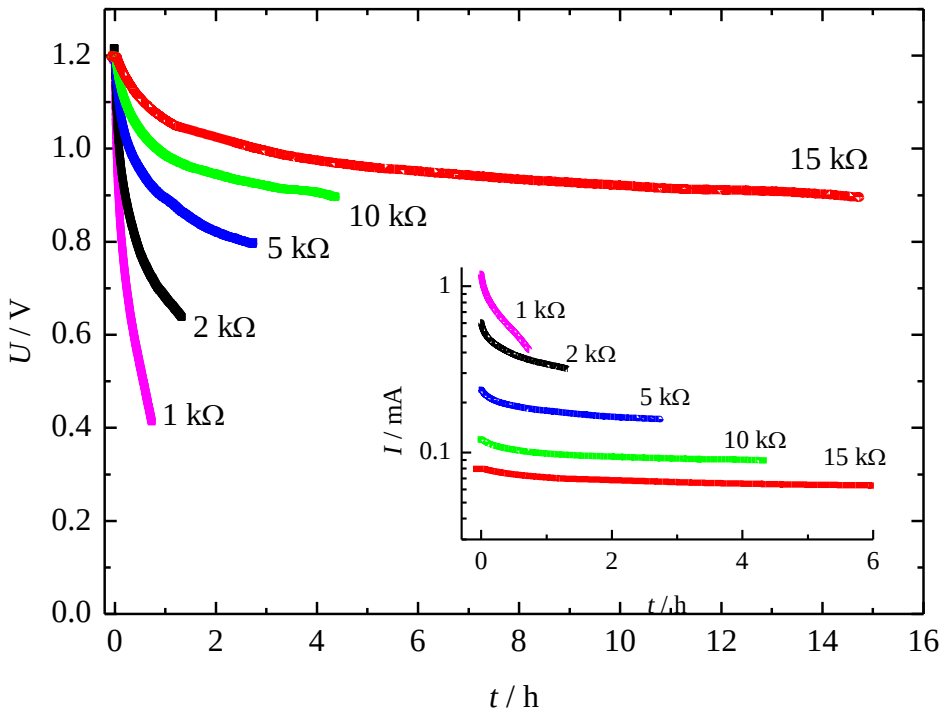

Figure 4.15. Continues discharge of the electrode (3.6 mAh) after 10 hours of reoxidation charge for different external loads. Inset: calculated discharge currents over time for different external loads.

By recalculating the voltage to current and current to specific capacity of the polypyrrole electrode by:

$$q = \frac{I \times t}{m(\mathrm{PPy})} = \frac{U(t)_{actual} \times t}{R \times m(\mathrm{PPy})} \tag{4.17}$$

the dependence of the cell voltage on specific discharge capacity can be obtained, as shown in Fig. 4.16.

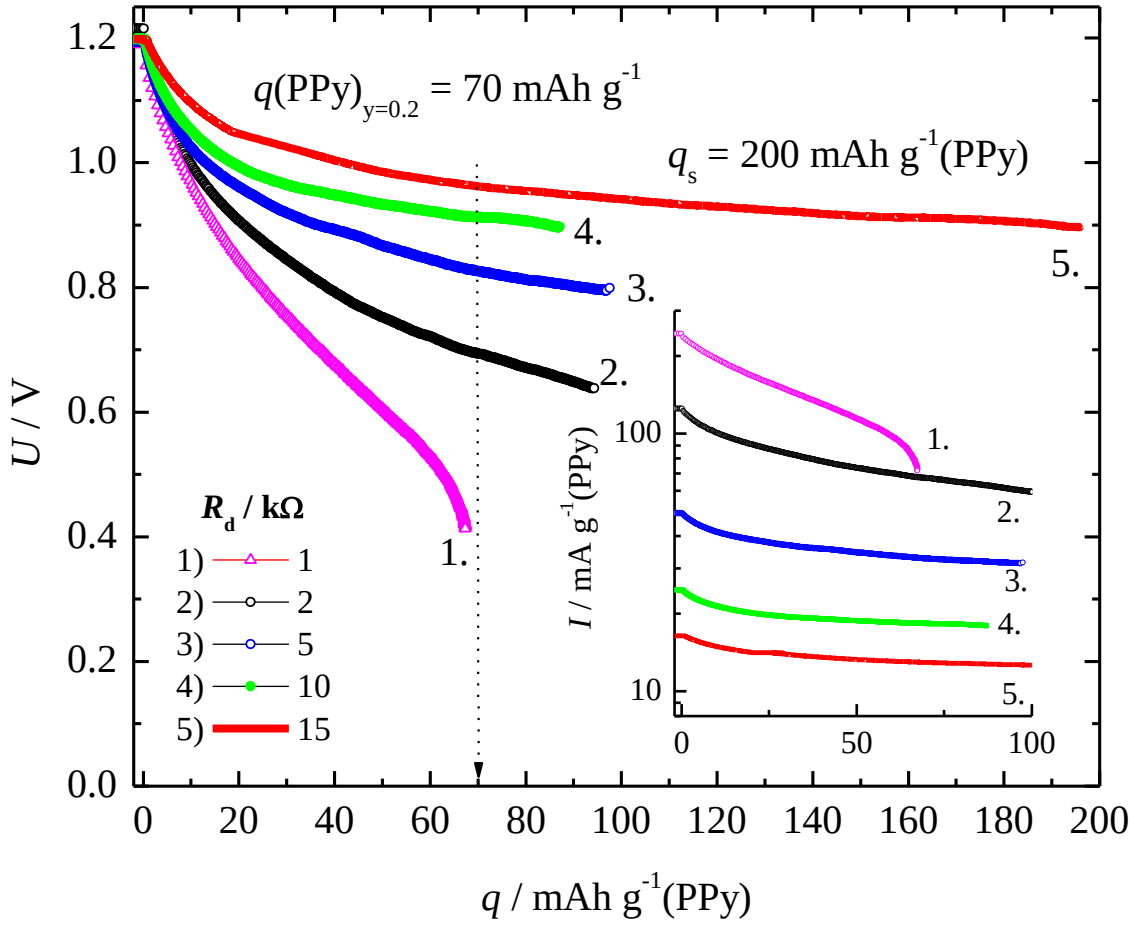

Figure 4.16. Discharge curves for different external load (marked in figure) for electrode-3.6 mAh. Inset: The dependence of the specific currents on specific discharge capacity.

The established open circuit cell voltage of 1.2 V, corresponded to the PPy electrode potential of ~0.15 V. From Fig. 4.8, it can be estimated that doping degree, *y*, for that potential is 0.2, which from Eq 4.8 yields discharge dedoping capacity in the range of 70 mAh g^{-1} of PPy. For the external load of 1 kΩ discharge capacity is in that range, but increasing the value of the external load, the discharge capacity will exceed available capacity which leads from the dedoping reaction. For example, under external load of 15 kΩ discharge capacity is 200 mAh g^{-1} of PPy, with discharge voltage above 0.9 V. Corresponding specific currents given in inset Fig. 4.16, varies between 15 mA g^{-1} of PPy for load of 15 kΩ, to 250 mA g^{-1} of PPy for load of 1 kΩ. Hereafter, for the high discharge rate, the electrode discharge capacity is limited mainly to the rate of dedoping reaction. For low discharge rate the obtained capacity suggested that among dedoping reaction, oxygen reduction reaction occurred, producing hydrogen peroxide which simultaneously chemically oxidized PPy. In that manner, stable discharge voltage plateau can be obtained for low discharge rates for example. 10-20 mA g^{-1} of PPy, achieving high discharge capacity.

Specific energy, w_{sp}, of the system can be estimated using following equation:

$$w_{sp} = qU(t) = \frac{I \times t}{m(\mathrm{PPy})} = \frac{U^2(t)_{actual} \times t}{R \times m(\mathrm{PPy})} \tag{4.18}$$

The dependence of the specific energy over time is given in Fig. 4.17. For the lower value of external load e.g. 1 kΩ, the maximum energy of 32 mWh g^{-1} of PPy is generated. By increasing the external load values, the generated specific energy increase as well, and reached 180 mWh g^{-1} of PPy after 15 h of discharge, which is more than six times higher than classical lead acid battery which is in the range of 20 to 30 mWh g^{-1}. It is worth to mentioned that investigated cell, even it works at minimum oxygen concentration in the electrolyte, possess comparable value of energy density as most advanced Li-polymer cells (100–250 mWh g^{-1}) [117]. In that way the long lasting energy supply of the zinc polypyrrole cell, is demonstrated. In the prolonged discharge, the specific energy will linearly increase.

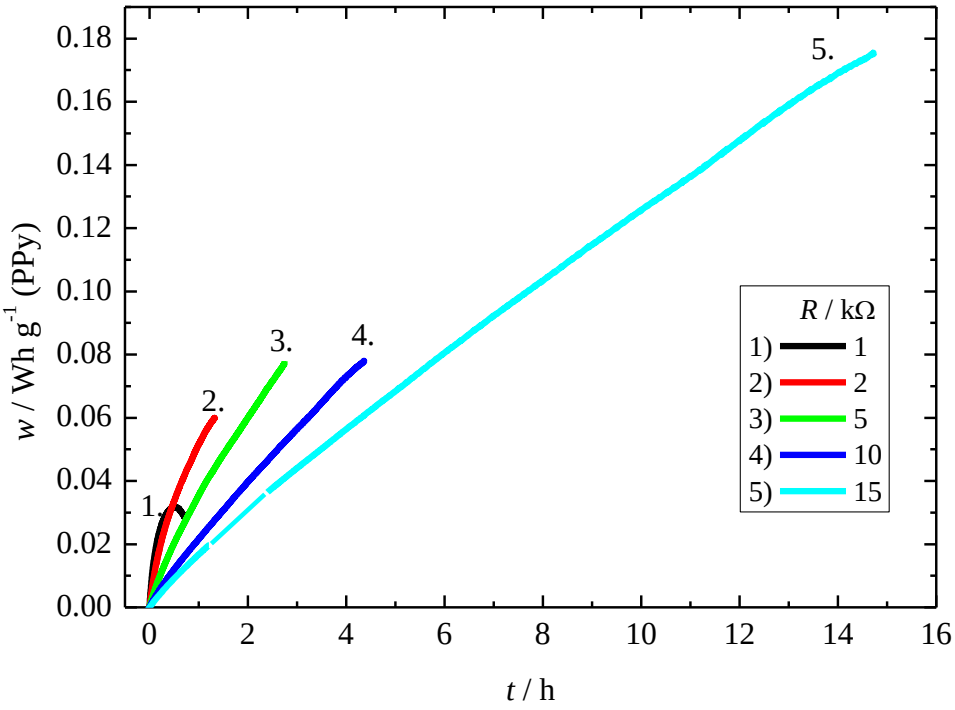

Figure 4.17. The dependence of the discharge specific energy over time for the Zn|PPy system.

The specific power is very important parameter of the electrochemical power sources. Specific power, P_{sp}, of the system can be obtained by dividing the specific energy by discharge time:

$$P = \frac{w_{sp}}{t} = \frac{UI}{m(\text{PPy})} = \frac{U^2(t)_{actual}}{R \times m(\text{PPy})} \tag{4.19}$$

The dependence of the specific energy on power is shown in Fig. 4.18 in the form of Ragone plot. For the low value of external load, e.g. 1 kΩ, the very high value of specific power in the range of 200 to 300 mW g^{-1} of PPy is reached, but the values of specific energy is relatively low from ~1 to 30 mWh g^{-1} of PPy. Specific power at low and medium discharging rates are around 10 to 30 mW g^{-1} of PPy, with much higher specific energy up to ~200 mWh g^{-1} of PPy. From this results it can be concluded that

low power high energy discharge is suitable for constant works, for example during the sensors data acquisition mode, and high power low energy during the data transition mod.

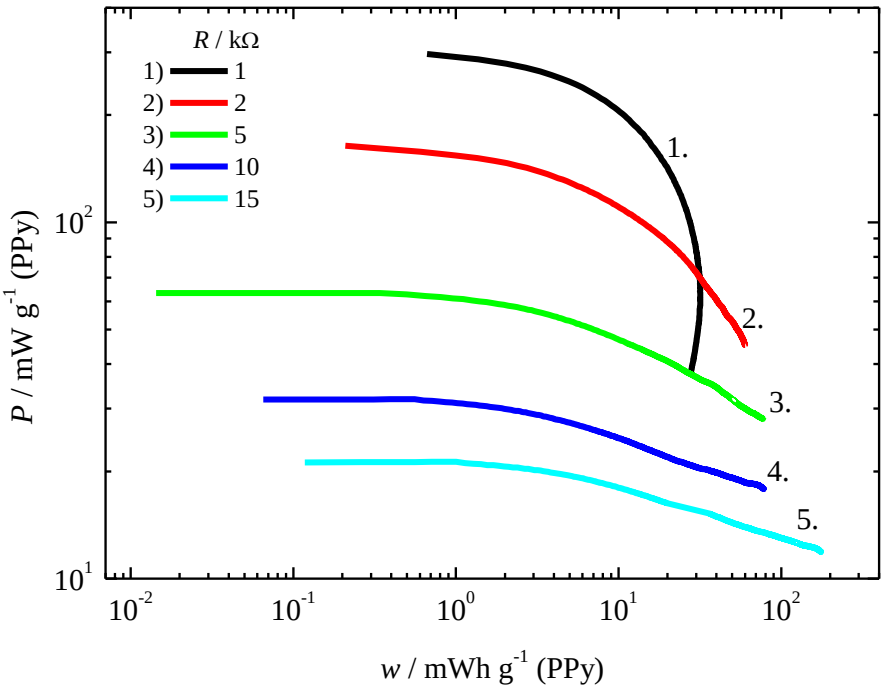

Figure 4.17. The dependence of the discharge specific energy over time for the Zn|PPy system, in the form of Ragone plot.

4.2.3. The influence of the oxygen transport on the zinc-polypyrrole system characteristics

All previous experiments are conducted in naturally aerated solution. To investigate the influence of the oxygen transport (for example, under windy conditions with waves), the following experiments are done. The PPy electrode is charged 24 hours in the reoxidation mod, and the cell is discharged under an external load of 1 kΩ to the voltage of 0.7 V, as shown in Fig. 4.18. After that, the air is introduced into the cell by bubbling. The cell voltage is increased to ~0.9 V, as well as the PPy potential to ~-0.25 V. After 25 minutes of discharge, the external load is switched off, provoking, a fast increase of the cell voltage, and PPy potential. Switching the oxygen supply off and external load on, relatively fast discharge is again obtained. Hence, an additional gain of

0.15 V can only be obtained with constant oxygen supply. In the same figure, the characteristic of the Zn/graphite cell is also shown for comparison, which shows a significantly poorer characteristic. During the discharge of the cell under constant air supply and with the external load of 2 kΩ, the stable voltage plateau of ~0.92 V was obtained over two hours. It is important to note that the fluctuation of the cell voltage and PPy potential is not observed by changing the air supply on and off. This indicates that chemical step in the oxygen reduction reaction mechanism, is the rate determining, which is not sensitive to the hydrodynamic conditions. The only chemical step, given in the mechanism above, is the adsorption of the molecular oxygen from the electrolyte to –OH group in the pyrrole ring, given by Eq. 4.12.

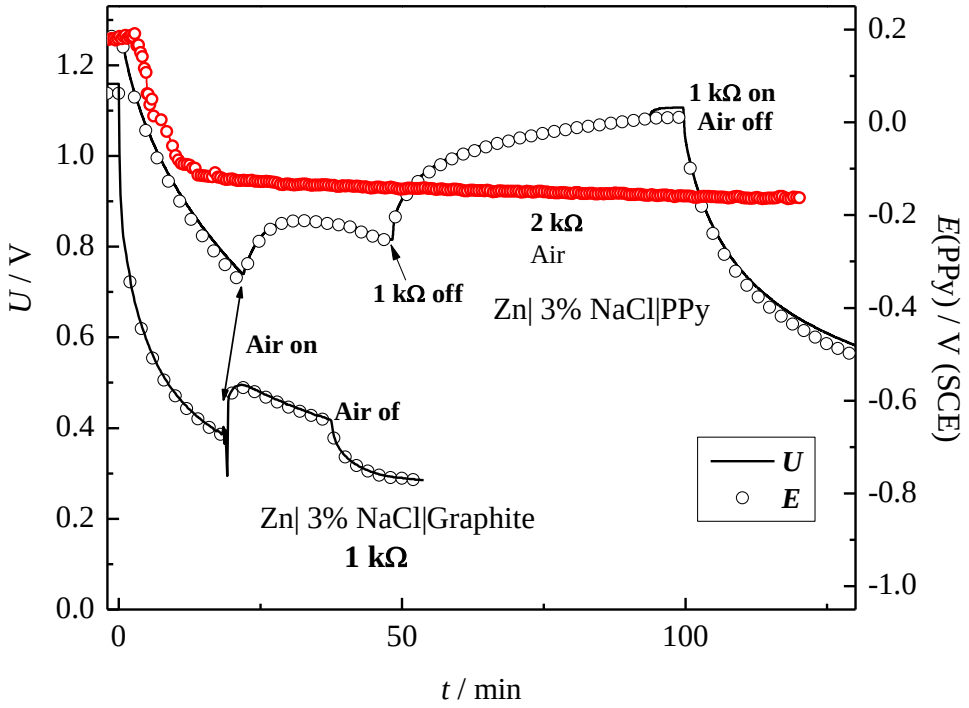

Figure 4.18. The dependence of the cell voltage and PPy potential, during discharge under external load, and different oxygen supply conditions.

Figure 4.19 shows continuous discharge of the cell under an external load of 1 kΩ and constant air supply during one hour discharge and one hour reoxidation charge, without external load. The stable discharge voltage plateau of ~0.85 V with discharge current of 0.85 mA (190 mA g^{-1} of PPy), Fig. 4.19a, is obtained over 27 hours, producing

almost 2.5 Ah g^{-1} of PPy. The specific energy during the discharge of 2.1 Wh g^{-1} of PPy can be calculated by Eq. 4.19, which is an extraordinary value. Some small decrease in the voltage can be observed over time and this can be connected with zinc electrode, which shows increase of the corrosion potentials for ~20 mV during 20 hours of exposure to the electrolyte, as shown in Fig. 4.19b. This increase of the potential can be explained by the formation of insoluble zinc hydroxide species onto the surfaces:

$$Zn \rightarrow Zn^{2+} + 2e \tag{4.19}$$

$$Zn^{2+} + 2OH^{-} \rightarrow Zn(OH)_2 \tag{4.20}$$

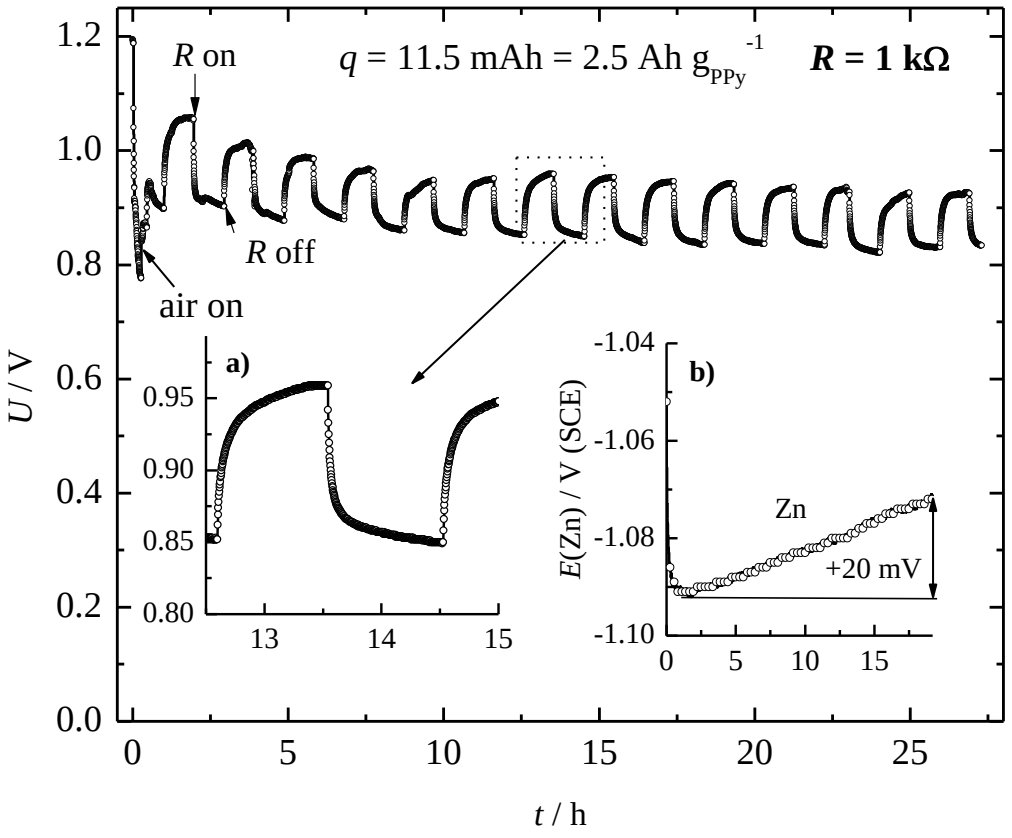

Figure 4.19. Continuous discharge of the cell under external load of 1 kΩ and constant air supply, during one-hour discharge and one-hour reoxidation charge. a) Magnification of the marked charge-discharge cycle. b) Dependence of the zinc corrosion potential over time.

4.2.4. The effect of the storage and external power charge

The Zn/PPy cell is considered to work as an immersion system. In order to evaluate the influence of the storage time on the system characteristics the following experiments are performed. Consequently, the previously used PPy electrode is charged 24 hours under the reoxidation mode, removed from the solution, washed with distiled water, and stored at ambient conditions for one month. After that, the cell is again assembled, and filed with the electrolyte. The established open circuit voltage is 1.22 V (Figure 4.20) and has discharge capacity of 0.6 mAh and discharge voltage above 0.7 V under external load of 2 kΩ (1), in Fig. 4.20a.

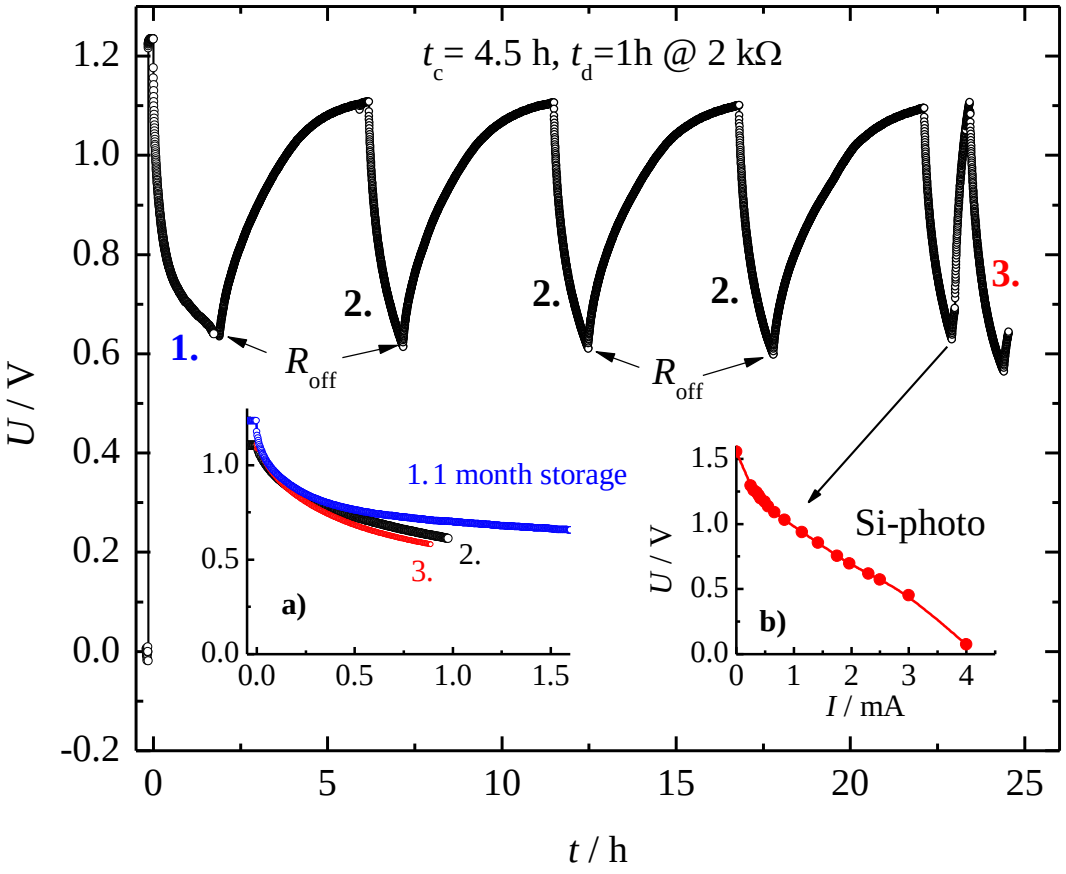

Figure 4.20. Discharge of the cell under external load of 2 kΩ after one month of storage (1), after reoxidation charge for 4.5 h (2), and charged with Si-photovoltaic cell, with voltage-current characteristics given in b); in naturally aerated solution.

From Fig. 4.20, it can be also seen that reoxidation characteristics have been retained. After 4.5 hours of being charged in reoxidation mode, slightly weaker characteristics are obtained (2) in Fig. 4.20a. After four discharge and reoxidation charge cycles cell is attached to a small Si-photovoltaic cell of which the voltage-current characteristics under polychromatic light with the intensity of ~ 40 mW cm^{-2} is shown in Fig. 4.20b. Electrode is practically fully charged within 20 minutes, with similar discharge characteristics as obtained after 4.5 hours of reoxidation charge (3) in Fig. 4.20a. Hence, this method can be used for fast charging of the cell, during the day.

The same electrode is tested again in the mode of six-hour reoxidation charge and 20 minutes discharge at external load of 1 kΩ, and results are shown in Fig. 4.21. Under this extended discharge, system practically retained discharge characteristics, inset in Fig. 4.20 over 50 hour.

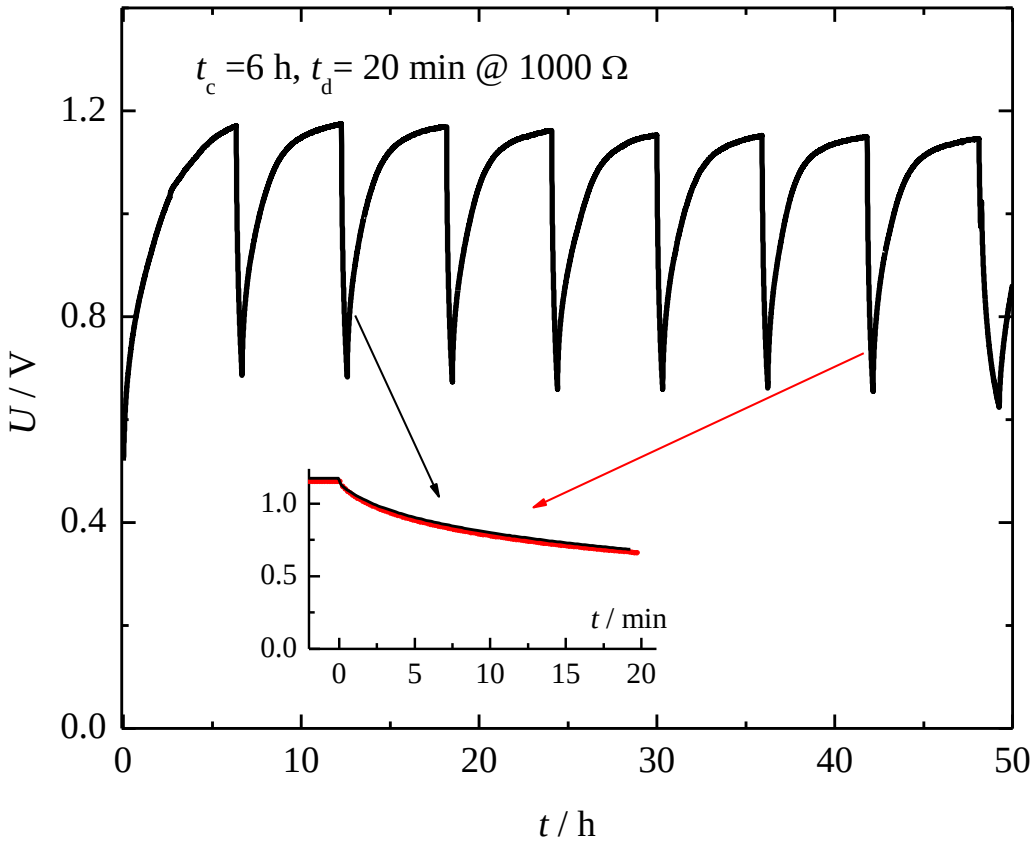

Figure 4.21. Extended six-hour reoxidation charge and 20 minutes discharge at external load of 1 kΩ in naturally aerated solution.

The structure of the cell potential on applied current during charge and discharge with external power supply, are as shown in Fig. 4.22. To avoid overoxidation, the PPy electrode is charged to the anodic potential limits of 0.4 V (SCE). The potential of PPy electrode during charge occurs practically linearly in the range of -0.4 to 0.4 V, while discharge occurs linearly in the potential range of ~0.3 to –0.8 V, followed by a sharp decrease of the potential due to diffusion limitations of Cl^- ions. Corrosion potential of the zinc electrode is –1.1 V. Anodic dissolution of the zinc occurs with relatively small overpotentials of 50-100 mV, depending on applied current, Fig. 4.22a, while cathodic overpotentials are much higher between 100-250 mV.

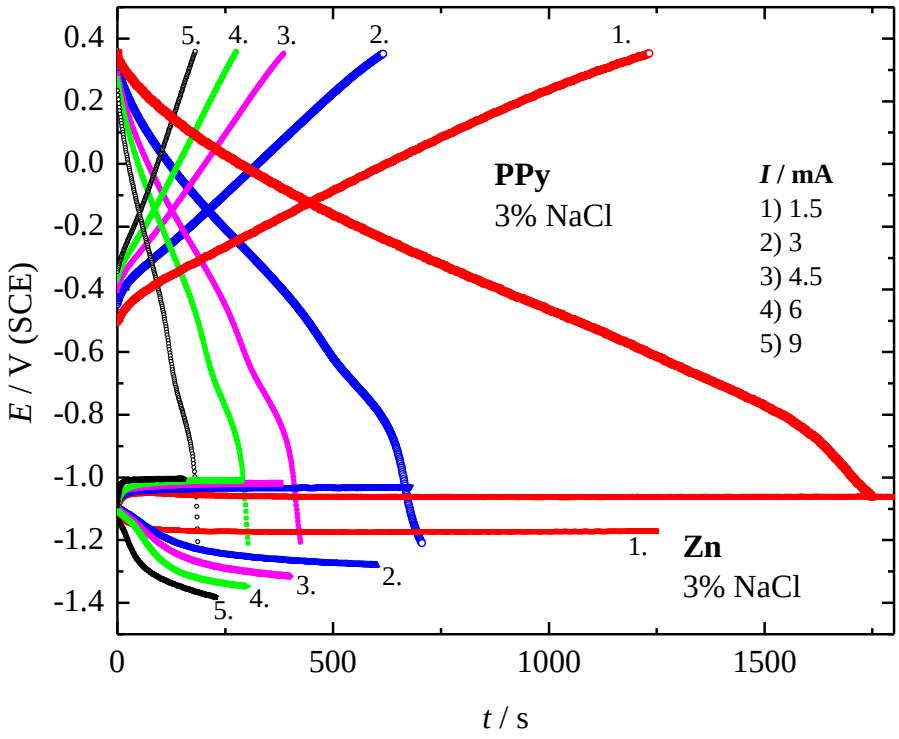

Figure. 4.22. The structure of the cell potentials of the polypyrrole and zinc electrode during charge and discharge with external power supply.

Simultaneously with the potential measurement, the voltage of the cell is also recorded, and results are shown in Fig. 4.23, in the form of cell voltage dependence on the polypyrrole areal electrode capacity. The charge cell voltage increase from 0.5–0.8 V

to around 1.7 V, which is for a 1 V lower values than in classical zinc-air rechargeable cell [118], which is a great improvement. The discharge of the cell linearly occurred in the voltage range between 1.5 V to ~0.2 V. Obtained discharge specific capacity of 0.4 to 0.5 mAh for the higher currents are in agreement with estimated doping degree (0.4 mAh for y = 0.26). For the moderate current of 1.5 mA or current density of 0.25 mA cm^{-2}, specific capacity of 0.8 mAh is obtained, again suggesting that oxygen reduction reaction is involved during the discharge process.

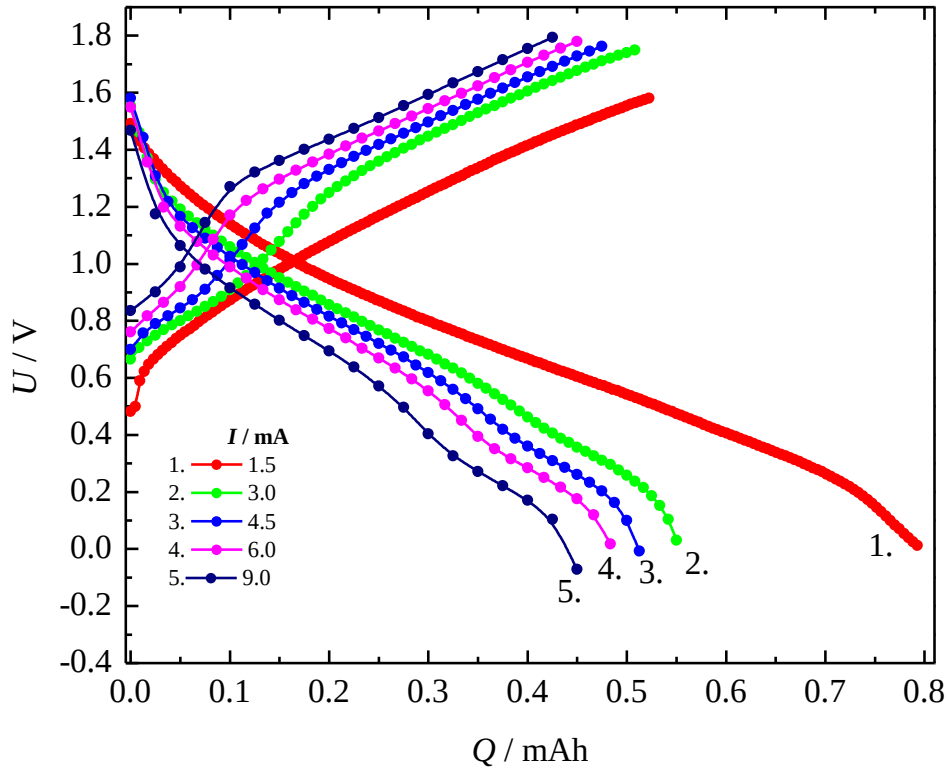

Figure 4.23. The dependence of the cell voltage on the areal polypyrrole electrode capacities during charge and discharge.

In Fig. 4.24, the diagram shown in Fig. 4.23 is recalculated based on the polypyrrole mass giving the specific capacities. It can be seen that for the applied currents in the range of 1.5 to 9 mA or ~300 to 2000 mA g^{-1} of PPy, the specific charge to the cut-of voltage of ~0.7 V are 90 to 45 mAh g^{-1} of PPy. It should be noted that those specific currents are very high, and can be used for high power applications of the systems, for example during the short data transmission periods. The corresponding specific energy is estimated between 45 mWh g^{-1} to 80 mWh g^{-1}.

Relatively low voltage of the cell during discharge could be increased by serial connection of two or three cells with proper elimination of the current leaking, or by simple electronic miniature micro-power synchronous step-up DC/DC converters like LT3525-3 V; LTC3525-3.3 V; LTC3525-5 V (see below).

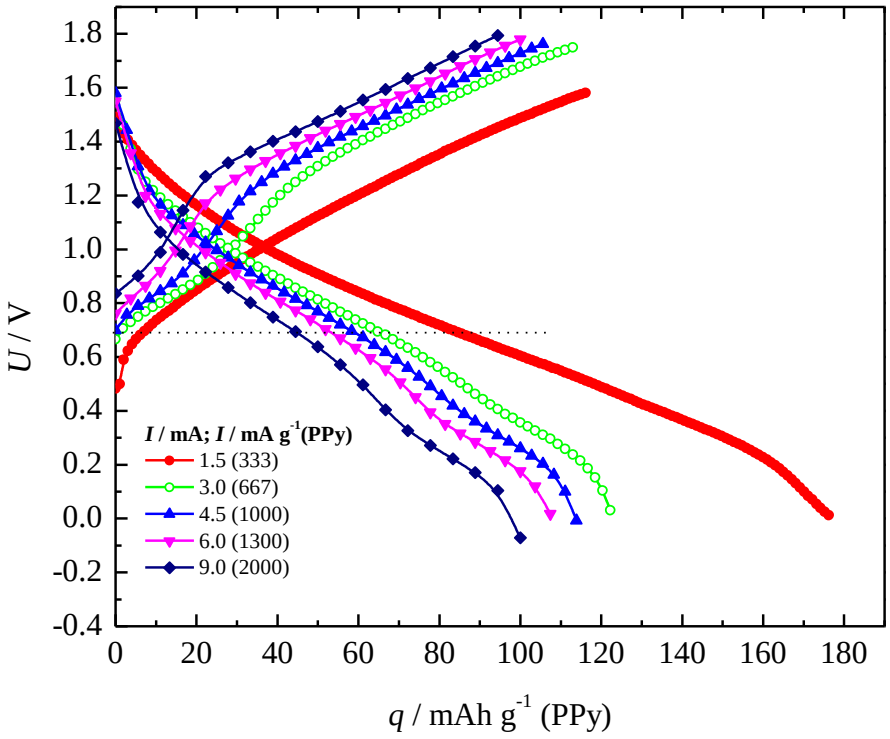

Figure. 4.24. The dependence of the cell voltages on specific polypyrrole electrode capacities during charge and discharge.

Interestingly from Figs 4.23 and 4.24, it can be seen that the charge voltage has the shape of S-curve, which cannot be connected with PPy charge, Fig. 4.22. For that reason, the galvanostatic curve for pure zinc is recorded as shown in Fig. 4.25. It can be seen that hydrogen evolution on the zinc (reaction during charging) has an S-shape. Generally, the limiting current-like behavior of the polarization curves for the hydrogen evolution reaction on Zn can be explained by a mechanism in which the surface oxide plays an active role according to [119]:

$$Zn\text{-}OH + H_2O + e = Zn\text{-}OH_2 + OH^- \qquad (4.21)$$

$$Zn\text{-}OH_2 + e = Zn\text{-}H + OH^- \quad (4.22)$$

$$Zn\text{-}H + H_2O = Zn\text{-}OH + H_2 \quad (4.23)$$

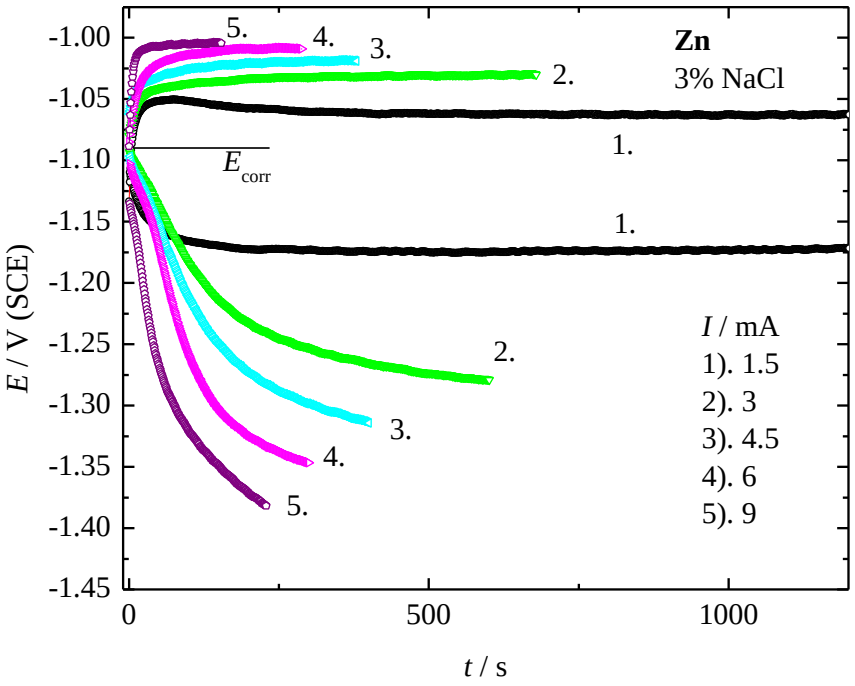

Figure. 4.25. The galvanostatic charge discharge curves for pure zinc in 3% NaCl solution.

One of the important characteristics of the investigated Zn|PPy system is corrosion current of zinc, which leads to lose of the anode active mass. In order to detemine the corrosion current density, the polarization curve of the pure zinc is recorded and shown in Fig. 4.26. Anodic Tafel slope has a value of 38 mV dec^{-1}, which is the main reasons for low polarization of the zinc electrode during Zn|PPy cell discharge. Cathodic branch of the polarization curve is more complex with existence of the limiting like current in the potential range of –1.1 to –1.3 V (SCE). The nature of the limiting current is explained above. Below ~–1. V (SCE), the hydrogen evolution reaction (so-called gassing) from water occurred:

$$2H_2O + 2e \rightarrow H_2\uparrow + 2OH^- \qquad (4.24)$$

The gassing reaction of the hydrogen is important, because under these conditions the oxide zinc covered surfaces can be regenerated to metallic zinc.

From the intercept of the anodic Tafel line to corrosion potential, E_{corr} = –1.1 V (SCE), the corrosion current density of 30 μA cm^{-2} is obtained. Using this value the mass loss of the zinc due corrosion in term of g day^{-1} can be calculated from the Faraday law:

$$\Delta m(\mathrm{Zn}) = \frac{j_{corr} \times t \times M(\mathrm{Zn})}{n \times F} \qquad (4.25)$$

where Δm, g, is a mass loss, t is 24 h, M(Zn) = 65.4 g mol^{-1}, and F = 26.8 Ah mol^{-1}. The estimated mass loss is around 0.8 mg cm^{-2} per day, or in a yearly base only 0.3 g cm^{-2} of the electrode area, which is practically negligible value. Knowing the zinc density of 7.140 g cm $^{-3}$, the thickness loss of only 0.4 mm per year can be estimated. It should be mentioned that thickness of zinc electrode could be in the order of few centimeters.

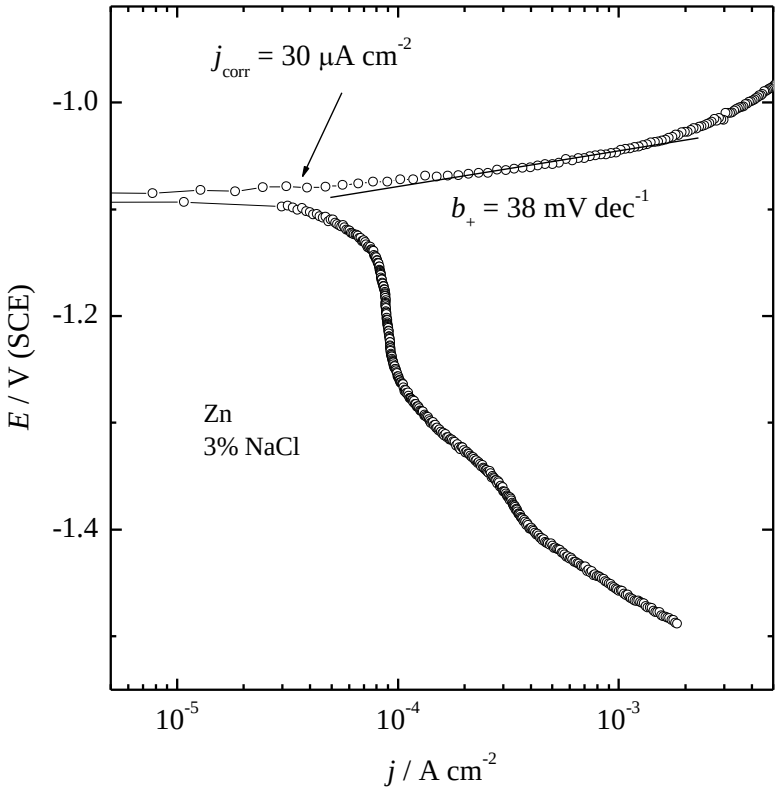

Figure 4.26. Polarization curve of the pure zinc in 3% NaCl.

In order to test the ability for fast charge and discharge, cyclization of the cell is performed during fifteen successive fast charge-discharge cycles with current of 9 mA (2 A g^{-1} of PPy) to the potential of 0.5 V (SCE), at which overoxidation could occur, Fig. 4.27. As it can be seen, practically no deterioration of the characteristics is observed, which can be characterized by the maximum charge cell increase, inset in Fig. 4.27. It is interesting to note that charge-discharge curves are supercapacitors-like [120, 121, 122]. These conditions of charge-discharge can be meet using the small external photocell.

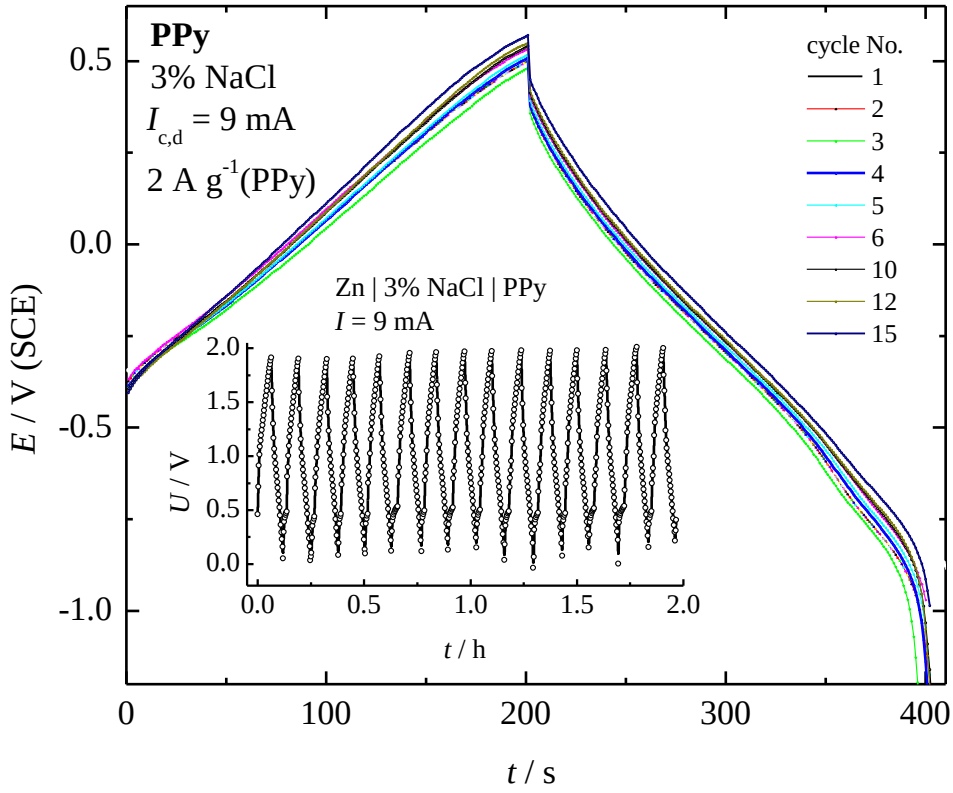

Figure 4.27. Dependence of the PPy potential, and cell voltage (inset) during fifteen successive fast charge-discharge cycles with current of 9 mA (2 A g^{-1} of PPy).

The anodic potential can influence the characteristics of the polypyrrole by the means of the overoxidatio, which could lead to lose of the conjugation and conductivity. The maximum charging potential is estimated from the cyclic voltammetry experiment, shown in Fig. 4.28. Increae of the anodic potential limit from 0.3 V to 0.5 V, the only small increase of the cathodic charge is observed. At higher potentials, thermodynamic conditions for oxygen evolution reaction occurred. The potentials of $E_r(O_2|H_2O)$ = 0.57

V(SCE) is the theoretical potential for oxygen evolution, marked in Fig. 4.28. Increase of the current above potential of 0.5 V, indicate that oxygen evolution reaction is possible, accompanied with the polypyrrole overoxidation. The current is extremely high, ~60 mA, at potentials higher than 0.8 V, inset in Fig. 4.28, but the shape of the voltamogram did not change dramaticall, except for the potentials above 1 V. Hence, from this experiment it could be concluded that PPy electrode can be occasionally charged at higher potentials without significant degradation.

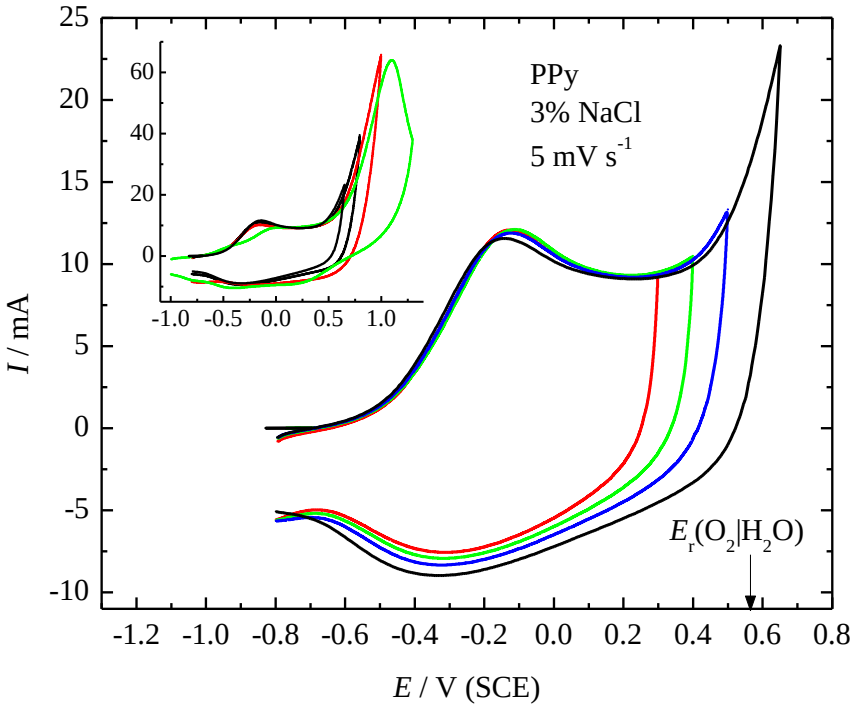

Figure 4.28. Cyclic voltammograms of the PPy electrode with increased anodic potential limits.

The overoxidation is an irreversible degradation process that results in the shortening of the polymer chain length and formation of defects and pores along the PPy chain [123]. Figure 4.29 shows the sequence of reactions that occur during the overoxidation [124]. At potentials higher than 0.6 V (SCE) an additional anion is doped in the polymer chain, simultaneously with oxygen evolution in a small rate. Molecular oxygen in a next step attack pyrrole ring producing the quinone like species, and stop the conjugation along the polymer chain, and prevent further doping of that chain part.

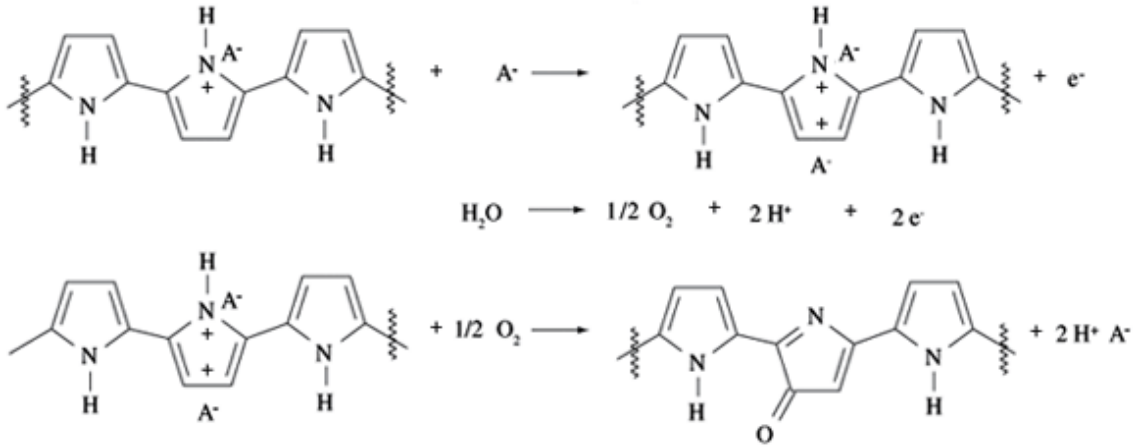

Figure 4.29. Possible reactions during overoxidation of polypyrrole at potentials higher than 0.6 V (SCE) [124].

4.3. High area carbon-polypyrrole zinc cell

In order to simulate the real characteristics of the sea-water zinc -polypyrrole cell, the polypyrrole is electropolymerized on the carbon felt electrode and investigated in a 3.5% of sodium chloride solution.

Figure 1 shows galvanostatic electropolymerization of pyrrole onto carbon felt (CF) electrode, which construction is also shown as an image in Fig. 4.30. Electropolymerization with a current of 48 mA (j = 2 mA cm^{-2}) occurred at potential around 0.6 V. Discharge capacity (Q) can be connected with electropolymerization charge (Q_P) according to Eq. 4.6:

$$Q = \frac{y}{2+y} Q_p = \frac{y}{2+y} I_p t_p \tag{4.6}$$

where y is doping degree. Theoretically for y = 0.33, one chloride anion pre three pyrrole monomer units. Hence, for the electropolymerization charge of 30 mAh, the corresponding maximum available discharge capacity will be 4.25 mAh. More applicable value of 3.3 mAh can be obtained using the previously determined value for y = 0.25. The

mass of the electropolymerized polypyrrole (PPy) is related with the electropolymerization charge, and is represented Eq. 4.9 [19]:

$$m(\mathrm{PPy}) = \frac{Q_{\mathrm{p}}[M_{\mathrm{M}} - 2M(\mathrm{H}^{+}) + yM_{\mathrm{A}}]}{(2+y)F} \tag{4.9}$$

where, M_{M} and M_{A} the molar masses of the monomer unit (M = 67.1 g mol^{-1}) and the chloride anion (M = 35.5 g mol^{-1}). For the available doping degree of y = 0.25 the mass of the electropolymerized PPy is estimated to ~37 mg.

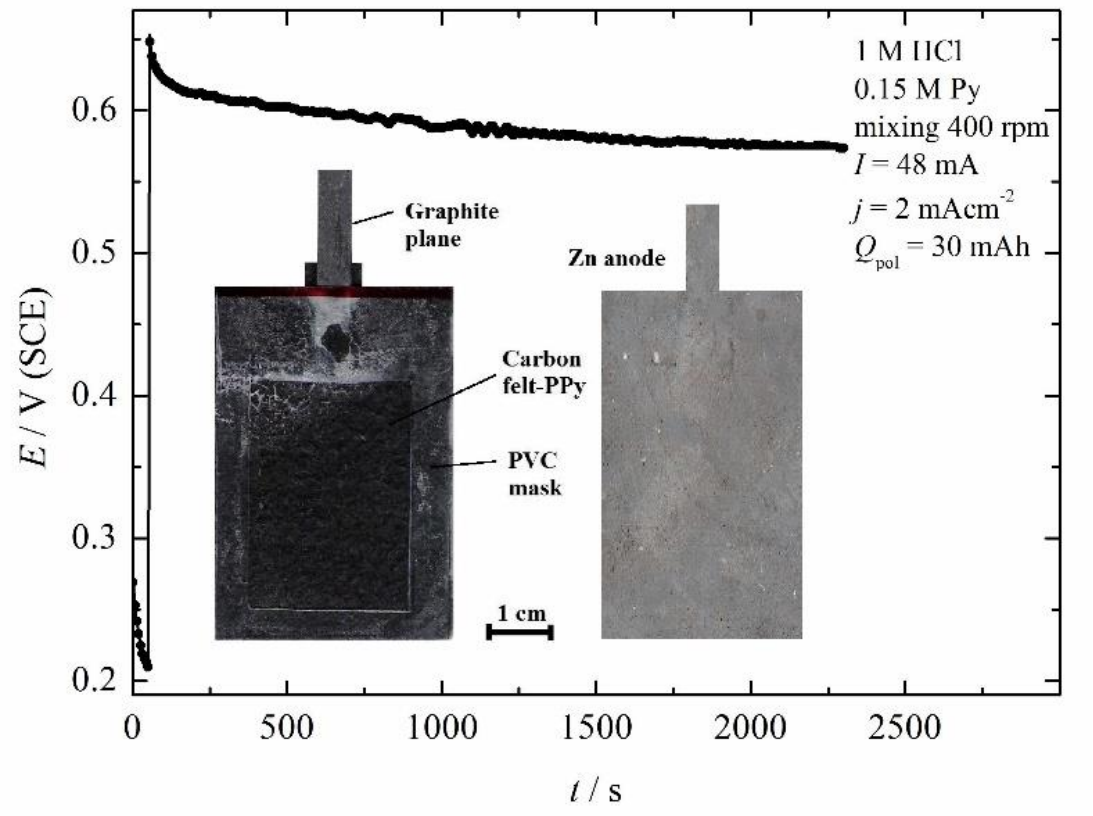

Figure 4.30. Galvanostatic electropolymerization of the pyrrole with current of 48 mA (j = 2 mA cm^{-2}) onto carbon felt electrode, shown in the figure.

The discharge characteristics of the cells with the zinc anode and CF or CF-PPy cathode for different external loads are shown in Fig. 4.31. It is obvious that CF-PPy electrode possess much better discharge characteristics than pure CF, because dedoping of the chloride ions and oxygen reduction reactions occurred simultaneously. For example, at 500 Ω the voltage of the Zn|CF cell was 0.6 V (I = 1.2 mA), while for the

Zn|CF-PPy cell the voltage was ~1.1 V (I = 2.2 mA). After recording the discharge curves, the external load was switched off and the open circuit voltages over time were recorded, shown in the inset in Fig. 4.31. The Zn|CF cell recovered initial voltage of 1.1 V within 30 min. On the other hand, for Zn|CF-PPy much longer time of ~6 h is required for recovery of the open circuit voltage. This can be connected with two reactions occurred at the CF-PPy electrode, similar as in the case of corrosion reaction. First is the oxygen reduction to the peroxide ions as cathodic reaction, and the second is the doping (reoxidation) of the dedoped polypyrrole units in the polymer chain as anodic reaction, partially assisted with chemical oxidation with released hydrogen peroxide ions. Henceforth, in the interaction with molecular oxygen, PPy can recover its initial charge. It should be mentioned that small degree of PPy reoxidation by hydrogen peroxide ions can occur also during discharge.

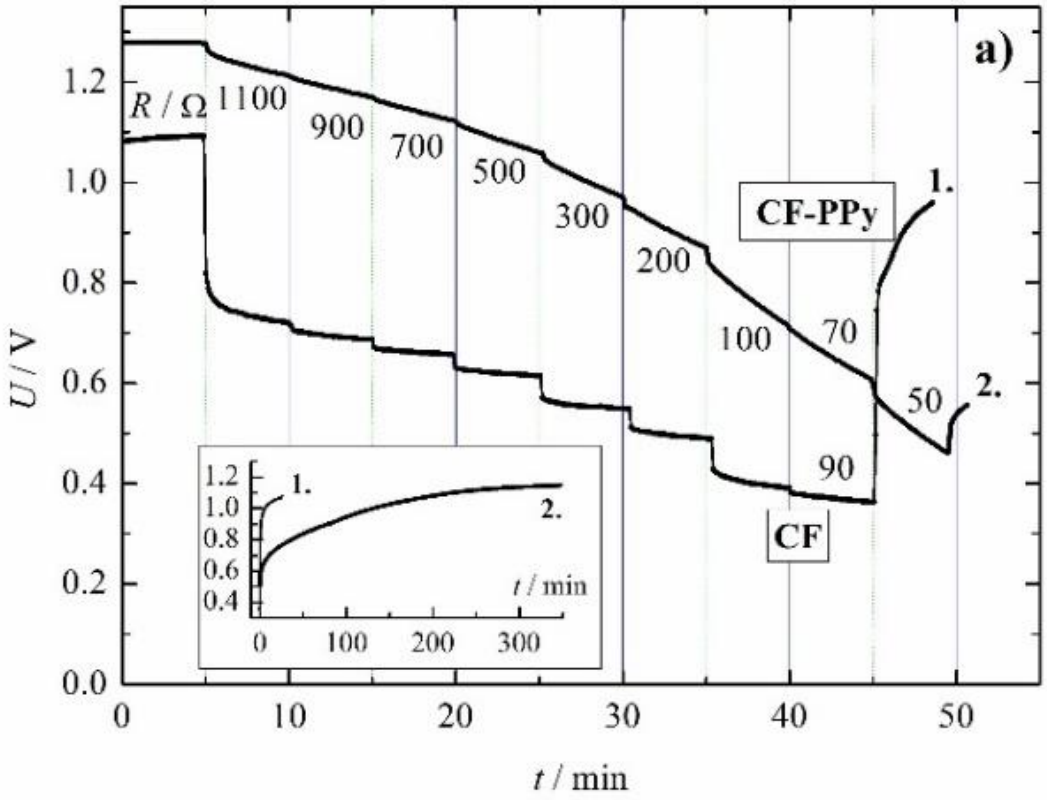

Figure 4.31. The discharge characteristics of the cells with zinc anode and CF or CF-PPy cathode for different external load (marked in the figure) in the non-mixed air saturated 3.5% NaCl. Inset: Dependence of the cell open circuit voltages after discharge over time.

Figure 4.32, shows polarization curves of the cells extrapolated from Fig. 4.31, as well as dependence of power on applied current. Discharge characteristics of the Zn|CF cell are limited by the low molecular oxygen concentration in the sea-water, ranging from 0.35 mM at 0°C to ~0.2 mM at 30°C, and the slow reaction kinetics [125]. Voltage above 0.6 V is obtained only at the low current density below ~0.05 mA cm^{-2}, inset in Fig. 4.32. Mixing of the electrolyte practically did not affect reaction rate, suggesting chemical rate determining step. According to Hossain et al. [126] oxygen reduction can be described by following reaction scheme:

$$GF\text{-}Q + e \rightarrow GF\text{-}Q^{-} \quad (4.26)$$

$$GF\text{-}Q^{-} + O_2 \rightleftarrows GF\text{-}Q\text{-}O_2^{-} \quad (4.27)$$

$$GF\text{-}Q\text{-}O_2^{-} + H_2O + e \rightleftarrows GF\text{-}Q + HO_2^{-} + OH^{-} \quad (4.28)$$

where Q in GF-Q, represents quinone-like surface active centers. The rate determining step was probably chemisorption of molecular oxygen, Eq. 4.27, as the only chemical step in the mechanism.

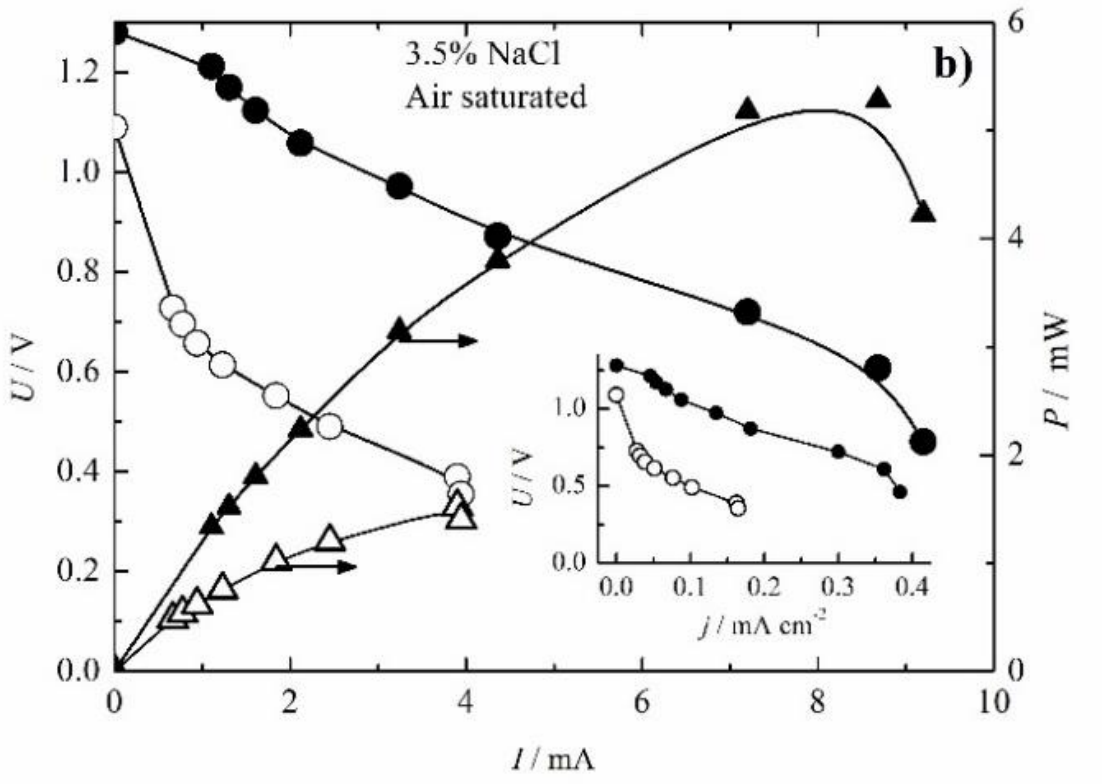

Figure 4.32. Polarization curves of the cells extrapolated from Fig. 4.31, and dependence of power on applied current (open symbols Zn|CF, full symbols Zn|CF-PPy cell). Inset: polarization curves with respect on the current density.

Much higher discharge voltage, 0.75 V, for the Zn|CF-PPy cell is obtained even with the current density of ~0.3 mA cm^{-2}, due simultaneous dedoping-doping and oxygen reduction reaction, inset in Fig. 4.31. At the lower current densities e.g. <0.15 mA, voltage is above 1 V.

Obtained maximum power was ~1.5 mW for Zn|CF cell at current of ~4 mA and corresponding voltage of only 0.35 V, and ~5 mW for Zn|CF-PPy cell at current of ~8 mA and corresponding voltage of 0.7 V.

Reactions which are likely to occur during PPy discharge and reoxidation charge can be anticipated by the following simplified reaction scheme as explained above, Eqs. 4.10-4.13 in more details. During discharge at higher voltages, partial dedoping of $[PPy^{y+}(Cl^{-})_y]_n$ is the main reaction, accompanied with hydrogen peroxide ion production on the –Py=O moieties:

$$[PPy^{y+}(Cl^{-})_y]_n \rightarrow [PPy^{y+}(Cl^{-})_y]_{(n-m)}\text{-}[PPy^{0}]_m + myCl^{-} + mye$$

and:

$$[PPy^{y+}(Cl^{-})_y]_n\text{–Py=O} + H_2O + e \rightarrow [PPy^{y+}(Cl^{-})_y]_n\text{–Py–OH} + OH^{-}$$

$$[PPy^{y+}(Cl^{-})_y]_n\text{–Py–OH} + O_2 \rightarrow [PPy^{y+}(Cl^{-})_y]_n\text{–Py=O} + HO_2^{-}$$

The produced hydrogen peroxide ion (HO_2^-) is able to chemically reoxidize partially dedoped PPy, (-[PPy^0]), in the polymer chain:

$$[PPy^{y+}(Cl^{-})_y]_{(n-m)}\text{-}[PPy^{0}]_m + myCl^{-} + my\,HO_2^{-} + myH_2O \rightarrow [PPy^{y+}(Cl^{-})_y]_n + 3myOH^{-}$$

producing better discharge characteristics. At lower voltages and higher currents, the main reaction is dedoping of the PPy, *via* reaction given by the first reaction in the reaction scheme, which gone through diffusion limitations of the counter ions. For the better visualization, all the reaction steps are schematically shown in Fig. 4.33.

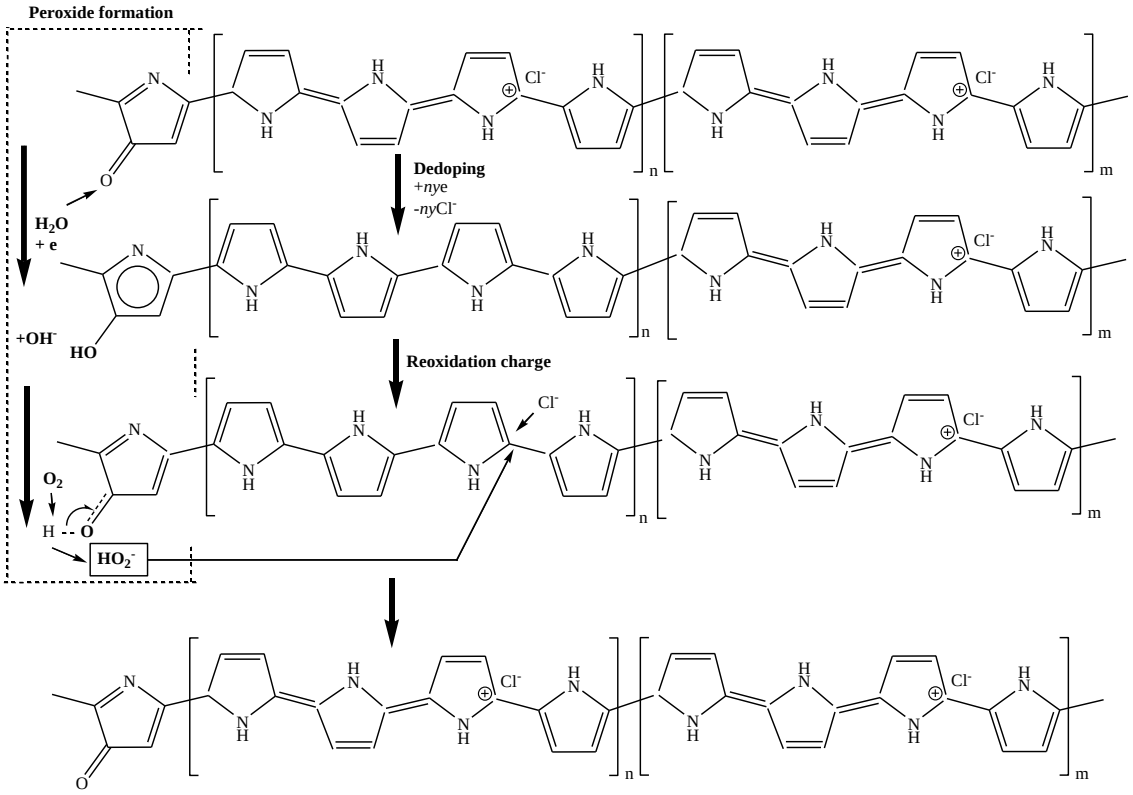

Figure 4.33. Schematic presentation of the reactions occurring at polypyrrole during discharge.

The advantage of the Zn|CF-PPy cell can be further used for impulse discharge-reoxidation charge for long lasting cell operation. In order to investigate the potentiality of the cell, the following experiments are conducted, which results are shown in Fig. 4.34. During constant load (250 Ω) discharge, the cell voltage gradually decreases to 0.6 V over 45 min with average current of 3.2 mA and capacity of ~2.4 mAh. Discharge is conducted in air saturated, but not mixed conditions to simulate different oxygen transport, which can occur in shallow sea-water. After voltage recovery, the discharge is conducted with 2 min under the load (250 Ω), and 2 min without the load (reoxidation charge). Practically the same discharge capacity is obtained, as in continuous discharge. Increasing the reoxidation charge time to 5 min, the stabilization of the average discharge voltage to ~0.65 V is observed. Introducing the air in the solution (simulating mixing of the sea-water under mild, windy conditions), an increase of the cell voltage to ~1 V is observed. This can be explained by different oxygen reduction mechanisms: at low voltages which corresponds67 to low PPy potentials in air saturated solutions, to mainly hydroxyl ions

via bridge-type oxygen-carbon adsorption complexes [66,67] as explained in the theoretical part, and mainly to the hydrogen peroxide mechanism under constant oxygen over-pressure and higher potentials [19]. Changing the values of the external load to 100 Ω or 500 Ω under air mixing conditions, the stable average discharge currents of ~9 mA and ~2.5 mA respectively, are obtained, with the average cell voltage above 0.8 V.

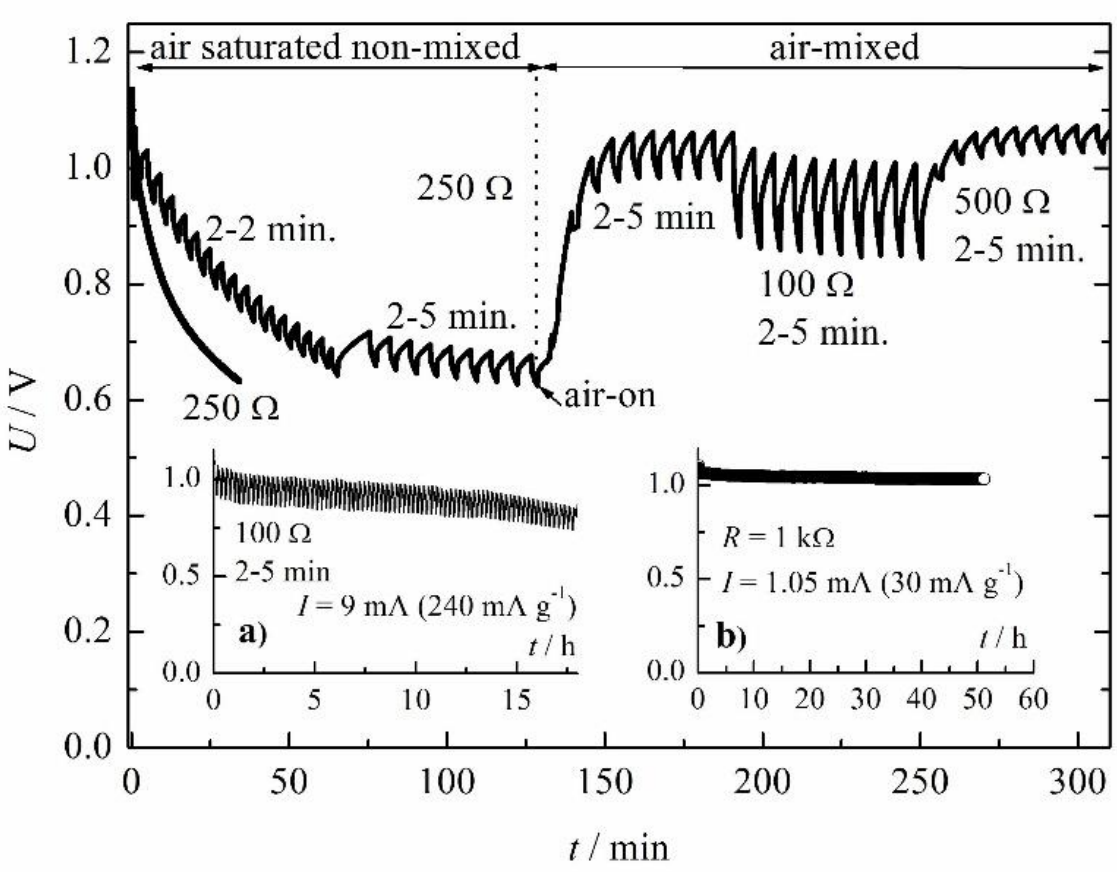

Figure 4.34. Characteristics of the Zn|CF-PPy cell under continuous and pulsed discharge. a) Constant load (100 Ω) pulsed discharge under air mixing conditions with 2 min. discharge, 5 min recharge period, over time. b) Continuous discharge under air mixing conditions with external load of 1 k Ω over time.

For the pulsed discharge (2 min.) and reoxidation charge (5 min.) under constant load of 100 Ω electrode is discharged over 18 h. with the voltage above 0.8 V, Fig. 4.34a. The corresponding average discharge current was 9 mA or ~240 mAh g^{-1} of PPy (taking into account that PPy is the main limiting factor of the cell characteristics). The obtained discharge capacity of the cell is 45 mAh (~1.25 Ah g^{-1} of PPy) which fourteen times

exceed available PPy dedoping capacity of 3.3 mAh estimated using the previously determined value for y = 0.25. On the other hand, during the continuous discharge under 1 kΩ load, the cell voltage was above 1 V over 50 h., Fig. 4.34b with corresponding constant current of 1.1 mA (~30 mAh g^{-1} of PPy) and a capacity of 55 mAh (~1.5 Ah g^{-1} of PPy).

According to the results shown in Fig. 4.34, pulsed discharge-recharge under constant loads and two different on-off conditions are shown in Fig. 4.35.

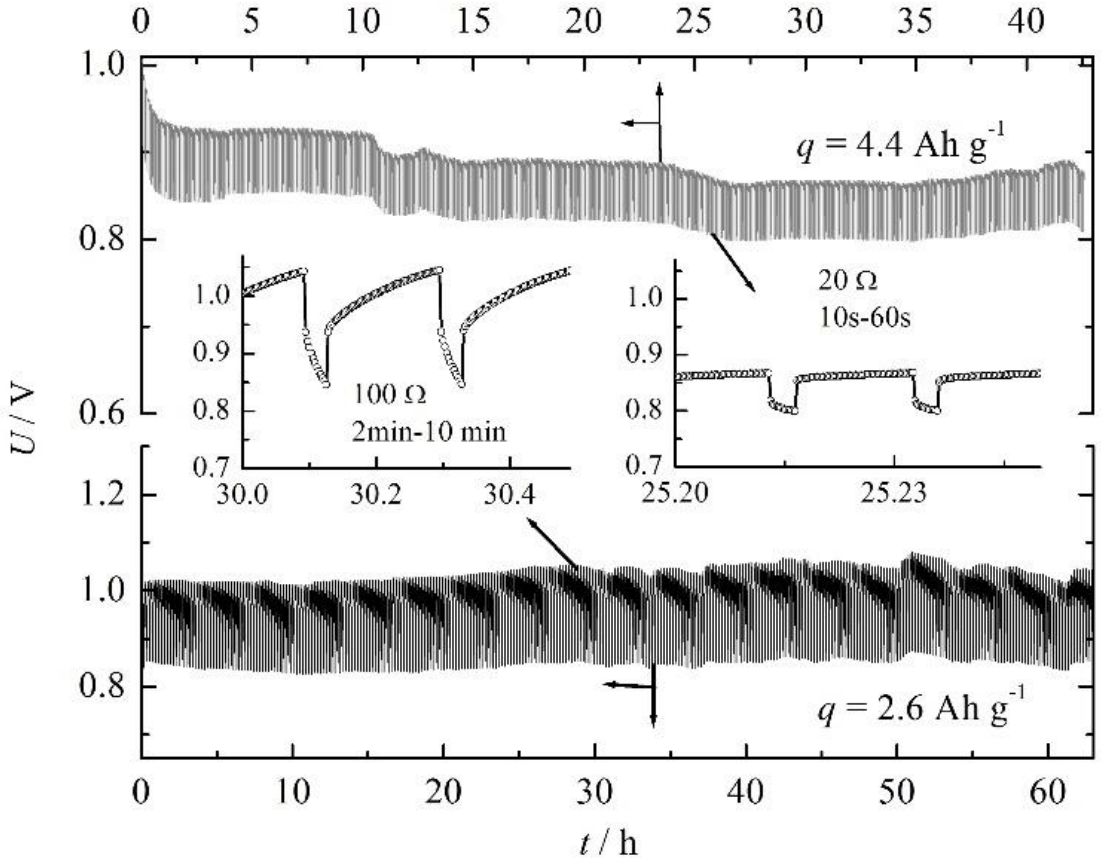

Figure 4.35. Pulsed discharge-recharge of Zn|CF-PPy cell for external loads of 100 Ω (discharge 2 min, recharge 10 min) and 20 Ω (discharge 10 s, recharge 60 s) in air mixed electrolyte over time.

For the conditions of 10 s discharge under the load of 20 Ω, which corresponds to high discharge rare during collected data transmission, and reoxidation charge for 60 s, the voltage gradually decreased from 1 V to ~0.8 V over 42 h, while the average current is ~40 mA (~1.1 A g^{-1} of PPy). The delivered capacity is in the range of 4.4 Ah g^{-1} of PPy.

Accordingly, to the average discharge potentials of 0.8 V, right inset in Fig. 4.34, the specific energy can be estimated to 3.5 Wh g^{-1} of PPy. The estimated specific power is in the range of 0.8 W g^{-1} of PPy.

For the conditions of 2 min. discharge under the load of 100 Ω, data collecting and storage mode, and reoxidation charge for 10 min., the average voltage of 0.9 V did not change significantly over 60 h. The average current was ~9 mA (~240 mA g^{-1} of PPy), and the delivered capacity is in the range of 2.6 Ah g^{-1} of PPy. The average discharge potentials is ~0.9 V, left inset in Fig. 4.34, so the specific energy can be estimated to 2.3 Wh g^{-1} of PPy, and specific power to ~0.23 W g^{-1} of PPy.

In both modes, estimated power and energy during the prolonged discharge and reoxidation charge can significantly excide all the existing electrochemical power sources.

4.4. Possible construction of the battery and reqired accessories

The investigated high area CF-PPy cell shows extraordinary characteristic of specific capacity, energy and power. The cell is proposed to operate as a long lasting power supply for different devices used in a remote sensor buoy system for monitoring shallow marine environments in two modes. In the low discharge mode (10–20 mA g^{-1}), it can be used for data acquisition, and at the fast discharge mode (up to 2 A g^{-1}) for collected data transmission.

Unfortunately, the discharge voltage of the single cell, which is lower than 1 V, is insufficient to be applied as autonomy power source in the buoy systems. The required voltages for the most electronic components and devices are from 3.3 V to 5 V.

One possible ways is to attach four cells by serial connections, with proper elimination of plastic leaking currents eliminators, in a single cell which schematic presentation is shown in Fig. 4.36.

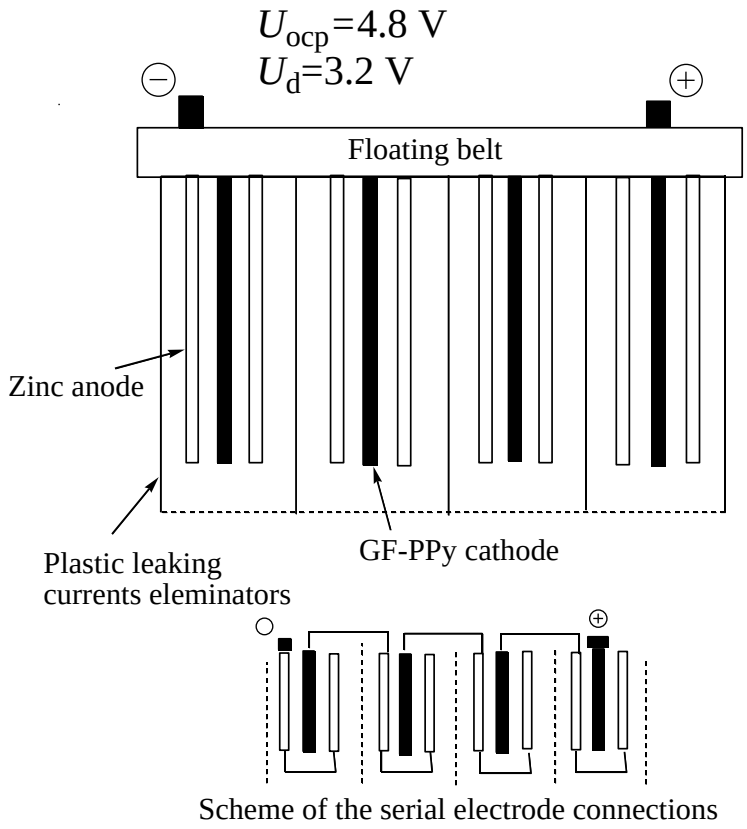

Figure 4.36. Serial connections of four identical Zn|CF-PPy cells.

In that way, the open circuit voltage of ~4.8 V, and discharge voltage of ~3 V can be obtained. However, the average discharge voltage could significantly vary, depending on the load conditions. To avoid this voltage fluctuation, the simple DC/DC converter electronic circuit can be applied, for example LTC3225 by Linear Technology Corporation [127].

The LT3525-3; LTC3525-3.3 and LTC3525-5 are high efficiency synchronous step-up DC/DC converters with output disconnect that can start up with an input as low as 1V. They offer a compact, high efficiency alternative to "charge pumps" in single cell or dual cell alkaline or Li-ion applications. Only three small external components are required as shown in Fig 4.37.

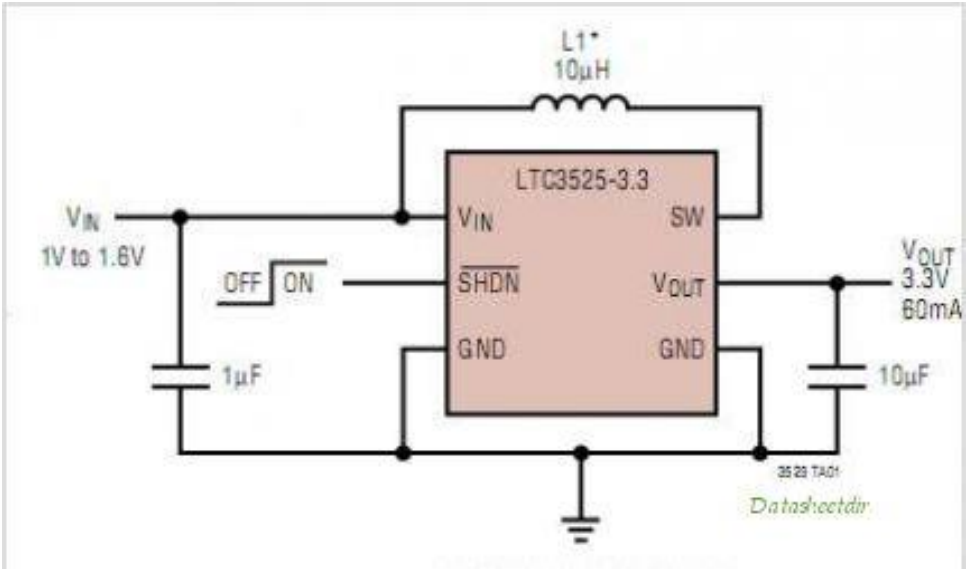

Figure 4.37. Electronic scheme for the LTC3525-3.3 (Linear Technology Corporation).

The LTC3525 is offered in fixed output voltages of 3V, 3.3V or 5V. The device includes a 0.5 n-channel MOSFET switch and a 0.8 p-channel synchronous rectifier. Peak switch current ranges from 150 mA to 400 mA, depending on load, providing enhanced efficiency. Quiescent current is an ultralow 7 µA, maximizing battery life in portable applications. Other features include <1A shutdown current, antiringing control and thermal shutdown. The LTC3525 is available in a tiny 6-pin SC70 package. To further save space, it requires only three external components (two small ceramic capacitors and a small inductor). The LTC3525-3.3 and LTC3525-5 are both packaged in the 2mm × 2mm × 1mm SC70 package, and operate over an input voltage range of 0.8 V to 4.5 V. This flexibility makes them suitable for compact applications powered by 1 to 3

alkaline/NiMH cells, or a single Li- ion battery. The 3.3V version can even maintain regulation with input volt- ages exceeding the output voltage.

Hence, this circuit can be applied for DC/DC conversion of the two serially connected Zn|CF-PPy cells.

4. CONCLUSIONS

The electrochemically formed thin film polypyrole-air regenerative electrode in combination with zinc anode has been tested as a potential material in the seawater based batteries. Due to reversible doping and dedoping reaction of the polypyrrole, and the possibility of polypyrrole reoxidation after discharge with the oxygen contained in the electrolyte, the battery can renew its capacity. The findings also show that during short impulse discharge-reoxidation charge with low currents e.g. ~20-100 mA g^{-1} battery can operate few days with voltage above 0.9 V. For the fast discharge, very high value of specific power in the range of 200 to 300 mW g^{-1} of PPy is reached, but the values of specific energy is relatively low from ~1 to 30 mWh g^{-1} of PPy. Specific power at low and medium discharging rates are around 10 to 30 mW g^{-1} of PPy, with much higher specific energy up to ~200 mWh g^{-1} of PPy. From this results it can be concluded that low power high energy discharge is suitable for constant works, for example during the sensors data acquisition mode, and high power low energy during the data transition mod.

The battery can be also be charged with an external power supply, such as Si-photovoltaic cell, and discharged with specific discharge currents of 300 to 2000 mA g^{-1}. Based on these findings, it is proposed that Zn|PPy-air regenerative cell could be applied as an environmentally friendly battery, in the seawater as the electrolyte. Such cell could work as a long-term power supply for different sensor devices in two modes: In the low discharge mode for data acquisition and at fast discharge mode for the collection of data transmission.

The carbon felt electrode modified with polypyrrole possess improved discharge characteristics as a cathode, in comparison with pure carbon felt, in the Zn sea water based cell. Such behavior was explained with ability that polypyrrole can be reoxidized in the interaction with dissolved molecular oxygen. Under the conditions of mild air mixing the cell can operate with constant discharge current of ~30 mA g^{-1} of PPy over at least 50 h, with the voltage above 1 V. Under pulsed discharged-reoxidation charge conditions, the

cell can deliver specific currents in the ranges of 0.1 to 1 A g^{-1} of PPy with average discharge voltage above 0.8 V, over significant period of time. Specific discharge capacity obtained in this work for investigated times were in the rages of few Ah g^{-1} of PPy, suggesting that such cell with proper mass of zinc anode could be potentially considered as at least secondary power sources, in combination with smaller Li-polymer battery and photovoltaic panel, in the remote sensor buoy system for monitoring shallow marine environments, for example to power microcontrollers during sleep period. Also it should be pointed out that, proposed cell is an environmentally friendly devices which does not contain toxic organic solvents, or highly reactive lithium compounds. Relatively low average discharge voltage, can be increased by serial connections of three cell (2.5-3 V) with proper elimination of leaking currents, or by using simple miniature micro-power synchronous step-up DC/DC converters like LT3525-3 V; LTC3525-3.3 V; LTC3525-5 V.

REFERENCES

[1] C. Albaladejo, F. Soto, R. Torres, P. Sánchez and J.A. López, A low-cost sensor buoy system for monitoring shallow marine environments, Sensors, 12 (2012) 9613- 9634.

[2] G. Mills, G. Fones, A review of in situ methods and sensors for monitoring the marine environment, Sensor Rev., 32 (1) (2012) 17-28.

[3] J. Barton, M. Begoña González-García, D. Hernández-Santos, P. Fanjul-Bolado, A. Ribotti, M. McCaul, D. Diamond, P. Magni, Screen-printed electrodes for environmental monitoring of heavy metal ions: a review, Microchim. Acta, 183 (2016) 503-517.

[4] C.I.L. Justino, A.C. Freitas, A.C. Duarte, T.A.P. Rocha Santos, Sensors and biosensors for monitoring marine contaminants, Trends Environ. Anal. Chem. 6–7 (2015) 21-30.

[5] C. Albaladejo, P. Sánchez, A. Iborra, F. Soto, J.A. López, R. Torres, Wireless sensor networks for oceanographic monitoring: A systematic review, Sensors, 10 (2010) 6948 - 6968.

[6] B. Huang, C.C. Cook, S. Mui, P.P. Soo, D.H. Staelin, A.M. Mayes, D.R. Sadoway, High energy density, thin-film, rechargeable lithium batteries for marine field operations, J. Power Sources, 97–98 (2001) 674-676.

[7] C. Gong, D. Ruzmetov, A. Pearse, D. Ma, J.N. Munday, G. Rubloff, A.A. Talin, and M.S. Leite, Surface/interface effects on high-performance thin-film all-solid-state Li-ion batteries, ACS App. Mater. Interfaces, 7 (47) (2015) 26007 –26011.

[8] F. Cheng, J. Chen, Metal–air batteries: from oxygen reduction electrochemistry to cathode catalysts, Chem. Soc. Rev., 41 (2012) 2172- 2192.

[9] M. Armand and J.-M. Tarascon, Building better batteries, Nature, 451 (2008) 652-657.

[10] G. Li, M.A. Mezaal, R. Zhang, K. Zhang, W. Liu, L. Lei, Electrochemical Evaluation of La1-xCaxMnO3 in Zinc-air Batteries, Int. J. Electrochem. Sci., 10 (2015) 8412-8422.

[11] Md. Arafat Rahman, Xiaojian Wang, Cuie Wen High Energy Density Metal-Air Batteries: A Review, J. Electrochem. Soc. 160(10) (2013) A1759-A1771

[12] R.K. Sen, S.L. Van Voorhees, T. Ferrel, Metal-Air Battery Assessment, Office of Energy Storage and Distribution Conservation and Renewable Energy the U.S. Department of Energy under Contract DE-AC06-76RLO 1830, Battelle Memorial Institute. USA, Springfield, Vorginoa, 1988

[13] R.P. Hamlen, T.B. Atwater, Metal/air batteries, chapter 38. In: Linden, D., Reddy, T.B. (eds.) Handbook of batteries, 3rd edn. McGraw-Hill, New York (2002)

[14] M.A. Rahman, X. Wang, C. Wen, High energy density metal–air batteries: a review. J. Electrochem. Soc. 160 (2013) A1759–A1771.

[15] F. Cheng, J. Chen, Metal–air batteries: from oxygen reduction electrochemistry to cathode catalysts. Chem. Soc. Rev. 41 (2012) 2172–2192.

[16] X.G Zhang, Secondary batteries—zinc systems, zinc electrodes: overview. In: Jürgen, G. (ed.) Encyclopedia of electrochemical power sources, pp. 454–468. Elsevier, Amsterdam (2009)

[17] Y. Ding, S. Kan, J. Gu and J. Kan, Studies on new type current collectors for polyaniline batteries, Int. J. Electrochem. Sci., 9 (2014) 6281-6293.

[18] B.N. Grgur, M.M. Gvozdenović, J. Stevanović J, B.Z. Jugović, V.M. Marinović, Polypyrrole as possible electrode materials for the aqueous-based rechargeable zinc batteries, Electrochim Acta, 53(14) (2008) 4627-4632.

[19] B.N. Grgur, Metal | polypyrrole battery with the air regenerated positive electrode, J. Power Sources, 272 (2014) 1053-1060.

[20] W.S.D. Wilcock, P.C. Kauffman, Development of a seawater battery for deep-water applications, J. Power Sources, 66 (1997) 71-75.

[21] M. Shinohara, E. Araki, M. Mochizuki, T. Kanazawaa, K. Suyehiro, Practical application of a sea-water battery in deep-sea basin and its performance, J. Power Sources, 187 (2009) 253–260.

[22] N. Wang, R. Wang, C. Peng, Y. Feng, B. Chen, Effect of hot rolling and subsequent annealing on electrochemical discharge behavior of AP65 magnesium alloy as anode for seawater activated battery, Corros. Sci., 64 (2012) 17–27.
[23] Y. Zhu, P. Gao, X. Teng, H. Hu, S as additive in Mg–Cu2O seawater batteries using Ni foam-supported electrode, Ionics, 17 (2011) 853–857.
[24] R.F. Koontz, R. David Lucero, Magnesium water-activated batteries, Chapter 17, in: Handbook of batteries 3rd edition, Ed: Linden D, McGraw-Hill, New York, (1995).
[25] T. Zhang, Z. Tao, J. Chen, Magnesium–air batteries: from principle to application, Mater. Horiz., 1 (2014) 196–206.
[26] B.M.L. Rao, W. Kobasz, W.H. Hoge, R.P. Halmen, W. Halliop, N.P. Fitzpatric, Advances in aluminium-air salt water batteries, in: Electrochemistry in Transition, Conway, Brian E., Murphy, O.J., Srinivasan, S, Eds., Plenum Press, New York, 1992, pp 629-639.
[27]Q. Li, N.J. Bjerrum, Aluminum as anode for energy storage and conversion: a review, J. Power Sources, 110 (1) (2002) 1-10.
[28] N. Wang, R. Wang, C. Peng, B. Peng, Y. Feng, C. Hu, Discharge behavior of Mg-Al-Pb and Mg-Al-Pb-In alloys as anodes for Mg-air battery, Electrochim. Acta, 149 (2014) 193–205.
[29] R. Mori, Capacity recovery of aluminium–air battery by refilling salty water with cell structure modification, J. Appl. Electrochem., 45 (2015) 821–829.
[30] J. Maa, J. Wen, J. Gao, Q. Li, Performance of Al-0.5 Mg-0.02 Ga-0.1 Sn-0.5 Mn as anode for Al-air battery in NaCl solutions, J. Power Sources 253 (2014) 419-423.
[31] Y. Ma, N. Li, D. Li, M. Zhang, X. Huang, Performance of Mg–14Li–1Al–0.1Ce as anode for Mg-air battery, J. Power Sources, 196 (2011) 2346–2350
[32] M. Pino, D. Herranz, J. Chacón, E. Fatás, P. Ocón, Carbon treated commercial aluminium alloys as anodes for aluminium-air batteries in sodium chloride electrolyte, J. Power Sources, 326 (2016) 296-302.
[33] B.M. Praveen, T.V. Venkatesha, Y. Arthoba Naik, K. Prashantha, Corrosion studies of carbon nanotubes–Zn composite coating, Surf. Coat. Tech., 201 (2007) 5836–5842.
[34] D. Wittmaier, T. Danner, N. Wagner, K.A. Friedrich, Screening and further investigations on promising bi-functional catalysts for metal–air batteries with an aqueous alkaline electrolyte, J Appl. Electrochem., 44 (2014) 73–85.

[35] Z. Ma, P. Pei, K. Wang, X. Wang, H. Xu, Y. Liu, G. Peng, Degradation characteristics of air cathode in zinc air fuel cells, J. Power Sources, 274 (2015) 56-64.
[36] S.C. Popat, D. Ki, M.N. Young, B.E. Rittmann, C. I. Torre, Buffer pKa and transport govern the concentration overpotential in electrochemical oxygen reduction at neutral pH, Chem. Electro. Chem., 1(11) (2014) 1909–1915.
[37] A. Morozan, B. Jousselme and S. Palacin, Low-platinum and platinum-free catalysts for the oxygen reduction reaction at fuel cell cathodes, Energy Environ. Sci., 4 (2011) 1238–1254.
[38] EPA. (2012). 5.2 Dissolved oxygen and biochemical oxygen demand. In Water Monitoring and Assessment: http://water.epa.gov/type/rsl/monitoring/vms52.cfm
[39] P.K. Shen, A.C.C. Tseung, C. Kuo, Development of an aluminum/sea water battery for subsea applications, J. Power Sources, 47 (1994) 119-127.
[40] Steve P. Lund, Environmental Science – I, TOPIC 8: Biogeochemical cycling in the earth system, ENST-501/502, 2000.
[41] A. Malinauskas, J Malinauskienė, A Ramanavičius, , Conducting polymer-based nanostructurized materials: electrochemical aspects Nanotechnology, 16 (2005) R51–R62.
[42] P. Rüetschi, Energy storage and the environment: the role of battery technology, J. Power Sources, 42 (1993) 1-7.
[43] F. Beck, P. Rüetschi, Rechargeable batteries with aqueous electrolytes, Electrochim. Acta, 45 (2000) 2467–2482.
[44] G. A. Snooka, P. Kao, A. S. Best, Conducting-polymer-based supercapacitor devices and electrodes, J. Power Sources, 196 (2011) 1–12.
[45] D. Nguyen Nguyen, H. Yoon, Recent advances in nanostructured conducting polymers: from synthesis to practical applications, Polymers, 8 (2016) 118-156.
[46] E. Frackowiak, V. Khomenko, K. Jurewicz, K. Lota, F. Béguin, Supercapacitors based on conducting polymers/nanotubes composites, J. Power Sources, 153 (2006) 413–418.
[47] E. Smela, W. Lu, and B. R. Mattes, Polyaniline Actuators, Part 1: PANI(AMPS) in HCl, Synth. Met., 151 (1), 25–42 (2005).
[48] R. de Surville, M. Josefowicz, L.T. Yu, J. Perichon, R. Buvet, Electrochemical chains using protolytic organic semiconductors, Electrochi. Acta, 13 (1968) 1451-1458.

[49] M. Kaya, A. Kitani, K. Sasaki, Polyaniline as the positive electrode of storage batteries, Denki Kagaku 52 (1984) 847-848.

[50] A. Kitani, M. Kaya and K. Sasaki, Performance study of aqueous polyaniline batteries, J. Elecrochem. Soc., 133 (1986) 1069-1073.

[51] M.S. Rahmanifar, M.F. Mousavi, M. Shamsipur, M. Ghaemia, What is the limiting factor of the cycle-life of Zn–polyaniline rechargeable batteries?, J. Power Sources, 132 (2004) 296-301.

[52] H.N. Dinh, J. Ding, S.J. Xia, V.I. Birss, Multi-technique study of the anodic degradation of polyaniline films, J. Electroanal. Chem., 459 (1998) 45-56.

[53] D.E. Stilwell, S.-M. Park, Electrochemistry of conductive polymers IV: Electrochemical studies on polyaniline degradation - Product identification and coulometric studies, J. Electrochem. Soc., 135 (1988) 2497-2502.

[54] H-K. Song, G.T.R. Palmore, Redox-active polypyrrole: Toward polymer-based batteries, Adv. Mater., 18 (2006) 1764–1768.

[55] G. Nyström, A. Razaq, M. Strømme, L. Nyholm, A. Mihranyan, Ultrafast all-polymer paper-based batteries, Nano Lett., 9(10) (2009) 3635-3639.

[56] M. Pasta, C.D. Wessells, R.A. Huggins, Yi Cui, A high-rate and long cycle life aqueous electrolyte battery for grid-scale energy storage. Nat. Commun., 3 (2012) 1149.

[57] Y. Kong, C. Wang, Y. Yang, C.O. Too, G.G. Wallace, A battery composed of a polypyrrole cathode and a magnesium alloy anode—Toward a bioelectric battery, Synthetic Met., 162 (2012) 584– 589.

[58] C. Wang , W. Zheng , Z. Yue , C.O. Too, G.G. Wallace, Buckled, stretchable polypyrrole electrodes for battery applications, Adv. Mater., 23 (2011) 3580–3584.

[59] S. Li, I. Sultana, Z. Guo, C. Wang, G.G. Wallace, H-K. Liu, Polypyrrole as cathode materials for Zn-polymer battery with various biocompatible aqueous electrolytes, Electrochim. Acta, 95 (2013) 212–217.

[60] S. Li, Z. Ping, G.C. Yun Wang, G.G. Wallace, H.K. Liu, Flexible cellulose based polypyrrole–multiwalled carbon nanotube films for bio-compatible zinc batteries activated by simulated body fluids, J. Mater. Chem. A, 1 (2013) 14300–14305.

[61] B.N. Grgur, M.M. Gvozdenović, J. Stevanović, B.Z. Jugović, V.M. Marinović, Polypyrrole as possible electrode materials for the aqueous-based rechargeable zinc batteries, Electrochim. Acta, 53(14) (2008) 4627-4632.

[62] P. Audebert. Recent Trends in Polypyrrole Electrochemistry, Nanostructuration, and Applications, in: S. Cosnier and A. Karyakin (Eds.), Electropolymerization: Concepts, Materials and Applications, Wiley-VCH Verlag GmbH & Co. KGaA, Weinheim, Germany. 2010, pp 77-91.

[63] S.B. Saidman, Influence of anion and pH on the electrochemical behavior of polypyrrole synthesised in alkaline media, Electrochim. Acta, 48 (2003) 1719-1726.

[64] G.G. Wallace, G. Tsekouras, C. Wang, Inherently Conducting Polymers via Electropolymerization for Energy Conversion and Storage, Ch 11, in Electropolymerization: Concepts, Materials and Applications, Eds: S. Cosnier and A. Karyakin, Wiley-VCH Verlag GmbH & Co. KGaA, Weinheim, 2010.

[65] G.J. Wang, L.C. Yang, Q.T. Qu, B. Wang, Y.P. Wu, R. Holze, An aqueous rechargeable lithium battery based on doping and intercalation mechanisms, J. Solid State Electrochem., 14 (2010) 865–869.

[66] V. Z. Barsukov, V. G. Khomenko, A. S. Katashinskii, T. I. Motronyuk, Catalytic Activity of Polyaniline in the Molecular Oxygen Reduction: Its Nature and Mechanism, Russ. J. Electrochem., 40 (11) (2004) 1170–1173.

[67] V.G. Khomenko, V.Z. Barsukov, A.S. Katashinskii, The catalytic activity of conducting polymers toward oxygen reduction, Electrochim. Acta, 50 (2005) 1675–1683.

[68] V.Z. Barsukov, V.G. Khomenko, A.S. Katashinskii, T.I. Motronyuk, New concept for the metal-air batteries using composites: Conducting polymers/extended graphite as catalyst, I.V. Barsukov et al. (eds.), New Carbon Based Materials for Electrochemical Energy Storage Systems, 89–104. Springer, Netherlands, 2006.

[69] V.G. Khomenko, K.V. Lykhnytskyi, V.Z. Barsukov, Oxygen reduction at the surface of polymer/carbon and polymer/carbon/spinel catalysts in aqueous solutions, Electrochim. Acta ,104 (2013) 391– 399.

[70] A. Wu, E.C. Venancio, A.G. MacDiarmid, Polyaniline and polypyrrole oxygen reversible electrodes, Synthetic Met., 157 (2007) 303–310.

[71] K.B. Liew, W.R.W. Daud, M. Ghasemi, J.X. Leong, S.S. Lim, M. Ismail, Non-Pt catalyst as oxygen reduction reaction in microbial fuel cells: A review, Int. J. Hyd. Energy, 39 (2014) 4870-4883.

[72] Y. Yuan, S. Zhou, L. Zhuang, Polypyrrole/carbon black composite as a novel oxygen reduction catalyst for microbial fuel cells, J. Power Sources, 195 (2010) 3490–3493.

[73] X. Ji, C. Wang, C. Zhao, Y. Ge, G.G. Wallace, Toward biodegradable Mg–Air bioelectric batteries composed of silk fibroin–polypyrrole film, Adv. Funct. Mater., 2016, DOI: 10.1002/adfm.201503498

[74] K. Maksymiuk, Chemical reactivity of polypyrrole and its relevance to polypyrrole based electrochemical sensors, Electroanalysis, 18 (16) (2006) 1537 – 1551.

[75] A. Diaz, Electrochemical preparation and characterisation of conducting polymers, Chem. Scr., 17 (1981) 145 -148.

[76] G. B. Street, T. C. Clarke, M. Kronubi, K. Kanazawa, V. Lee, P. Pfluger, J. C. Scott, G. Weiser, Preparation and Characterization of Neutral and Oxidized Polypyrrole Films, Mol. Cryst. Liq. Cryst., 83 (1-4) (1982) 1285-1286.

[77] P. Pfluger, M. Kronubi, G. B. Street, G. Weiser, The chemical and physical properties of pyrrole-based conducting polymers: The oxidation of neutral polypyrrole, J. Chem. Phys., 78 (1983) 3212-3218.

[78] J. C. Scott, P. Pfluger, M. T. Kronubi, G. B. Street, Electron-spin-resonance studies of pyrrole polymers: Evidence for bipolarons, Phys. Rev. B., 28 (1983) 2140-2145.

[79] Y. Son, K. Rajeshwar, Potential-modulated ultraviolet–visible and Raman spectra of polypyrrole thin films in aqueous electrolytes : combination with voltammetric scanning and the influence of dioxygen on the stability of radical cations and dications of the conducting polymer, J .Chem. Soc. Faraday Trans., 88 (1992) 605-610.

[80] J. Lei, C. R. Martin, Investigations of the chemical interactions between molecular oxygen and pristine (undoped) polypyrrole, Chem. Mater., 7 (1995) 578-584.

[81] J. Kankare, I. A. Vinokurov, Potentiometric response of conducting polymer electrodes for oxygen in neutral aqueous solutions, Anal. Chem., 69 (1997) 2337-2342.

[82] J. Dumanska, K. Maksymiuk, Studies on Spontaneous Charging/Discharging Processes of polypyrrole in aqueous electrolyte solutions, Electroanalysis, 13 (2001) 567-573.

[83] D. Y. Kim, J. Y. Lee, D. K. Moon, C. Y. Kim, Stability of reduced polypyrrole, Synth. Met., 69 (1995) 471-474.

[84] J. T. Lei, W. Liang, C. R. Martin, Infrared investigations of pristine, doped and partially doped polypyrrole, Synth. Met., 48 (1992) 301-312.

[85] B. Tian, G. Zerbi, Lattice dynamics and vibrational spectra of polypyrrole, J. Chem. Phys., 92 (1990) 3886-3891.

[86] B. Tian, G. Zerbi, Lattice dynamics and vibrational spectra of pristine and doped polypyrrole: Effective conjugation coordinate, J. Chem. Phys., 92 (1990) 3892-3897.
[87] M. Nechtschein, F. Genoud, On the broadening of the ESR line in presence of air or oxygen in conducting polymers, Solid State Commun., 94 (1994) 471-473.
[88] A. Bartl, L. Dunsch, H. Naarmann, W. Göpel, ESR studies of polypyrrole films with a two-dimensional microstructure, Synth. Met., 61 (1993) 167-170.
[89] A. Bartl, L. Dunsch, D. Schmeiber, W. Göpel, H. Naarmann, Influence of oxygen on the paramagnetic properties of polypyrrole layers, Synth. Met., 69 (1995) 389-390.
[90] K. Kanemoto, J. Yamauchi, ESR broadening in conducting polypyrrole because of oxygen: Application to the study of oxygen adsorption, J .Phys. Chem. B, 105 (2001) 2117.
[91] K. G. Neoh, T. T. Young, E. T. Kang, T. Kang, Structural and mechanical degradation of polypyrrole films due to aqueous media and heat treatment and the subsequent redoping characteristics, J. Appl. Polymer Sci. 64 (1997) 519-526.
[92] A. Alumaa, A. Hallik, V. Sammelselg, J. Tamm, On the improvement of stability of polypyrrole films in aqueous solutions, Synth. Met., 157 (2007) 485-491.
[93] P. Manisankar, A. Gomathi, Electrocatalysis of oxygen reduction at polypyrrole modified glassy carbon electrode in anthraquinone solutions, J. Mol. Cat. A Chem., 232 (2005) 45-52
[94] J.C. Forti, R.S. Rocha, M.R.V. Lanza, R. Bertazzoli, Electrochemical synthesis of hydrogen peroxide on oxygen-fed graphite/PTFE electrodes modified by 2-ethylanthraquinone, J. Electroanal. Chem., 601 (2007) 63-67
[95] S. H. Cho, S. K. Tae, L. J. Ypoung, Recent Advances in Polypyrrole," in in Conducting Polymers-Theory, Synthesis, Properties and Characterization, T. Skotheim and J. Reynolds, (Eds.), Teyor & Francis Group, 2007, pp. 1–87.
[96] T.V. Vernitskaya, O.N. Efimov, Polypyrrole: a conducting polymer; its synthesis, properties, and applications, Russ. Chem. Rev. 66 (5) (1997) 443-457.
[97] M.M. Gvozdenović, B.Z. Jugović, J.S. Stevanović, B.N. Grgur, Electrochemical synthesis of electroconducting polymers, Hem. Ind. 68 (6) (2014) 673–684.
[98] L.A.P. Kane-Maguire, G.G. Wallace, Chiral conducting polymers, Chem. Soc. Rev., 39 (2010) 2545-2576.

[99] F. Wolfart, D.P. Dubal, M. Vidotti, R. Holze, P. Gómez-Romero, Electrochemical supercapacitive properties of polypyrrole thin films: influence of the electropolymerization methods, J Solid State Electrochem., 20 (2016) 901-910.

[100] S. Carquigny, O. Segut, B. Lakard, F. Lallemand, P. Fievet, Effect of electrolyte solvent on the morphology of polypyrrole films: Application to the use of polypyrrole in pH sensors, Synth. Met., 158 (2008) 453–461.

[101] E. M. Genies, G. Bidan, A. F. Diaz, Spectroelectrochemical study of polypyrrole films, J. Electroanal. Chem., 149 (1983) 101-113.

[102] K. Matyjaszewski and T. Davys, Eds., Handbook of Radical Polymerization. Hoboken, John Wiley & Sons, 2002.

[103] J. Kankare, Conducting polymers: Basic Methods of Synthesis and Characterization, in Electrical and Optical Polymer Systems: Fundamentals, Methods and Applications, Wise D.; Wnek G.; Trantolo D.; Cooper J.; Gresser D., (Eds.), New York, 1998, pp. 167–199.

[104] G.G. Wallace, G.M. Spinks, L.A.P. Kane-Meguire P.R. Teasdale, Conductive Electroactive Polymers, 3rd. ed. Boca Raton, London, New York, Telyor& Francis Group, 2009.

[105] J. Stejskal, M. Trchova, P. Bober, Z. Morávková, D. Kopecký, M. Vrnata, J. Prokeš, M. Varga and E. Watzlova, Polypyrrole salts and bases: superior conductivity of nanotubes and their stability towards the loss of conductivity by deprotonation, RSC Adv., 6 (2016) 88382-88391.

[106] A.S. Liu, M.A.S. Oliveira, Electrodeposition of polypyrrole films on aluminum from tartrate aqueous solution, J. Braz. Chem. Soc., 18 (1) (2009) 143-152.

[107] A.S. Liu, M. C. Bezerra, L.Y. Cho, Electrodeposition of polypyrrole films on aluminum surfaces from a p-toluene sulfonic acid medium, Materials Research, 12 (4) (2009) 503-507.

[108] S. Ardizzone, G. Fregonara, S. Trasatti, “Inner” and “outer” active surface of RuO_2 electrodes, Electrochim. Acta, 35 (1990) 263-268.

[109] H. Masuda, D. K. Asano, Preparation and properties of polypyrrole, Synthetic Metals, 135-136 (2003) 43-44.

[110] J.V. Thombare, M.C. Rath, S.H. Han, V.J. Fulari, Synthesis of hydrophilic polypyrrole thin films by SILAR method, Mat. Phys. Mech., 16 (2013) 118-125.

[111] P.M. Carrasco, M. Cortazar, E. Ochoteco, E. Calahorra, J.A. Pomposo, Comparison of surface and bulk doping levels in chemical polypyrroles of low, medium and high conductivity, Surf. Interface Anal., 39 (2007) 26–32.

[112] C. Weidlich, K.-M. Mangold, K. Jüttner, EQCM study of the ion exchange behaviour of polypyrrole with different counterions in different electrolytes, Electrochim. Acta, 50 (2005) 1547–1552.

[113] R. Mazeikiene, A. Malinauskas, Kinetics of the electrochemical degradation of polypyrrole, Polym. Degrad. Stab., 75 (2002) 255–258.

[114] M.A. Careem, Y. Velmurugu, S. Skaarup, K. West, A voltammetry study on the diffusion of counter ions in polypyrrole films, J. Power Sources, 159 (2006) 210–214.

[115] R. Stanković, O. Pavlović, M. Vojnović, S. Jovanović, The effect of preparation conditions on the properties of electrochemically synthesized thick films of polypyrrole, Eur. Polym. J., 30 (3) (1994) 385-393.

[116] A. Alumaa, A. Hallik, V. Sammelselg, J. Tamm, On the improvement of stability of polypyrrole films in aqueous solutions, Synthetic Met., 157 (2007) 485–491.

[117] https://en.wikipedia.org/wiki/Lithium_polymer_battery

[118] Y. Li, H. Dai, Recent advances in zinc–air batteries, Chem. Soc. Rev., 43 (2014) 5257-5275,

[119] T. Trišović, LJ. Gajić-Krstajić, N. Krstajić, M. Vojnović, On the kinetics of the hydrogen evolution reaction on zinc in sulfate solutions, J. Serb. Chem. Soc., 66 (11–12) (2001) 811–823.

[120] R. Kötz, M. Carlen. Principles and applications of electrochemical capacitors, Electrochim. Acta, 45(15-16) (2000) 2483-2498.

[121] Y. Zhang, H. Feng, X. Wu, L. Wang, A. Zhang, T. Xia, H. Dong, X. Li, L. Zhang, Progress of electrochemical capacitor electrode materials: A review, Int. J. Hyd. Energy., 34 (2009) 4889–4899.

[122] A. Burke, Ultracapacitors: why, how, and where is the technology, J. Power Sources 91, (2000) 37–50.

[123] Li Y, Qian R. Electrochemical overoxidation of conducting polypyrrole, nitrate film in aqueous solutions. Electrochim. Acta., 45(11) (2000) 1727-1731.

[124] A. Santos Liu, M.A.S. Oliveir, Corrosion control of aluminum surfaces by polypyrrole films: Influence of electrolyte, Mat. Research, 10 (2) (2007) 205-209.

[125] B.N. Grgur, B.Z. Jugović, M.M. Gvozdenović, Oxygen reduction on SILAR deposited iron oxide onto graphite felt electrode, Electrochimica Acta, 212 (2016) 254–259.
[126] M. S. Hossain, D. Tryk, E. Yeager, The electrochemistry of graphite and modified graphite surfaces: the reduction of O2, Electrochim. Acta, 34(12) (1989) 1733-1737.
[127] http://pdf.datasheetcatalog.com/datasheet/lineartechnology2/ltc3225.pdf

BIOGRAFIJA

Ali Hussien Al-Eggiely, master inženjer tehnologije, je rođen 27.10.1979. godine u mestu Souq Alkhamees, Libya. Diplomirao je na departmanu za hemijsko inženjerstvo školske 2001/2002 na Al-Mergheb, University, Alkhums, Libya. Master studije je uspešno završio 2006 godine na, Department of Chemical Engineering, National University of Malaysia, Malaysia. Tokom perioda od 2006 do 2012 radio je kao pomoćni predavač na Al-Mergheb University, Libya.
Školske 2014/2015 upisao je doktorske studije na Tehnološko-metalurškom fakultetu, Univerziteta u Beogradu, odsek za Hemijsko inženjerstvo. Do sada je koautor jednog rada u međunarodnom časopisu izuzetnih vrednosti (M21a) i autor i koautor dva rada u istaknutom međunarodnom časopis (M22), i autor rada u međunarodnom časopisu (M23).

BIOGRAPHY

Ali Hussien Al-Eggiely, Master Technology Engineer, was born on October 27, 1979. in Souq Alkhamees, Libya. He graduated from the Department of Chemistry 2001/2002 at Al-Mergheb, University, Alkhums, Libya. He successfully completed his master studies in 2006 at the Department of Chemical Engineering, National University of Malaysia, Malaysia. During the period from 2006 to 2012 he worked as an assistant lecturer at Al-Mergheb University, Libya.
School year 2014/2015 he enrolled in doctoral studies at the Faculty of Technology and Metallurgy, University of Belgrade, Department of Chemical Engineering.
He is the author and coauthor of four scientific papers.

Radovi proistekli iz doktorske disertacije/Papers from doctoral dissertation

Istaknuti međunarodni časopis M22.

1. Al-Eggiely Ali H., Alguail Alsadek A., Gvozdenović Milica M, Jugović Branimir Z., Grgur Branimir N., Seawater Zinc/Polypyrrole-air Cell Possessing Multifunctional Charge-Discharge Characteristics, - *Journal of Solid State Electrochemistry*, vol. 21, pp. 2769–2777, 2017 **(IF= 2.316)** (ISSN: 1432-8488)

Međunarodni časopis, M23.

1. Al-Eggiely Ali .H., Alguail Alsadek A., Gvozdenović Milica .M., Jugović Branimir Z., Grgur Branimir N., Zinc Polypyrrole-Air Sea Water Battery, - *International Journal of the Electrochemical Science*, vol. 11, pp. 10270 – 10277, 2016. **(IF= 1.469)** (ISSN 1452-3981)

Прилог 1.

Изјава о ауторству

Потписани-а Ali Hussien Al-Eggiely

број индекса 4042/2014

Изјављујем

да је докторска дисертација под насловом

Possible application of the polypyrrole-zinc system as a sea-water battery

- резултат сопственог истраживачког рада,
- да предложена дисертација у целини ни у деловима није била предложена за добијање било које дипломе према студијским програмима других високошколских установа,
- да су резултати коректно наведени и
- да нисам кршио/ла ауторска права и користио интелектуалну својину других лица.

Потпис докторанда

У Београду, 07.11.2017.

Прилог 2.

Изјава о истоветности штампане и електронске верзије докторског рада

Име и презиме аутора Ali Hussien Al-Eggiely

Број индекса 4042/2014

Студијски програм Хемијско инжењерство

Наслов рада Possible application of the polypyrrole-zinc system as a sea-water battery

Ментор Др Бранимир Гргур, ред. проф.

Потписани/а Ali Hussien Al-Eggiely

Изјављујем да је штампана верзија мог докторског рада истоветна електронској верзији коју сам предао/ла за објављивање на порталу **Дигиталног репозиторијума Универзитета у Београду.**

Дозвољавам да се објаве моји лични подаци везани за добијање академског звања доктора наука, као што су име и презиме, година и место рођења и датум одбране рада.

Ови лични подаци могу се објавити на мрежним страницама дигиталне библиотеке, у електронском каталогу и у публикацијама Универзитета у Београду.

Потпис докторанда

У Београду, 07.11.2017.

Прилог 3.

Изјава о коришћењу

Овлашћујем Универзитетску библиотеку „Светозар Марковић“ да у Дигитални репозиторијум Универзитета у Београду унесе моју докторску дисертацију под насловом:

Possible application of the polypyrrole-zinc system as a sea-water battery

која је моје ауторско дело.

Дисертацију са свим прилозима предао/ла сам у електронском формату погодном за трајно архивирање.

Моју докторску дисертацију похрањену у Дигитални репозиторијум Универзитета у Београду могу да користе сви који поштују одредбе садржане у одабраном типу лиценце Креативне заједнице (Creative Commons) за коју сам се одлучио/ла.

1. Ауторство

2. Ауторство - некомерцијално

3. Ауторство – некомерцијално – без прераде

4. Ауторство – некомерцијално – делити под истим условима

5. Ауторство – без прераде

6. Ауторство – делити под истим условима

(Молимо да заокружите само једну од шест понуђених лиценци, кратак опис лиценци дат је на полеђини листа).

Потпис докторанда

У Београду, 07.11.2017.

1. Ауторство - Дозвољавате умножавање, дистрибуцију и јавно саопштавање дела, и прераде, ако се наведе име аутора на начин одређен од стране аутора или даваоца лиценце, чак и у комерцијалне сврхе. Ово је најслободнија од свих лиценци.

2. Ауторство – некомерцијално. Дозвољавате умножавање, дистрибуцију и јавно саопштавање дела, и прераде, ако се наведе име аутора на начин одређен од стране аутора или даваоца лиценце. Ова лиценца не дозвољава комерцијалну употребу дела.

3. Ауторство - некомерцијално – без прераде. Дозвољавате умножавање, дистрибуцију и јавно саопштавање дела, без промена, преобликовања или употребе дела у свом делу, ако се наведе име аутора на начин одређен од стране аутора или даваоца лиценце. Ова лиценца не дозвољава комерцијалну употребу дела. У односу на све остале лиценце, овом лиценцом се ограничава највећи обим права коришћења дела.

4. Ауторство - некомерцијално – делити под истим условима. Дозвољавате умножавање, дистрибуцију и јавно саопштавање дела, и прераде, ако се наведе име аутора на начин одређен од стране аутора или даваоца лиценце и ако се прерада дистрибуира под истом или сличном лиценцом. Ова лиценца не дозвољава комерцијалну употребу дела и прерада.

5. Ауторство – без прераде. Дозвољавате умножавање, дистрибуцију и јавно саопштавање дела, без промена, преобликовања или употребе дела у свом делу, ако се наведе име аутора на начин одређен од стране аутора или даваоца лиценце. Ова лиценца дозвољава комерцијалну употребу дела.

6. Ауторство - делити под истим условима. Дозвољавате умножавање, дистрибуцију и јавно саопштавање дела, и прераде, ако се наведе име аутора на начин одређен од стране аутора или даваоца лиценце и ако се прерада дистрибуира под истом или сличном лиценцом. Ова лиценца дозвољава комерцијалну употребу дела и прерада. Слична је софтверским лиценцама, односно лиценцама отвореног кода.